AN ANALOGUE COMPUTER STUDY OF COSMIC RAY THRESHOLD RIGIDITIES

THESIS

submitted by

PETER CHARLES HEDGECOCK

for the degree of

DOCTOR OF PHILOSOPHY

in the

UNIVERSITY OF LONDON

May 1964

ABSTRACT

Cosmic ray threshold rigidities have been investigated by an analogue technique which involved a study of the trapping of an electron beam in a magnetic dipole field. This method of analysis has produced useful data on the general features of the penumbra both at the Earth's surface and at satellite altitudes. In addition, measurements of the threshold perturbation produced by superimposing weak magnetic fields on the dipole system have indicated the type of perturbation to be expected during periods of geomagnetic disturbance.

Where comparison may be made, acceptable agreement between the present results and the theoretical analyses of other workers has been found. In confirmation of the earlier work of Bland, discrepancies in the transparency of the penumbra are apparent at latitudes in the range 20° to 30°.

This investigation has revealed longitude-dependent threshold perturbations which are produced by asymmetric magnetic field configurations. These are discussed in relation to the observation of cosmic ray intensity variations.

Finally, evidence is presented which suggests the existence within the model field of a trapped 'radiation belt' of low energy electrons.

INDEX

CHAPTER 1

COSMIC RAYS AND THE GEOMAGNETIC FIELD

1.1 General Introduction

Since the propagation of cosmic ray particles through space depends on the ratio between the Larmor radius of the particles and the scale size of the magnetic fields in their paths, some properties of the interplanetary magnetic field may be deduced by comparing the characteristics of the cosmic ray flux in different energy ranges. Fortunately, the geomagnetic field restricts the access of charged particles to the Earth's surface in such a way that the field may be used as a form of magnetic spectrometer for the particles which have magnetic rigidities of the order 10^9 volts. Therefore, measurements of the latitude variation of the cosmic ray flux provide information on the spatial and temporal variations of the particle flux which is most susceptible to solar influence. Best use of this type of measurement is possible only if the influence of the geomagnetic field is understood adequately. The work to be described in this thesis provides additional information on these geomagnetic effects and on the disturbances which may occur during magnetic storms.

1.2 Historical development

A theoretical study of the motion of cosmic ray particles in the geomagnetic field has revealed the existence of threshold momenta which define the minimum values of particle momentum in the incident primary cosmic radiation at positions on the Earth's surface. These threshold values depend on the zenith and azimuth co-ordinates of the arrival direction. In addition, some momenta which are larger than these threshold values are

not present in the incident radiation because they correspond to trajectories which intersect the Earth at positions remote from the point of observation. By analogy with geometrical optics the range of momenta which contains these forbidden rigidities has been called 'the penumbra'.

Many years ago, comparisons of the latitude distribution of the cosmic ray flux (Clay 1927, Compton 1933) with theoretical predictions (e.g. Lemaitre and Vallarta 1933) indicated the momentum of some of the particles which were contained in the primary cosmic radiation. The sign of the electric charge which was carried by these particles also was revealed by the discovery that the incident flux from the West at any given location was larger than the flux from the East (Johnson and Street 1933).

Following these two discoveries many surveys of the distribution of the cosmic ray flux were made (e.g. Compton 1933, Compton and Turner 1937, Bowen et. al. 1938, Neher et. al. 1953). These showed that although the flux contours follow the general contours of the geomagnetic surface field many large differences occur. Attempts to relate the flux contours to the field contours of an eccentric dipole which had been fitted to the Earth's surface field surveys (Vallarta 1935, Kodama et. al. 1957, Webber 1958) provided fair agreement between the theoretical and experimental flux contours.

Simpson et. al. (1956) and Kodama and Miyazaki (1957) concluded that the differences between these flux contours could be explained in terms of a longitude displacement of the position of the eccentric dipole; however, Marsden and Wilson (1958) showed that an observed distribution of the flux of solar flare radiation was inconsistent with any simple dipole interpretation. The latter observation and measurements of the effects of geomagnetic field anomalies on the flux distribution (Rothwell and Quenby

1958, Sandström 1958, Storey 1959), indicated that the non-dipole field components must be included in the theoretical representation of the geomagnetic field.

Since the theoretical equations are complicated by the introduction of non-dipole terms in the field representation several approximate methods of deriving threshold values have been suggested. Rothwell (1958) has related threshold values to local values of the geomagnetic field strength and dip angle; however, Quenby and Webber (1959) have described a more accurate general method of calculating threshold values which involves a study of the magnetic field line geometry at large latitudes and the assessment of the contribution of the magnetic field terms of order less than six at latitudes less than 20°. Quenby and Wenk (1962) have revised these threshold values and have used the experimental cosmic ray flux contours to relate the thresholds at positions near the equator to the calculated thresholds at the equator where the penumbral effects are known. They illustrate the accuracy of their values by a comparison of the theoretical and experimental distributions of the radiation from three solar flares. Recent experimental results have confirmed the general accuracy of the Quenby - Wenk threshold values (e.g. Pomerantz and Agarwal 1962, du Plooy et. al. 1963) and an analogue computer technique (Bland 1962) has checked the validity of the method.

Several calculations of the threshold rigidities at specific locations have involved the use of digital or mechanical computers to integrate the equations of motion of a particle in a close simulation of the geomagnetic field (e.g. Schwartz 1959, Kasper 1959, Kellogg 1960, Vallarta 1961, McCracken 1962). In general, the differences between these thresholds and

the Quenby - Wenk values are small.

Anisotropies in the primary radiation have been studied by observing the diurnal variation in the counting rate of directional detectors due to the rotation of the Earth. Useful information can be obtained only if the atmospheric effects are eliminated and the deflection of the cosmic ray trajectories in the geomagnetic field is known. Malmfors (1945) and Brunberg and Dattner (1953) have used an analogue computer to determine these trajectory data.

The trajectories of low rigidity particles which arrive at various positions on the Earth's surface have been calculated by several workers (e.g. Firor 1954, Jory 1956, Lüst 1957, Schluter 1958, Kellogg 1960, McCracken 1962, McCracken et. al. 1962). Quenby and Wenk have suggested an approximate general method of estimating the effects of the non-dipole field terms at large latitudes and recently, Webber (1963) has extended this type of approximation by using the single parameter trajectories (nullbahnen) of Schluter to provide a general method for determining the trajectories which reach the Earth at latitudes larger than 45°. Ray (1956) and Webber (1963) have estimated the perturbation of these trajectories by the magnetic field of a magnetospheric 'ring current'.

Since the cosmic ray monitors on the Earth's surface record the secondary particle flux which is produced in cascade nuclear interactions in the atmosphere, it is necessary to obtain a measure of the response of a given detector to primary particles with different energies (e.g. Webber 1962). These response curves and known threshold values may be used to relate the counting rate variations in detectors at different locations on the Earth's surface to changes in the rigidity spectrum of the primary

radiation during solar disturbances.

Although the counting rate of a cosmic ray monitor on the Earth's surface increases if the monitor is moved away from the equator this increase does not continue if the latitude of the monitor exceeds $\sim 60^{\circ}$ because the atmospheric attenuation absorbs the energy of the less energetic particles. This 'air cut - off' phenomenon has been reduced by the use of balloons to carry nuclear emulsions and a variety of electronic instruments to an atmospheric depth of a few grammes per square centimetre. In particular, an instrument which was originally developed by McDonald (1956) may be used to determine parts of the rigidity and charge spectra of the primary radiation at rigidities slightly larger than the local threshold.

The recent use of satellites has provided thresholds which are limited only by instrumental and geomagnetic effects. This method observation also has the advantage that the orbital motion of the satellite may be used to scan the integral spectrum of the primary radiation through the range of geomagnetic threshold values. An assessment of the penumbra at satellite altitudes is important in this respect.

Alternatively, changes in the flux of low rigidity particles during solar disturbances may be detected by observing the variation in the degree of ionisation in the ionosphere. This is usually accomplished by using the riometer technique to measure changes in the ionospheric attenuation of cosmic radio noise (Little and Leinbach 1959, Hultqvist 1962) or by studying the propagation of radio signals (e.g. Bailey 1962).

The use of this wide range of techniques has yielded a wealth of data on the primary rigidity spectrum, its time variations and probable variations in the geomagnetic threshold values.

1.3 Specific problems

a) The penumbra.

The existing data on the latitude variation of the penumbra are restricted to relatively few latitudes and arrival directions. Even at latitudes where the most data are available, the general characteristics of the penumbra which would be 'seen' by a detector with a large angle acceptance cone are difficult to predict. However, Bland's analogue computer (Bland 1962) has provided some information on the average properties of the penumbra which would exist within a small range of angles about the zenith at latitudes less than 30^{o}.

Since the Earth subtends a smaller solid angle at satellite altitudes than at the surface the penumbra should be more transparent at high altitudes. Little information on this effect is available although Bland's results have indicated the type of altitude variation to be expected.

At positions where penumbral effects are large the thresholds may be defined by comparing the integral primary spectrum with the counting rates of detectors of known response. These thresholds depend on the assumed primary spectrum and on the geometries of the acceptance cones of the detectors (e.g. Schwartz 1959). Knowledge of the shapes of the penumbral differential transparency curves (section 5.2) would permit a more detailed study of this relationship.

b) Threshold perturbations.

Many recent observations have indicated that the geomagnetic threshold values have changed during the main phase periods of certain geomagnetic storms (e.g. Webber 1962, Mathews et. al. 1961, Kellogg and Winckler 1961). In addition, there is evidence which suggests that the threshold perturbation

has been a function of longitude during some of the events (Hatton and Marsden 1962). In view of these observations, a knowledge of the way in which superimposed magnetic fields perturb the geomagnetic thresholds might permit the use of cosmic ray data to monitor continuously the magnetospheric distortions and weak interplanetary magnetic fields.

Due to computing difficulties, threshold perturbations have been deduced only for the combination of the geomagnetic field with an axially symmetric 'ring current' (Treiman 1952, Ray 1956) or with a uniform magnetic field which is superimposed parallel to the axis of the dipole (Obayashi and Hakura 1960, Obayashi 1961, Kodama 1959, Quenby 1960). There is no available information on the threshold perturbations which may be produced by asymmetric field configurations although there is no reason to suppose that these configurations are impossible (chapter 9).

1.4 Additional information presented in this thesis

The specific problems which were mentioned in the preceding section may be investigated conveniently by the analogue computer technique. This has been demonstrated by the work of Bland (1962) which involved the use of a scale model of the geomagnetic field to study the penumbra and various perturbations of the threshold values.

A similar technique has been used in the present experiment to obtain data on the penumbra at the Earth's surface and at satellite altitudes. In addition, an analysis of the threshold perturbations which were produced when a uniform magnetic field was applied at various angles to the dipole axis has revealed the existence of significant perturbations which have a complex dependence on longitude, latitude, and field orientation. Other studies have indicated the longitude dependence of the threshold perturbations

which may accompany asymmetric 'ring currents'.

Some evidence which suggests that a trapped electron distribution existed in the model also is presented.

CHAPTER 2

GEOMAGNETIC THEORY

2.1 General

There are two difficulties in the theoretical analysis of the motion of charged particles in the geomagnetic field. The first - a result of the lack of axial symmetry in the magnetic field - is that the variables R, λ , ϕ which represent the radius, latitude and longitude of a point on the trajectory may not be separated. Therefore, the differential equation of motion may not be integrated easily. A simplification which removes this difficulty, is the representation of the geomagnetic field by a dipole. Necessary conditions for the arrival of a particle at a given latitude then may be obtained by analysing the motion in a meridian plane. This method was developed by Störmer in an attempt to explain the auroral phenomenon.

The second difficulty occurs because this method does not include two important conditions - that the co-ordinates of the trajectory must not pass through a value of R which is smaller than one Earth radius before the particle reaches the given point, and that trajectory length in the magnetosphere must not be infinite. These conditions exclude some rigidities which are larger than the Störmer threshold values. This produces the penumbral effects. The forbidden rigidities may be predicted only by computing the individual orbits.

2.2 Störmer theory

In the e.s.u. system of units, the geomagnetic field may be represented by a dipole with a vector potential $\underline{A}$ which is given by :-

$$\underline{A} = \frac{M_e \cos\lambda}{r^2}\,\underline{i}_\phi \qquad \ldots\ldots (2.A)$$

where: $\underline{i}_\phi$ is a unit vector directed to the west,

M_e is the Earth's equivalent dipole moment,

r is the radius from the dipole,

λ is the latitude.

Thus, considering a particle of rest mass m_o, charge Ze, velocity $\underline{v}$, the Lagrangian

$$L = -m_o c^2(1-\beta^2)^{\frac{1}{2}} + \frac{Ze}{c}(\underline{A}\cdot\underline{v}) \qquad \ldots\ldots (2.B)$$

is independent of the longitude co-ordinate ϕ. An inspection of the Lagrangian equation of motion in generalised co-ordinates q_i

$$\frac{\partial}{\partial t}\frac{\partial L}{\partial \dot{q}_i} = \frac{\partial L}{\partial q_i} \qquad \ldots\ldots (2.C)$$

then indicates that, since $\frac{\partial L}{\partial \phi} = 0$, $p_\phi = \frac{\partial L}{\partial \dot{\phi}}$ is a constant of the motion. This equation is integrated (e.g. Fermi 1949) to yield an equation containing the co-ordinates of the motion in a meridian plane:-

$$r\cos\lambda\cos\psi + \frac{M_e}{P_e}\frac{\cos^2\lambda}{r} = \text{constant} \qquad \ldots\ldots (2.D)$$

where: P_e is the particle rigidity ($P_e = \frac{pc}{Ze}$), and

ψ is the angle between $\underline{v}$ and $\underline{i}_\phi$.

It is convenient to render this equation dimensionless by substituting $r = \frac{M_e}{P_e}R$. This is equivalent to expressing length in terms of a new unit $\frac{M_e}{P_e}$ which is called the Störmer unit. The resulting equation is:-

$$R\cos\lambda\cos\psi + \frac{\cos^2\lambda}{R} = 2\gamma = \text{constant} \qquad \ldots\ldots (2.E)$$

Since ψ must be such that $0 \leq |\cos \psi| \leq 1$ for any value of γ, a range of values of R, λ is forbidden. Thus the R plane is split into allowed and forbidden regions. In general it can be shown that, for a dipole field, the allowed region is divided into two parts if $\gamma = 1$. Using this value and putting the conditions $\cos \psi = \pm 1$ into equation (2.D), the loci of the edges of the forbidden regions may be found. Figure (2.1) is a polar plot of the R, λ plane showing the location of the forbidden regions. In this plot the Earth's surface is represented by semicircles about the origin of radius $\frac{P_e}{M_e} r_e$. These have been drawn for various values of rigidity. The intersection of the locus obtained by putting $\cos \psi = 0$ with the semicircle representing the surface of the Earth gives the condition of vertical arrival of the particle at the surface.

Putting $\gamma = 1$ in equation (2.E) and solving for R gives an expression for the threshold rigidity in terms of λ and ψ, i.e. :-

$$P_e = \frac{M_e}{r_e^2} R_e^2 = \frac{M_e}{r_e^2} \left[\frac{1 - (1 - \cos \psi \cos^3 \lambda)^{\frac{1}{2}}}{\cos \psi \cos \lambda} \right]^2 \quad \ldots\ldots \quad (2.E)$$

Since this is independent of zenith angle in the N - S direction there is no predicted asymmetry in this plane.

Putting $\psi = 90^\circ$ and expanding, we have the condition for vertical incidence :-

$$P_e = \frac{M_e}{4r_e^2} \cos^4 \lambda \quad \text{e.s.u.} \quad \ldots\ldots \quad (2.G)$$

$$\text{i.e.} \quad P_e = \frac{75 M_e}{r_e^2} \cos^4 \lambda \simeq 14.9 \cos^4 \lambda \quad \text{G.V. (practical units)} \quad (2.H)$$

Alternatively, ψ may be found as a function of the rigidity at a given

latitude. This locates the boundary of the Störmer cone of allowed trajectories which opens towards the west.

From figure (2.1) it is seen that the radius of the equatorial pass between the inner and outer allowed regions is one Störmer unit. Since from equation (2.G) the radius of the Earth in these units is $R = (1/2)\cos^2\lambda$, the radius of the pass in units of one Earth radius is $2/\cos^2\lambda$. Hence:-

$$r_j = \frac{2r_e}{\cos^2\lambda}. \qquad \ldots\ldots (2.J)$$

2.3 Modifications to Störmer theory - the penumbra

The theory outlined in the preceding section imposes no restrictions on the type of trajectory described by the particle prior to the arrival at the point of observation. In particular the trajectory may pass through a value of radius which places it below the Earth's surface. This type of trajectory must be forbidden (Vallarta 1938). Additional trajectories are asymptotic to periodic orbits in the dipole field (Lemaitre 1935). These describe a path length in the dipole field which tends asymptotically to infinity for certain values of rigidity.

These additional rigidities occupy the region between the Störmer threshold and a rigidity of the order 20% greater than this. Information on the subject is obtained from the step-by-step integration of orbits using the two boundary conditions - that the minimum orbit radius is greater than the radius of the Earth and that the orbit traverses the equatorial pass before a given number of minima in radius occurs. This rejects trajectories which are obscured by the Earth and also those which are asymptotic to the periodic orbits of Vallarta. It is reasonable to reject the latter owing to the high probability of collision or scatter of the cosmic ray particle in

the residual magnetospheric plasma.

The penumbral effects which are observed at a given latitude may be represented by diagrams which indicate the allowed values of rigidity for certain combinations of zenith and azimuth arrival directions at the Earth (figure 2.2). Since the structure of these diagrams varies considerably with the arrival direction, the penumbra which is 'seen' by a cosmic ray telescope with a finite angle acceptance cone must be deduced by an averaging process. For this purpose the most convenient diagram would indicate the percentage of allowed trajectories within the acceptance cone as a function of rigidity.

Curves which provide this information have been obtained from an analogue computer by Bland (1962). Alternatively, approximate curves may be deduced from line trajectory diagrams similar to figure (2.2) by averaging the transparency over a range of rigidity which corresponds to the limits of threshold in the acceptance cone. The result of performing this process for an averaging interval of 0.5 G.V. is indicated in figure (2.2). This represents the use of a 10° acceptance cone at latitude 30°.

Lemaitre and Vallarta (1936 a,b) investigated the limits of the penumbra in detail and expressed their results in terms of an allowed 'main cone' by analogy with the Störmer method. Since this 'cone' has an irregular cross - section in the meridian plane their calculation predicts the asymmetry of the radiation flux in this plane which is observed at the Earth's surface (Lemaitre and Vallarta 1936 a). All the trajectories which arrive within the 'main cone' are allowed.

These investigators also demonstrated the existence of an irregular 'shadow cone' between the Störmer and main cones. The trajectories which arrive between the Störmer and shadow cones are simple forbidden trajectories

which pass through one minimum in radius below the surface of the Earth. The shadow cone has been studied by Schremp (1938) but Kasper has obtained further information which has modified Schremp's shadow cone geometry (Kasper 1959). Kasper demonstrates that the shadow cone coincides with the main cone at small and medium latitudes provided that the arrival direction of the trajectory is near the zenith. The region between the shadow cone and the main cone contains complicated trajectories which pass through many minima in radius, some of which may lie below the surface of the Earth. Hence this region contains several groups of allowed or forbidden trajectories.

The early penumbral calculations of Lemaitre and Vallarta (1936 a,b.), Bouckaert (1934) and Hutner (1939) have been extended by Schwartz (1959) who has assessed the transparency of the penumbra as a function of latitude.

2.4 Perturbation of the dipole threshold rigidities by non-dipole terms

If non-dipole terms are included in the vector potential (equation 2.A), the Lagrangian is a function of ϕ and an equation similar to (2.D) cannot be obtained by simple integration. Störmer thresholds may be calculated by using a digital computer to perform a numerical integration.

Quenby and Webber have introduced an alternative method which provides approximate values of the Störmer thresholds in the geomagnetic field (Quenby and Webber 1959). When the equatorial pass is relatively near the Earth (figure 2.1) distortions in the dipole field near the pass are significant. Quenby and Webber allow for this distortion by introducing a dipole moment which is a function of the geomagnetic horizontal field strength and dip angle at the point where the threshold is required. They use this modified dipole moment for M_e in equation (2.G) to obtain the approximate Störmer thresholds.

Since there is no penumbra near the zenith at the equator the Quenby - Webber thresholds at this position should equal the experimental thresholds. Quenby and Wenk (1962) use this assumption to derive more accurate thresholds for stations at latitudes less than 20° by comparing the cosmic ray flux at these stations with the flux at various longitudes on the equator. This avoids the errors which might be introduced by the use of inaccurate penumbral corrections to obtain experimental thresholds from the Quenby - Webber thresholds at latitudes between 10° and 20°.

Quenby and Webber use a different approximation at latitudes larger than 30° because the pass is removed sufficiently from the Earth's surface for the high order field terms to make a negligible contribution to the field at the pass. They notice that particles with rigidities near the threshold describe close spirals round the field lines near the Earth. Since these field lines are displaced, by the high order terms, from the dipole line which would cross the equator at the same geocentric radius, Quenby and Webber assign an effective latitude to the point of contact of the geomagnetic field line with the Earth's surface which is equal to the latitude of contact of the dipole line.

Quenby and Wenk (1962) have used the field line calculations of Hultqvist (1958) to identify the effective latitudes more precisely. In addition, they have incorporated the penumbral corrections of Schwartz (1959).

Other workers have used the guiding centre approximation (Alfvén 1950) to describe the motion of the particles near the Earth and have combined this with the Störmer treatment. In this way directions of arrival at the surface of the Earth were related to the directions of arrival at a 'transition radius' from the Earth. At larger radii the geomagnetic field has been

represented as a dipole. This approach has been used to obtain information on the Störmer threshold values (Sauer 1963, Sauer and Ray 1963, Ray 1963) and on the asymptotic trajectories at latitudes larger than $\sim 40^{\circ}$ (Webber 1963). It has been shown that the contours of constant threshold are related to the contours of constant 'L' (McIlwain 1961) if this parameter is evaluated at the position of the guiding centre of the particle (e.g. Ray 1963).

2.5 The theoretical effects of external magnetic fields

Although these calculations involve the use of a vector potential which represents the combination of the external field with the geomagnetic field a dipole representation of the latter must be used to provide a Lagrangian which is longitude invariant. However, a difficulty occurs in the calculation because if the vector potential represents a 'ring current' or a uniform field which is parallel to the geomagnetic axis the integration constant 'γ' in equation (2.E) is a function of the field strength and ring radius. A solution may be obtained only by graphical or numerical analysis. The theoretical data which are available for these two field configurations may be summarised :-

A) Ring current effects.

Treiman (1952) represents the 'ring current' by a spherical current sheath which is concentric with the Earth and has a current density which is proportional to the cosine of the latitude. This system produces a magnetic field which is parallel to the geomagnetic axis within the sheath; however, the field everywhere outside the sheath is that of a dipole. The vector potential which is used in equation (2.A) represents the sum of two dipole fields if the equatorial pass is situated outside the sheath or the sum of a dipole field and the above uniform field if the pass is within the sheath. The threshold perturbations at large latitudes correspond to a reduced dipole moment of the

geomagnetic field while the perturbations at the smaller latitudes are those which would be produced by superimposing a uniform magnetic field parallel to the geomagnetic axis.

Ray has calculated the perturbations which would be produced by an equatorial filamentary ring current. This required the use of a vector potential which contained elliptic functions. Ray's curves indicate the perturbed threshold rigidities as a function of latitude for several values of ring radius and current strength.

The calculations of both Ray and Treiman indicate that the equatorial pass is distorted by the ring current field to produce two pass regions (figure 2.1) which impose different restrictions on the entry of particles to the inner allowed region. Since the threshold effect is controlled by the inner pass at small latitudes and by the outer pass at large latitudes the two parts of the curve of threshold as a function of latitude join with a rapid change of slope (figure 2.4).

In addition to the longitude drift of charge which was considered in the above approximations, the spiral motion and latitude oscillation of the 'ring current particles' contribute to the magnetic field of a real trapped particle system. Akasofu, Cain and Chapman (1961) also Apel, Singer and Wentworth (1962) have considered these effects and by using an interation procedure, have made some allowance for the distortion of the trapping field which is produced by the presence of the particle system. Although these authors disagree on the details of the effects which would be produced by the presence of a large energy density of trapped particles their predictions are similar for small energy densities.

The field line plot of Akasofu et. al. indicates that the geometry of the field of the 'ring current' is approximately the mean of the field geometries

of Ray and Treiman. Therefore, if the theoretical field of Akasofu et. al. is a fair approximation, the field of a real trapped particle system probably produces the threshold perturbations which are represented in figure (2.4) by the dash curve.

In the construction of figure (2.4) data for the filamentary approximation were obtained from Ray's paper; however, Treiman's method of solving the equations which contain a vector potential term to represent a uniform field could not be used for superimposed field strengths of 150 γ at a latitude $\sim 50^{\circ}$. Thus the line which represents the Treiman approximation at the larger latitudes has been joined smoothly to the line which represents the predictions of the method of numerical solution (Appendix A).

Since the 'ring current' produces threshold perturbations which are a function of the dipole moment of the 'ring current' at large latitudes but are a function of both the dipole moment and the radius of this current at small latitudes (Kellogg 1961) the geometry of the 'ring current' may be deduced from a knowledge of the latitude dependence of any real perturbations.

B) Uniform field effects.

Several authors have determined the threshold perturbations which are produced by superimposing uniform magnetic fields parallel to the geomagnetic axis.

Rothwell (1958) and Kodama (1959) have obtained approximate expressions for the threshold perturbations which are valid for small field strengths and latitudes. A similar result may be obtained from Treiman's calculations by placing the equatorial pass within the current sheath.

Obayashi and Hakura (1960) also Obayashi (1961) have obtained a more rigorous solution of an equation which corresponds to the Störmer equation (2.E) but contains an additional term to represent the uniform magnetic field.

They have demonstrated that the thresholds are reduced to zero at latitudes larger than a minimum value which is a function of the superimposed field strength.

Recently Quenby (1960) has used a numerical method of solution of the Störmer equation which is valid for all latitudes and field strengths to obtain the perturbed threshold values (Appendix A). This method was used to deduce the latitude dependence of the threshold perturbations which are produced by superimposing a 150 γ uniform field antiparallel to the geomagnetic equatorial field. Since this field strength is produced at the Earth's surface by the ring currents which are represented in figure (2.4) the results of the above calculation and of Quenby's similar calculation for a 20 γ field (Quenby 1960) have been included in figure (2.4) for comparison.

Quenby and Obayashi, independently, have calculated similar values for the latitude at which the threshold is reduced to zero as a function of the strength of the uniform magnetic field which is superimposed antiparallel to the geomagnetic equatorial field. These results (figure 2.5) indicate that if the average interplanetary magnetic field is of the order 3 - 5 γ near the orbit of Earth, the thresholds would be zero at latitudes larger than $\sim 75^{\circ}$ if this field penetrates the magnetosphere. This will be discussed further in Chapter 9.

Obayashi and Hakura also have shown that the geomagnetic field is confined within a cavity if a uniform magnetic field is superimposed antiparallel to the geomagnetic equatorial field. This observation is deduced from the fact that the tangential field component is zero on a spherical surface which is concentric with the geomagnetic field for this field configuration.

Since a plasma with large electrical conductivity exists in the

magnetosphere and in interplanetary space the application of these theoretical results to the real geomagnetic field requires care. This is discussed in Chapter 9.

2.6 Summary

In this review of geomagnetic theory a method of calculating the Störmer thresholds for a dipole field and for combinations of a dipole field with simple axially symmetric fields has been indicated. The effects which are produced by non - axially symmetric fields cannot be determined from the Störmer equation in a simple way however.

The analysis of the penumbra is complicated even for a simple dipole field. Few quantitative details of the penumbra 'seen' by a wide angle cosmic ray telescope are available. Theoretical information may be obtained only by the extensive use of fast digital computers.

Thus, while the geomagnetic theory is able to predict the general distribution of the cosmic ray flux, there are many details which are only partially understood.

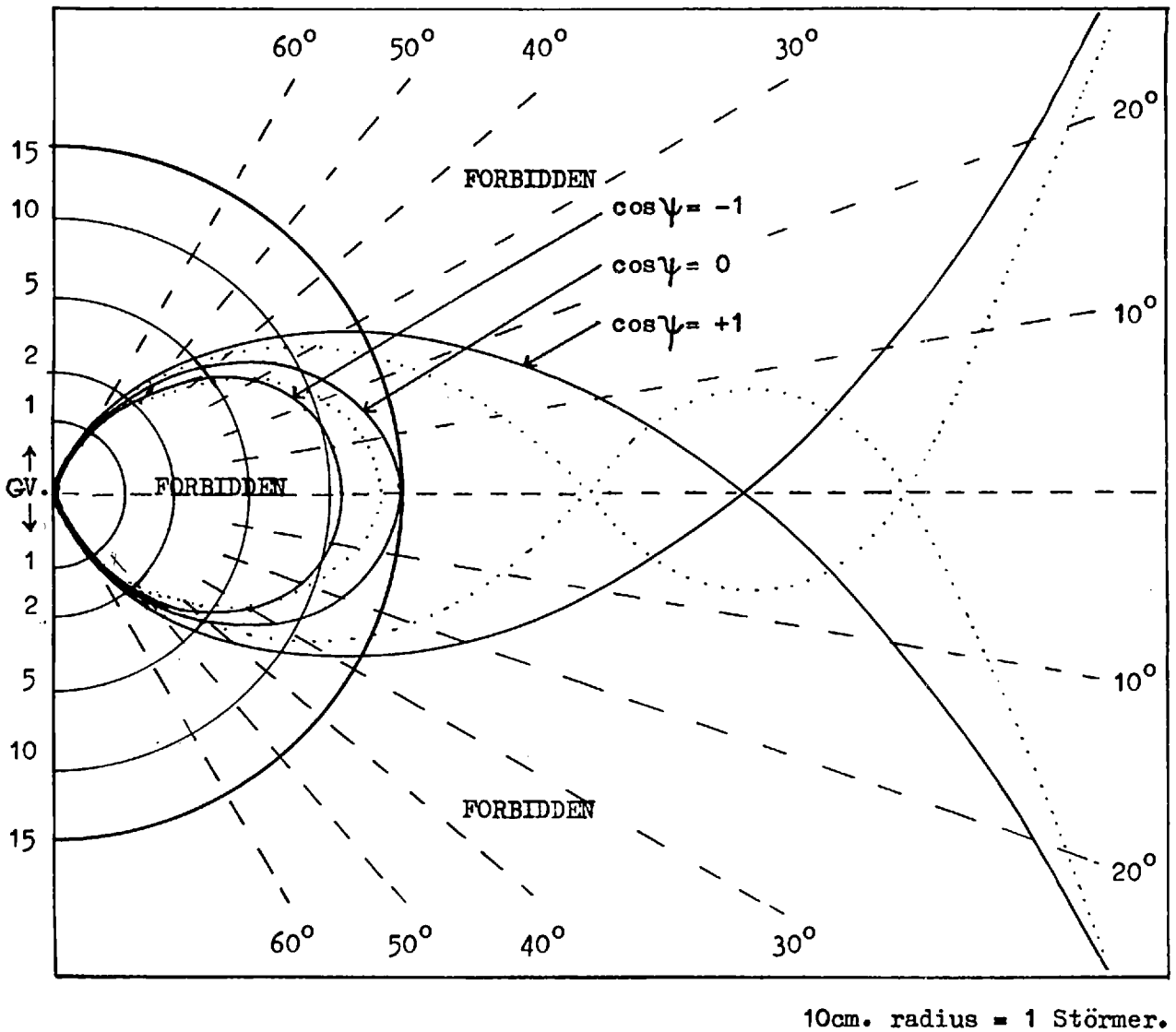

Figure 2.1 A meridian plane polar diagram of the Störmer allowed and forbidden regions for a dipole field. The semicircles about the origin represent the radius of the Earth for the given rigidities. The dotted curve illustrates the type of distortion produced by a 'ring current'; however, the shape of the curve is a function of the particle rigidity, the 'ring' radius and the 'ring current' amplitude in this case.

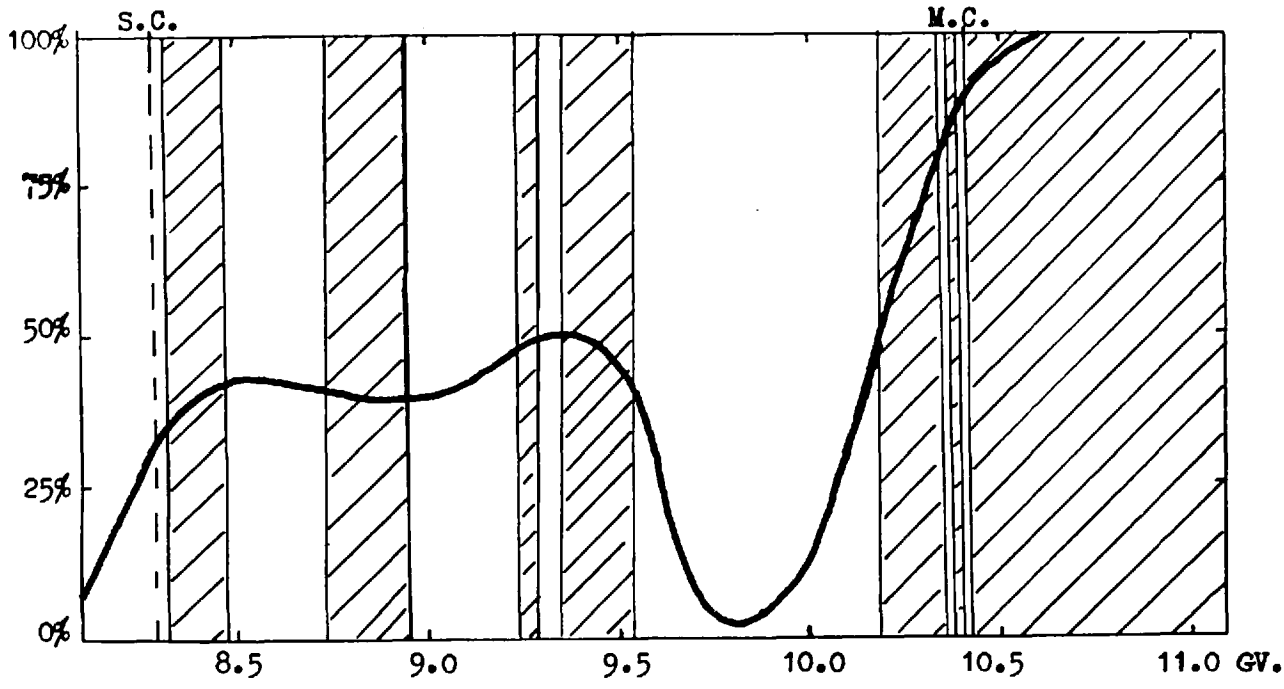

Figure 2.2 Differential transparency of the zenith penumbra at latitude $\lambda = 30^{\circ}$ as a function of rigidity. The hatched areas are the allowed regions of Schwartz. The curve is obtained by averaging the Schwartz transparency over a rigidity interval of 0.5 GV. representing an acceptance cone angle of $\sim 10^{\circ}$.

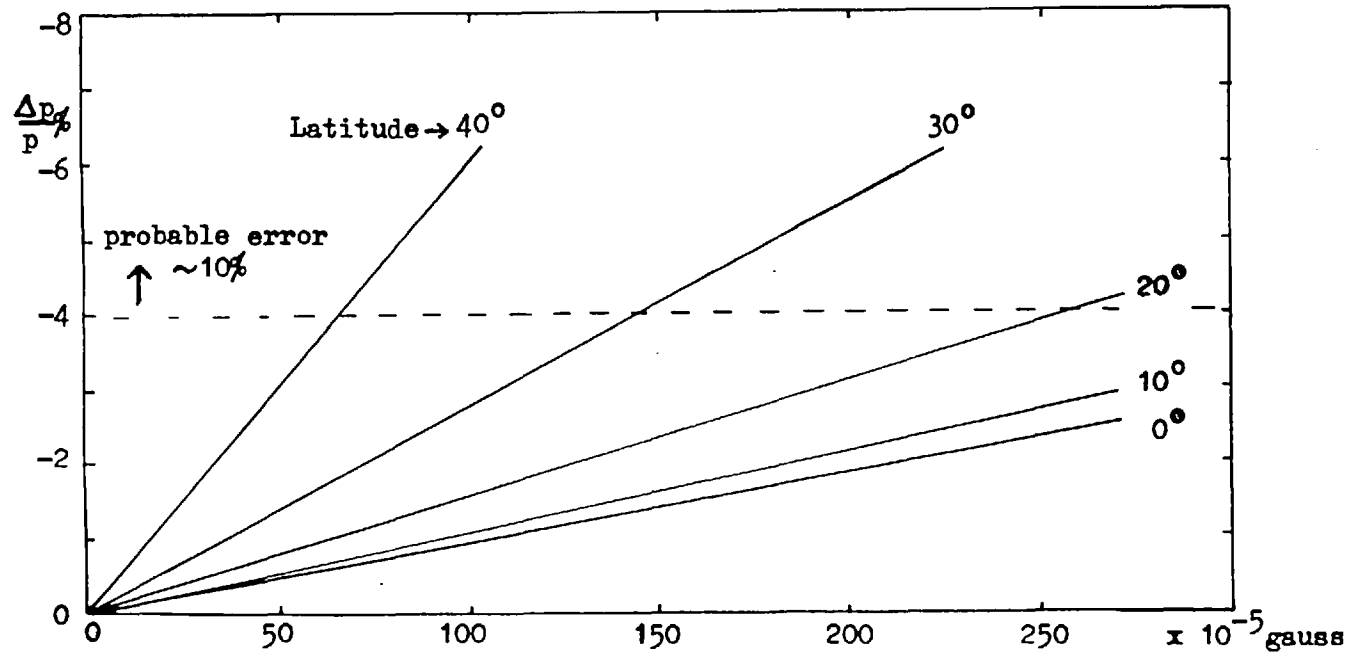

Figure 2.3 The percentage decrease of threshold as a function of field strength for a uniform field antiparallel to the geomagnetic equatorial field.

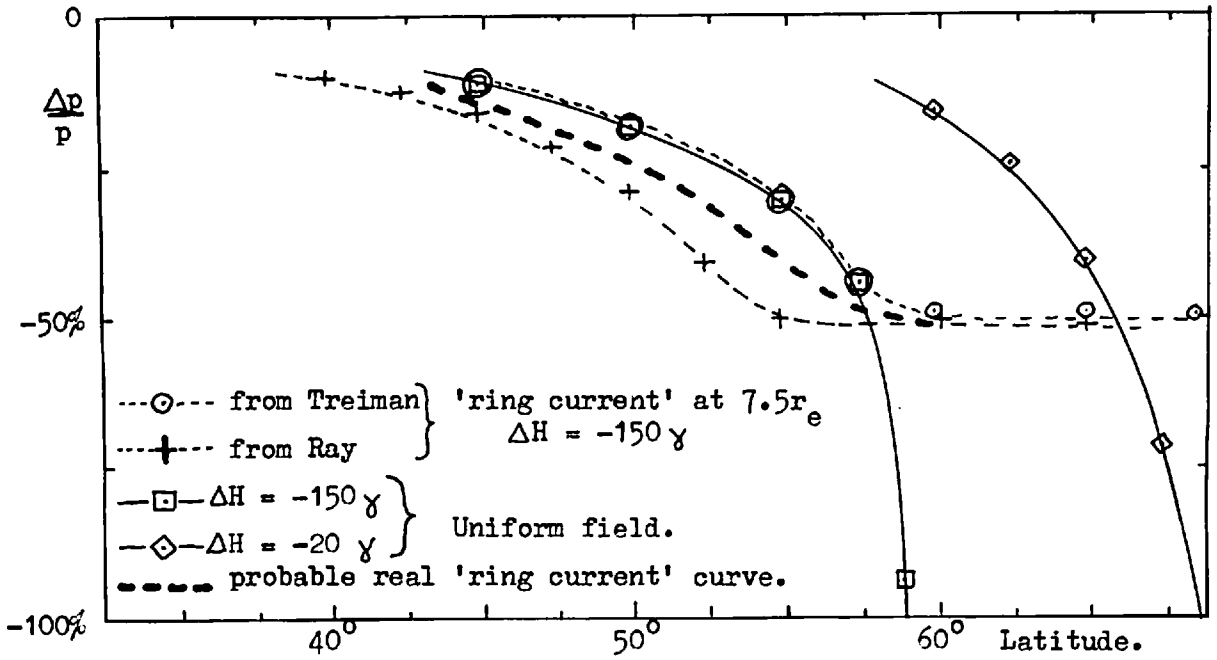

Figure 2.4 Percentage threshold reduction as a function of latitude produced by a uniform field parallel to the dipole axis and by two theoretical approximations to the field of a geomagnetic trapped particle system. The expected curve for the real particle system is indicated.

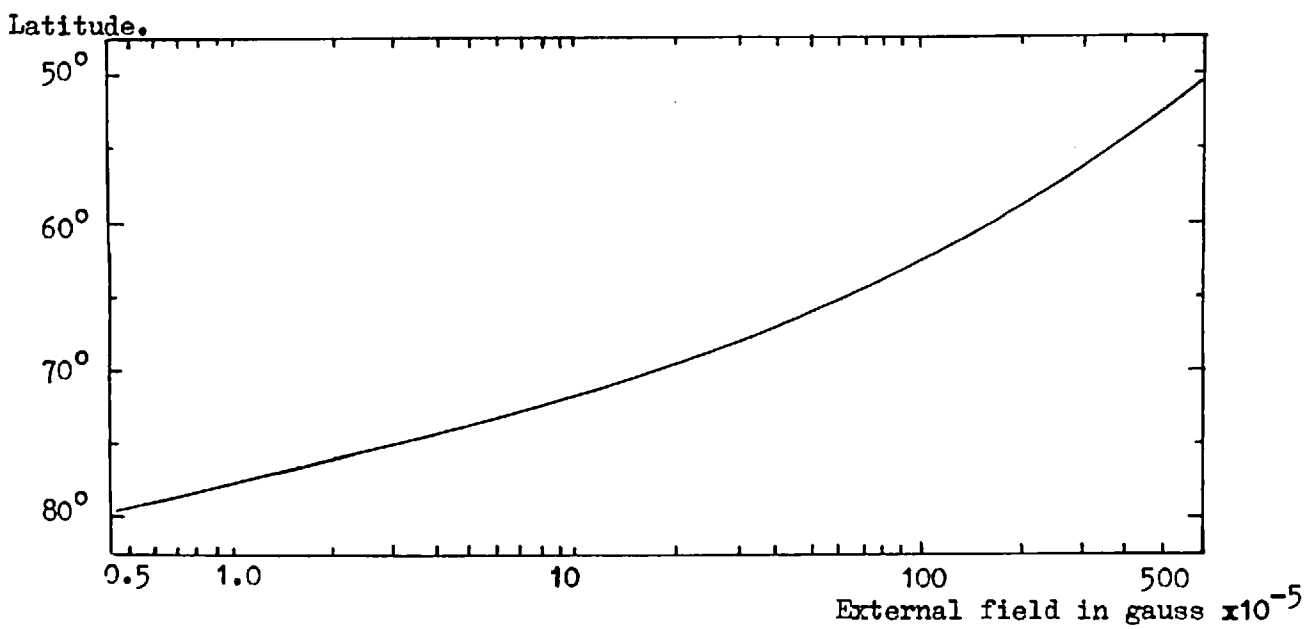

Figure 2.5 Minimum latitude of zero threshold as a function of the strength of the superimposed field for a uniform field antiparallel to the geomagnetic equatorial field.

CHAPTER 3

A REVIEW OF THE APPLICATION OF MODEL TECHNIQUES IN THE STUDY OF CHARGED PARTICLE MOTION IN THE GEOMAGNETIC FIELD

3.1 Introduction

In view of the difficulty of calculating the trajectories of charged particles in a magnetic dipole field it is not surprising that the first information on this subject was obtained by the laboratory use of scale models (Birkeland 1901). These experiments initiated Störmer's theoretical work which was reviewed in the preceding chapter. Several other experiments have yielded information on these trajectories.

3.2 The previous model experiments

Birkeland (1901) investigated the visible structure of a glow discharge near a model dipole field which was generated by a small spherical electromagnet. The electromagnet was placed in a vacuum tank between two plane electrodes and the gas pressure in the apparatus was adjusted to produce a diffuse electric discharge between these electrodes. A comparison of the geometry of the glow discharge which was visible near the poles of the model with auroral data which had been collected by the Norwegian Aurora Polaris Expedition of 1899 lead Birkeland to associate the aurora with the impact of charged particles in the upper atmosphere.

More recently, Block (1955, 1958) has performed similar experiments and has demonstrated the validity of the scaling factors which are used in this work (Block 1956). Photographs of the glow discharge near the model were compared with the records of all-sky cameras at various positions on the Earth's surface (Block 1958).

Villard (1906) obtained luminous trajectories by directing the filamentary beam of an electron gun through the field of an electromagnet which was placed in a vacuum tank. The gas focusing action which was used in early cathode ray tubes maintained the filamentary nature of the electron beam over a long path length. Although Villard's magnetic field differed significantly from a dipole field some of the visible trajectories were very similar to the simple theoretical dipole trajectories (Störmer 1907).

Bruche (1931) repeated the above experiment with an improved dipole field and found very good agreement between the experimental and theoretical orbits. Bruche also investigated an electric discharge of the Birkeland type and demonstrated that a westward flowing equatorial 'ring current' in the outer part of the model field decreased the latitude of the model 'auroral zone'.

The first quantitative investigation of the trajectories of particles which simulated cosmic rays was performed by Malmfors (1945). Later, this apparatus was modified by Brunberg and Dattner (1953) to permit trajectory measurements over an appreciably larger range of rigidities. Both experiments used an electron gun near the surface of the model to produce a filamentary electron beam; however, Brunberg and Dattner obtained a more flexible system by replacing Malmfors' spherical permanent magnet with an electromagnetic fluxball (Brown and Sweer 1945). Cosmic rays of various energy could be simulated by varying either the electron energy or the dipole moment of the model. These two experiments have provided data on the asymptotic trajectories of cosmic ray particles with energy between 10^9 and 10^{12} eV for a large range of latitudes and arrival directions.

Recently, Bennett (1958) has directed the filamentary beam of an electron gun towards a model dipole field which was generated by a small permanent

magnet. The pressure of the mercury vapour in the apparatus was adjusted to produce visible line trajectories which were photographed. Cosmic ray particles with $\sim 10^9$ eV energy were simulated.

Bland (1962) performed the first experimental investigation of cosmic ray threshold rigidities with a model which resembled the Brunberg - Dattner model. The threshold was measured at each latitude and longitude by determining the minimum rigidity at which the electrons were able to reach the walls of the vacuum tank. This is the practical analogue of the procedure which is used when threshold rigidities are calculated by the machine integration of the equation of motion (Lemaitre and Vallarta 1936 , McCracken 1962). Measurements of the electron currents in the system indicated when the electrons escaped from the model field. This experiment was the first to represent the geomagnetic field to a better accuracy than a dipole and provided a verification of the Quenby - Webber method of calculating threshold rigidities.

3.3 The present experiment

Bland's model geometry and method of observation were used to investigate the changes in theshold rigidity which were produced when additional magnetic fields were superimposed on the model dipole field. These additional fields were inclined at various angles to the dipole axis and the simulation of a geomagnetic 'ring current' was attempted.

Alterations were made to Bland's original design. The electron gun was recessed in the surface of the model to permit the observation of the penumbra from a position on the surface. The penumbra also was observed at a simulated altitude of 1100 km. Changes in the size and dipole moment of the model increased the maximum latitude at which thresholds could be observed to 57° and automation was introduced to facilitate the rapid accumulation of data.

3.4 The scaling equations

In order to produce a valid model the electrons must simulate cosmic ray particles which have atomic mass. Therefore it is necessary to equate the simulated cosmic ray rigidity to measurable quantities in the model system.

The Störmer theory (section 2.2) indicates that:-

$$R_e = \frac{.75\, M_e}{r_e^2} \cos^4 \lambda$$

where 'R_e' is the zenith threshold rigidity in 10^9 practical volts at latitude λ and 'M_e', 'r_e' are the dipole moment and radius of the Earth in C.G.S. units. Thus, if the subscripts 'e' and 'm' are used to denote the corresponding quantities in the Earth and model systems, at any latitude:-

$$\frac{R_e}{R_m} = \frac{M_e}{M_m} \left(\frac{r_m}{r_e} \right)^2 \qquad \ldots\ldots \quad (3.A)$$

It is assumed that magnetic fields which have a non-dipole origin and electric fields are absent in both systems. The importance of stray fields in the model is discussed in the following section; however, it will be assumed that equation (3.A) is valid for the real geomagnetic field if the 'effective latitudes' are used.

The electrons in the model have a momentum 'p' which is given by:-

$$p = \frac{1}{c} \left\{ (eV)^2 + 2\, m_o c^2\, eV \right\}^{\frac{1}{2}}$$

where, in C.G.S. units, 'V' is the electron accelerating voltage, 'e' and 'm_o' are the electron charge and rest mass, 'c' is the velocity of light and 'p' has units of eV/c. Now, for $V < 5$ e.s.u., $(eV)^2 \ll 2\, m_o c^2 eV$. Thus the electrons are non relativistic and to adequate accuracy:-

$$pc = (2\, m_o c^2\, eV)^{\frac{1}{2}}$$

Hence the electron rigidity in practical volts is:-

$$R_m = 300 \frac{pc}{e} = (1.01 \times 10^3) V^{\frac{1}{2}} \qquad \ldots\ldots \quad (3.B)$$

If equation (3.B) is substituted into equation (3.A) :-

$$R_e = 200 \frac{r_m^2 V^{\frac{1}{2}}}{M_m} \qquad \ldots\ldots \quad (3.C)$$

where 'R_e' is the simulated cosmic ray rigidity in units of 10^9 practical volts, 'V' is the electron accelerating voltage in practical units and the following values of the Earth's dipole moment and radius have been used:-

$M_e = 8.1 \times 10^{25}$ gauss cm^3. (Finch and Leaton 1957)

$r_e = 6.4 \times 10^8$ cms.

The selection of suitable practical values of 'r_m', 'M_m' and 'V' will be discussed in section (4.2).

3.5 The importance of stray magnetic and electric fields

In order to investigate the threshold perturbations which are produced by 50 γ fields on the geomagnetic scale the maximum stray field amplitude must be less than approximately 5 γ. Since the equatorial field of the model is approximately 300 times larger than the geomagnetic equatorial field the stray field strength must be less than 0.015 gauss. The degaussing system which will be described in section (4.6) fulfilled this condition.

The importance of stray electric fields may be assessed by Block's method (Block 1956):-

The equation of motion of a particle of mass 'm', charge 'e' and velocity 'v' in an electric field '$\underline{E}$' and magnetic field '$\underline{B}$' is:-

$$m \frac{d\underline{v}}{dt} = e\underline{E} + e(\underline{v} \wedge \underline{B}) \qquad \text{—— gaussian units.}$$

If the characteristic length 'λ', time 'τ', voltage 'ϕ', magnetic field strength 'β' and mass 'm' are used this equation becomes:-

$$\frac{m\lambda}{e\tau^2} = \frac{\phi}{\lambda} + \frac{\lambda}{\tau}\beta$$

The introduction of the scaling factors k_λ, k_τ, etc. in this equation

yields:-

$$\frac{m\, k_m \lambda\, k_\lambda}{e\, \tau^2\, k_\tau^2} = \frac{\phi\, k_\phi}{\lambda\, k_\lambda} + \frac{\lambda\, k_\lambda}{\tau\, k_\tau}\, \beta\, k_\beta$$

Thus, correct scaling of the particle trajectory is achieved if:-

$$\frac{k_m\, k_\lambda}{k_\tau^2} = \frac{k_\phi}{k_\lambda} = \frac{k_\lambda\, k_\beta}{k_\tau}$$

i.e.:-

$$k_\phi = \frac{(k_\lambda\, k_\beta)^2}{k_m}$$

Now if the stronger magnet is used in this experiment:-

$$k_\lambda = \frac{r_m}{r_e} = 7 \times 10^{-9}$$

$$k_\beta = \frac{H_m}{H_e} = 7 \times 10^{-2}$$

$$k_m = \frac{\text{electron mass}}{\text{proton mass}} = 5 \times 10^{-4}$$

(taking protons of 10^9 eV kinetic energy)

Thus a field of 1 volt / cm. simulates a field of the order 100 MV / Earth radius in the magnetosphere. Experiments were performed to determine the threshold perturbations which were produced by these small electric fields (section 4.8).

CHAPTER 4

THE DESIGN OF THE EXPERIMENT

4.1 General

The construction of suitable electron guns and the choice of the magnetic dipole moment and radius of the model were the two most serious difficulties in the design of the experiment. These problems and their solution are discussed at length since they determine the range and accuracy of the threshold measurements which may be attempted.

The experiment was performed in a existing vacuum tank which was equipped with pumps and degaussing coils. Since these components have been discussed in detail elsewhere (Bland 1962) they will be described here in outline only.

The latitude range of the measurements was restricted by the size of the vacuum tank; however, since the maximum latitude of observation could be increased from $\sim 60^{\circ}$ to $\sim 70^{\circ}$ only by increasing the linear dimensions of the tank by a factor of at least three, the dimensions of the present system are a reasonable compromise.

4.2 The design of the model

In order to observe threshold effects by detecting the escape of electrons from the model field the inner Störmer allowed region must be contained within the vacuum tank. Since the radius of this trapping region increases with the latitude of the electron gun (section 2.2) the radius of the model must be chosen to contain this region within the tank walls at the maximum latitude of observation. If the substitutions $r_t = r_j$ and $r_m = r_e$ are made in equation (2.J) this condition may be stated:-

$$r_m = \frac{r_t \cos \lambda_m}{2} \qquad \ldots\ldots \quad (4.A)$$

where r_t , r_m are the radii of the tank and model respectively.

A second practical limitation may be found by inserting this condition in the general scaling equation (3.C). Thus if R_e is replaced by the zenith Störmer threshold at λ_m :-

$$3 M_m = 10 r_t^2 V^{\frac{1}{2}} \qquad \ldots\ldots \quad (4.B)$$

Since the electron gun is 0.7 cm. long and there must be a 0.3 cm. gap between the magnet and the electron gun to allow for the presence of the magnet holder, the radius of the magnet must be at least 1 cm. smaller than the radius of the model. Therefore the maximum dipole moment of the magnet is:-

$$M_m = I \frac{\alpha}{6} (r_t \cos^2\lambda_m - 2)^3 \qquad \ldots\ldots \quad (4.C)$$

whence if this value is used in equation (4.B) :-

$$I = \frac{20 r_t^2 V^{\frac{1}{2}}}{(r_t \cos^2\lambda_m - 2)^3} \qquad \ldots\ldots \quad (4.D)$$

Subsidiary experiments indicated that the electron gun operated satisfactorily at voltages larger than approximately 30 volts (section 4.3). Therefore since r_t = 35 cm:-

$$I = \frac{42600}{(35 \cos^2\lambda_m - 2)^3} \qquad \ldots\ldots \quad (4.E)$$

This equation is plotted in figure (4.1). It will be noticed that 'I' must exceed $\sim$140 to permit threshold measurements at latitudes $\sim 60^\circ$.

Since a sufficiently strong steady magnetic field cannot be produced by an electromagnet at a convenient power dissipation the possibility of using a permanent magnet was investigated.

Rough calculations indicated that spherical samples of the Mullard materials 'Magnadur 2' or 'Ticonal G' should have intensities of magnetisation larger than 100 gauss. Although a spherical magnet of 'Magnadur 2' would

have the larger intensity of magnetisation, spherical samples of this ceramic material could not be obtained. Since 'Ticonal G' (an anisotropic metallic alloy) may be cast and ground by normal metal techniques two rough cast spheres of this material were obtained. These exhibited an intensity of magnetisation of approximately 110 gauss which would permit threshold measurements at a maximum latitude of approximately 59^{o} (figure 4.1). The use of this value of λ_m in equation (4.A) reveals that the radius of the model should be 4.65 cms. After the magnets were ground to the correct profile and the model was constructed the following values were obtained:-

$r_m = 4.58$ cms. $\qquad M_m = 21000$ gauss cm^3

$\lambda_m = 59^{o}$ $\qquad I = 110$ gauss

Unfortunately, if a single permanent magnet were used cosmic ray rigidities between 1 G.V. and 15 G.V. could be simulated only by varying the electron accelerating voltage between 30 and 6000 volts. Since the latter voltage was too large to apply to the electron guns which were used in this experiment at least two magnets were required. Satisfactory operation was achieved with two magnets which had dipole moments of 10^4 gauss cm^3 and 2×10^4 gauss cm^3. This limited the electron gun voltages to values between 30 and 1300 volts.

The geometry of the model is illustrated in figure (4.3). The model was suspended from the top of the vacuum tank by a stem which consisted of two concentric brass rods. The inner rod supported the magnet which was held in a brass ring while the outer rod supported the shell of the model on an insulating bush of 'Fluorosint'. Both rods could be rotated independently from the outside of the tank. During the threshold measurements the latitude of the gun was altered by rotating the shell of the model. This maintained

the magnet stationary relative to the external magnetic fields.

A flange on the body of the electron gun permitted the location of the gun at a known radius in the recess in the shell of the model. Thin brass rings were placed under this flange to adjust the altitude or direction of fire of the gun.

The possibility of mounting the axis of the magnet perpendicular to the stem was investigated since this geometry involves the simplest latitude adjustment. Unfortunately the threshold observations were seriously disturbed by the passage of the stem through the Störmer inner allowed region. Large distortions appeared in the differential transparency curves and the stem collected a large fraction of the electron beam current. Since the disturbance was insensitive to the longitude of the gun relative to the stem this effect demonstrates the complexity of the trajectories near the threshold.

Intersections between the stem and the allowed regions were avoided by mounting the magnetic axis of the model either parallel or at a small angle to the stem. In each series of measurements the choice was determined by the relative importance of maintaining either an easy latitude adjustment or a given aspect of the magnet with respect to external magnetic fields. During the observation of threshold effects the stray current which reached the stem was monitored to verify the absence of disturbances.

4.3 A survey of the model magnetic field

The type of magnetometer which was used to survey the field of the model has been described by Gregg (1947). This instrument has the following advantages:-

a) Since a null technique is used to determine the unknown field strength the

calibration is independent of temperature or changes in the electronic gain of the apparatus.

b) The probe measures the average value of the magnetic field in a cylinder 5 mm. long by 0.25 mm. diameter. Although the length of the probe was equivalent to 6° of latitude at the surface of the model the latitude range of a given measurement was reduced to a fraction of a degree by measuring the radial field component. This was essential for the detection of small local anomalies in the field.

c) The directional properties of the probe permit independent measurements of the field components. A check indicated that the calibration and zero stability of the probe were unaffected by the presence of strong fields transverse to the axis of the probe.

d) The accuracy of the instrument is of the order $\pm$ 3% or 1 gauss. There is also a possible systematic error of the same amplitude which is produced by errors in the construction of the calibration solenoid, in the measurement of the current in the calibration solenoid and in the location of the probe during the calibration.

The fields of both magnets were measured at 10° intervals on two orthogonal great circles. A perspex jig ensured correct alignment of the probe for the measurement of the three field components near the surface of the model. The maximum value of the E - W component was less than 0.5% of the polar radial field strength for both magnets. Since this was approximately equal to the residual noise level of the instrument the existence of an E-W component has been neglected.

A polar great circle survey of the radial field component of the weaker magnet is shown in figure (4.4). No significant departure from a dipole

field is apparent. Similar agreement between the experimental points and a sine curve was obtained in other surveys which were performed at different longitudes. It was concluded that any departure of the field of the weaker magnet from that of a dipole was too small to detect with the magnetometer.

No significant asymmetries were revealed in the later analysis of the threshold values which were obtained with this magnet at many positions on the surface of the model. Since the latter test is sensitive to variations of the order $\pm 1^{o}$ in effective latitude it is more sensitive than the magnetic survey for detecting the presence of magnetic anomalies.

Although the magnetometer failed to reveal irregularities in the field of the stronger magnet the distribution of threshold rigidities indicated that the effective latitude changed by approximately $\pm 2^{o}$ with longitude at latitudes larger than 45^{o} (section 6.2). These field distortions could have been produced by the more irregular surface of the stronger magnet. The existence of this asymmetry in the distribution of effective latitudes proved to be useful in the analysis of section (10.3).

4.4 The electron gun

Since the voltage which is applied to the electron gun must be varied during the observation of threshold effects the collimation and intensity of the beam must be independent of this voltage. The gun also must be small enough to fit in the recess in the shell of the model.

Since Bland's electron gun proved to be suitable this design was adopted; however, the dimensions were altered to improve the optics and to enable the gun to fit the space available. This gun is illustrated in figure (4.2). Three diaphragm electrodes and a pure Tungsten hairpin filament were used. The Pyrophillite former maintained accurate spacing between the stainless

steel electrodes which were cemented in position with a paste of aluminium oxide and potassium silicate. It was necessary to bake this paste at 800°C after it had set to harden the cement and to expel any trapped gas. The diaphragm apertures were drilled 'in situ' to ensure correct alignment and rough edges were removed by etching.

The dimensions 'a', 'b' and 'd' were chosen to provide the smallest beam divergence for a given total length 'a + b' (Klemperer 1953) and an additional electrode 'a_2' was added at a distance 'c' from 'a_1' to provide focus action. Since the Davisson - Calbick formula cannot be used to obtain the focal length from the electrode geometry and the applied voltages because the aperture diameters and gun length are comparable, the focusing action was investigated practically.

Several guns with different values of the dimension 'c' were constructed and the beam geometry of each was observed with a fluorescent target. This target was constructed by depositing a thin coating of zinc sulphide from an aqueous solution on a glass plate. A fine wire gauze which was maintained at a positive potential of approximately 1 kV was placed in contact with the zinc sulphide and a second similar gauze, which was connected electrically to the tank, was placed 5 mm. in front of the screen. Since the anode 'a_2' also was at the same potential as the tank the electron beam traversed a field-free distance of approximately 30 cms. between the gun and the screen. This arrangement provided sufficient electron energy to cause fluorescence even when small voltages were applied to the electron gun.

Each gun was tested over a large range of applied voltage. It was found that the gun which is illustrated in figure (4.2) produced a conical beam with a half angle of $\sim 1^\circ$ at $V_{g_1} = -6$ volts, $V_{a_1} = +80$ volts, $V_{a_2} = +300$ volts.

The divergence of the beam was approximately constant in the range $80 \leq V_{a_2} \leq 1300$ volts provided that the electrode voltages were obtained from a constant ratio potential divider (e.g. figure 4.5). Larger relative values of V_{g_1} and smaller aperture diameters produced an improvement in collimation. This, presumably, was the result of changes in the beam structure near the cross - over point within the electron gun. The use of the filament temperature to control the beam current maintained a constant beam divergence during the threshold measurements.

The filament consisted of 0.1 mm. diameter Tungsten wire which was spot welded to two supports of 1 mm. diameter Eureka wire. The 'hairpin' was held in position during the spot welding by a loop of the same Tungsten wire which was threaded through the electrode apertures. Finally, the tip of the filament was pinched with pliers to form a sharp point.

The Eureka support wires were bent to produce the correct value of 'a' when the tip was on the axis of the gun. The latter condition was determined by observing the parallax between the filament tip and the edges of the grid aperture. Although 'a' theoretically is the most critical dimension of the gun, no difficulty was experienced in obtaining reproducible results when filament wires were replaced.

Since the filament operated at a temperature of approximately $3000^{\circ}K$ the electron beam was not monoenergetic; however, the range of threshold rigidity which is found in an acceptance cone of 5° half angle is many times larger than the half width of the Boltzmann rigidity distribution which corresponds to the temperature of the filament. The thermal rigidity distribution of the electron beam therefore has been ignored.

The tetrode guns performed satisfactorily with the weaker magnet at latitudes less than 40°; however, they failed to produce a suitable beam in

field of the stronger magnet. This was expected since the presence of a strong magnetic field would destroy the focusing action of the gun at small values of applied voltage. Fortunately the threshold rigidity is a relatively slowly varying function of zenith angle at the larger latitudes and differential transparency curves which were suitable for revealing small threshold perturbations could be obtained with a much more divergent electron beam. Therefore a short triode gun was used for all measurements at latitudes larger than 40°. The divergence of the beam which was produced by this gun varied between 10° and 20° over the range of applied voltage.

A method of adjusting the gun mounting to allow for magnetic deflections of the beam within the gun is described in the following chapter.

4.5 The gun voltage supplies and threshold display unit

The electrical connections to the model system are shown in figure (4.5). The threshold effects were observed by plotting the percentage of the beam current which reached the walls of the vacuum tank as a function of the accelerating voltage 'V'. In practice, it is difficult to produce a simple instrument which is capable of indicating the ratio between two small currents conveniently. Therefore the current 'i_t' which was returned to the model and the beam current 'i_b' were measured as the voltage 'V' was varied. The stray current 'i_s' which was collected by the stem and the leakage current component of 'i_b' were monitored.

An automatic display of the threshold effects was obtained by recording the currents on a chart recorder which was coupled to a potentiometer. The latter swept the voltage 'V' through an appropriate range which could be selected by switch S_2 (figure 4.5). The response of the recorder was sufficient toprevent the introduction of significant distortion in the threshold curves. Since the variation of 'i_b' with time at constant voltage was small

the currents 'i_b', 'i_t', 'i_b', 'i_s' were recorded in time sequence on a single channel recorder which used a four inch wide chart and which produced a six inch length of chart for each voltage scan.

A Tektronix 515A oscilloscope was used to obtain a fast visual display of threshold effects. The X - axis time - base generator of this oscilloscope provides a D.C. coupled linear sweep output which has an amplitude of approximately 150 volts. Switch S_1 (figure 4.5) connects this sweep voltage between the positive terminal of the gun voltage supply and the earthed positive terminal of the voltage distribution network. The current 'i_t' was displayed on the Y - axis of the oscilloscope by connecting the latter to the simple valve - voltmeter which was coupled to the chart recorder. Since the above method of voltage sweep generation prevented the observation of the current 'i_b' in a similar way the oscilloscope could be used to observe threshold effects only when the variation of 'i_b' with voltage was small. The amplitude of the latter variation was checked manually. When the oscilloscope was used, the chart - driven potentiometer 'R' was automatically replaced by a manual type which permitted the fine adjustment of the mean value of 'V' during the sweep.

Capacitive time constants prevented the use of sweep periods which were shorter than 50 milliseconds; however, this period was sufficient to permit good photography of the traces at 1/10 second exposure.

The gun voltage supply contained six series-connected gas-filled stabilisers which provided several voltage outputs with adequate stability, small ripple content and low output impedance. Voltages larger than 900 volts were obtained by the inclusion of a 600 volt battery in series with the negative lead to the voltage distribution network. Precautions were taken to

maintain a large insulation resistance between the gun voltage supply and the tank which was earthed. Poor insulation could produce significant leakage currents which would confuse the measurement of 'i_b'.

A 50 c/s A.C. supply could not be used to provide the filament current because the small thermal time constant of the filament tip introduced a large ripple component in the electron beam current. Secondary lead cells were found to be the most suitable source of filament current.

In principle the time which was required for the correction of data could have been saved if 'i_b' were stabilised with respect to 'V' by a negative feedback system. The inclusion of a large resistance in the filament centre tap connection to provide a variable bias for the grid of the electron gun was attempted. Unfortunately the modulation of the beam current by stray voltages which were induced between the filament and the grid could be removed only by placing a large capacitance in parallel with the biassing resistor. The time constant of this combination was sufficient to distort the chart records and to render the stabilisation inoperative at the relatively short sweep period of the oscilloscope display.

The beam current might have been stabilised by using a variable amplitude oscillator, which could be controlled by the beam current, to supply heating current at a frequency of the order 1 kc/s to the filament via a transformer. Although time could not be spared for its development, this method possesses the advantage that the filament supply is isolated by the insulation of the transformer.

4.6 The vacuum system

The vacuum tank and pumps are shown in figure (4.6). The tank was fabricated from the non-ferrous aluminium alloy NP5/6 and neoprene 'O' rings

which were lubricated with 'Apiezon M' grease were used to seal the flange surfaces and the 'Armourplate' glass window. The controls of the model and the pressure guage may be seen at the top of the photograph.

The tank was evacuated to a pressure of 10^{-6} mm. Hg. by an Edwards F 603 three stage oil diffusion pump which was filled with Edwards 704 silicone oil. This pressure was attained approximately one hour after the pumping commenced provided that the system initially was clean and at backing pressure. A guard ring and chevron baffle were used to prevent back-streaming of the oil vapour from the pump. The diffusion pump was coupled to an Edwards 1SC/150/B single stage rotary backing pump and the backing pressure was monitored by a conventional 'thermocross' guage.

An Elliott cold-cathode ionisation guage provided a measure of the tank pressure. Since the sensor of this instrument contained no magnetised element and employed an electromagnet to generate the necessary magnetic field, the introduction of stray magnetic fields in the working volume of the tank could be avoided. In addition, a reservoir tank, vapour trap and isolation valve were included in the backing line so that the rotary pump could be inoperative for periods of approximately one hour during the threshold measurements which required the smallest values of stray field.

4.7 The degaussing coils

The degaussing system was required to produce a remnant magnetic field less than 15 milligauss in amplitude (section 3.5) over the maximum volume which was occupied by the Störmer inner allowed region - a sphere of radius 35 cms. centred at the model. Since the coils could be aligned in the E - W plane this cancellation of the geomagnetic field could be accomplished by a two -component degaussing system.

Since the model was situated in a steel frame building the uniformity of the geomagnetic field in the laboratory was checked by measuring the vertical and horizontal field components with a rotating coil and ballistic galvanometer at several positions in the working volume of the tank. The variation of either component within this volume was less than ± 2.5% from the mean value. The field strengths were:-

Vertical component : (0.44 ± 5%)

N - S component : (0.13 ± 4%)

Craig (1947) has calculated the field uniformity which is produced by two circular coils of the Helmholtz type as a function of the distance between the coils. From an inspection of his graphs it was noticed that, for a maximum deviation of ± 2% from the mean field strength, the radius of the working volume about the centre of the coil system must be less than 40% of the coil radius. To achieve this a coil separation equal to 87% of the coil radius is required. Two coils, each of radius one metre, were arranged in this configuration to cancel the N - S field component.

Vertical component cancellation was achieved by the rectangular coil system (figure 4.6) which is an enlarged version of a design by Haynes and Wedding (1951). The rectangular shape was convenient since it provided space near the removable ends of the tank to permit work in the latter without the removal of the coil system.

The two coil systems were energised by [redacted] independent power units which were operated from the A.C. mains. Sufficient filtering to reduce the ripple field to a peak value less than 1 milligauss was included in both power units. The lighting circuits of the building produced an A.C. magnetic field of equal amplitude.

The maximum deviation of the residual field from the value at the position of the model was of the order ± 2 milligauss. Even if the absence of electronic stabilisation could permit an uncorrected drift of 3% the residual field strength would not have exceeded 15 milligauss.

4.8 The reduction of stray electric and magnetic fields

Stainless steel and non-ferrous materials were used in the construction of the vacuum system. Therefore if the ionisation guage and rotary pump were inoperative the principal sources of stray magnetic field were removed. Measurements showed that the magnetic fields which were associated with the electronic equipment and ferrous instrument racks were negligible at the position of the model provided that the latter was at least two metres from the instruments.

Stray electric fields could be produced by the exposed electron gun leads, the charging of insulators by electron bombardment and the potential differences which were introduced by the current detectors. The first source was the most important.

The gun leads were shielded by passing them between the stem and a graphite-coated glass sheath which was maintained at the same potential as the vacuum tank. A groove was cut in the stem for this purpose. At the model the leads were recessed in the surface and covered with copper foil; however, the filament terminals near the gun could not be shielded. The charging of insulators was reduced by coating as much of their surfaces as possible with graphite which was maintained at the tank potential.

Two experiments were performed to discover the disturbances which might be produced by the exposed filament terminals and by the potential differences which were produced by the current detectors. In the first a variable

potential was applied to a spare lead which was included with the leads to the gun and exposed in the same way as the filament leads. The oscilloscope threshold trace suffered negligible distortion when positive or negative voltages equal to the mean accelerating voltage were applied to this lead.

The second experiment entailed placing a potential difference of 0.5 volt - the potential drop across the input impedance of the current detector - alternately in series with all of the leads which were used for current measurement while the oscilloscope threshold trace was observed. The only detectable distortion occurred at large latitudes where the threshold corresponds to a small accelerating voltage. Under these conditions the threshold curves suffered small displacements in rigidity which were approximately equivalent to the applied voltage. Since the largest of these displacements were equivalent to an error of only 0.5% in the absolute values of the thresholds it was concluded that this effect could be ignored.

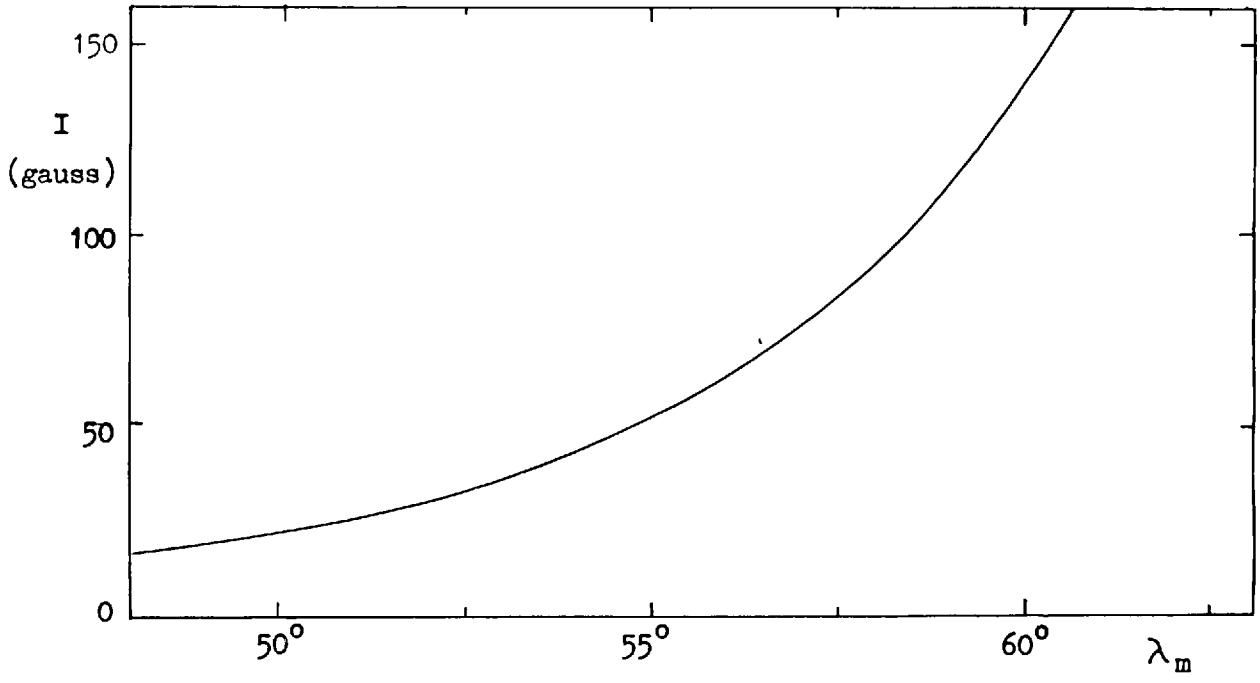

Figure 4.1 The required intensity of magnetisation as a function of the maximum latitude at which threshold effects can be observed for the present working volume of ~35cm. radius.

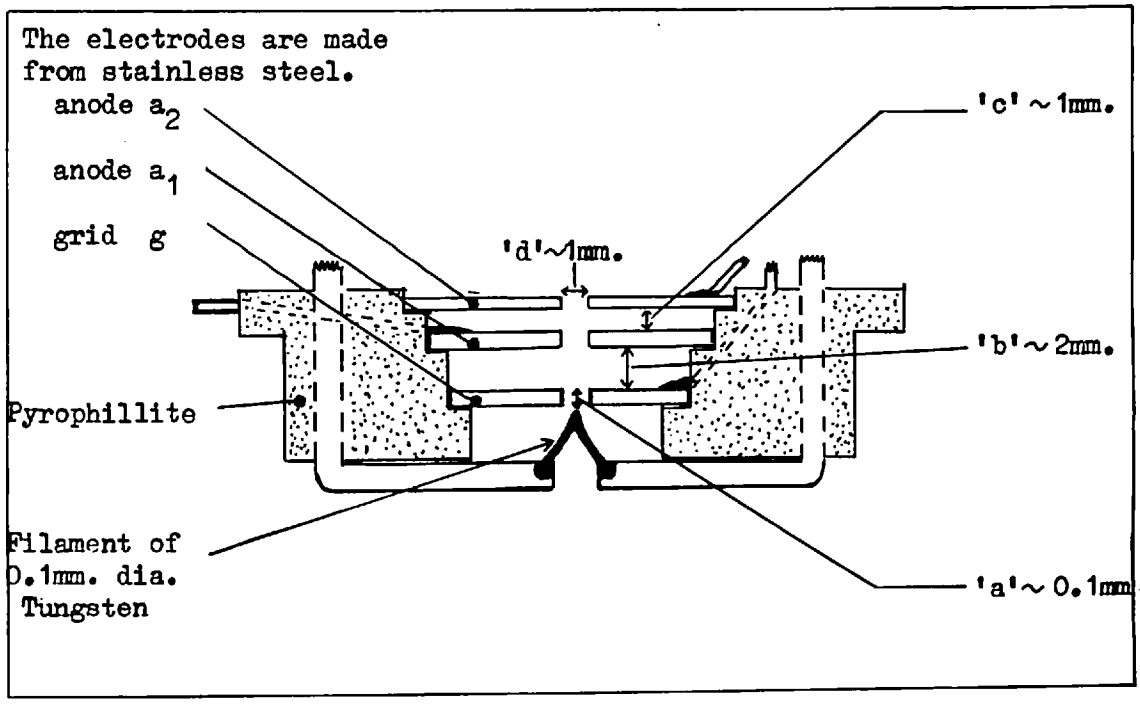

Figure 4.2 The electron gun (approximately 4 x actual size - section)

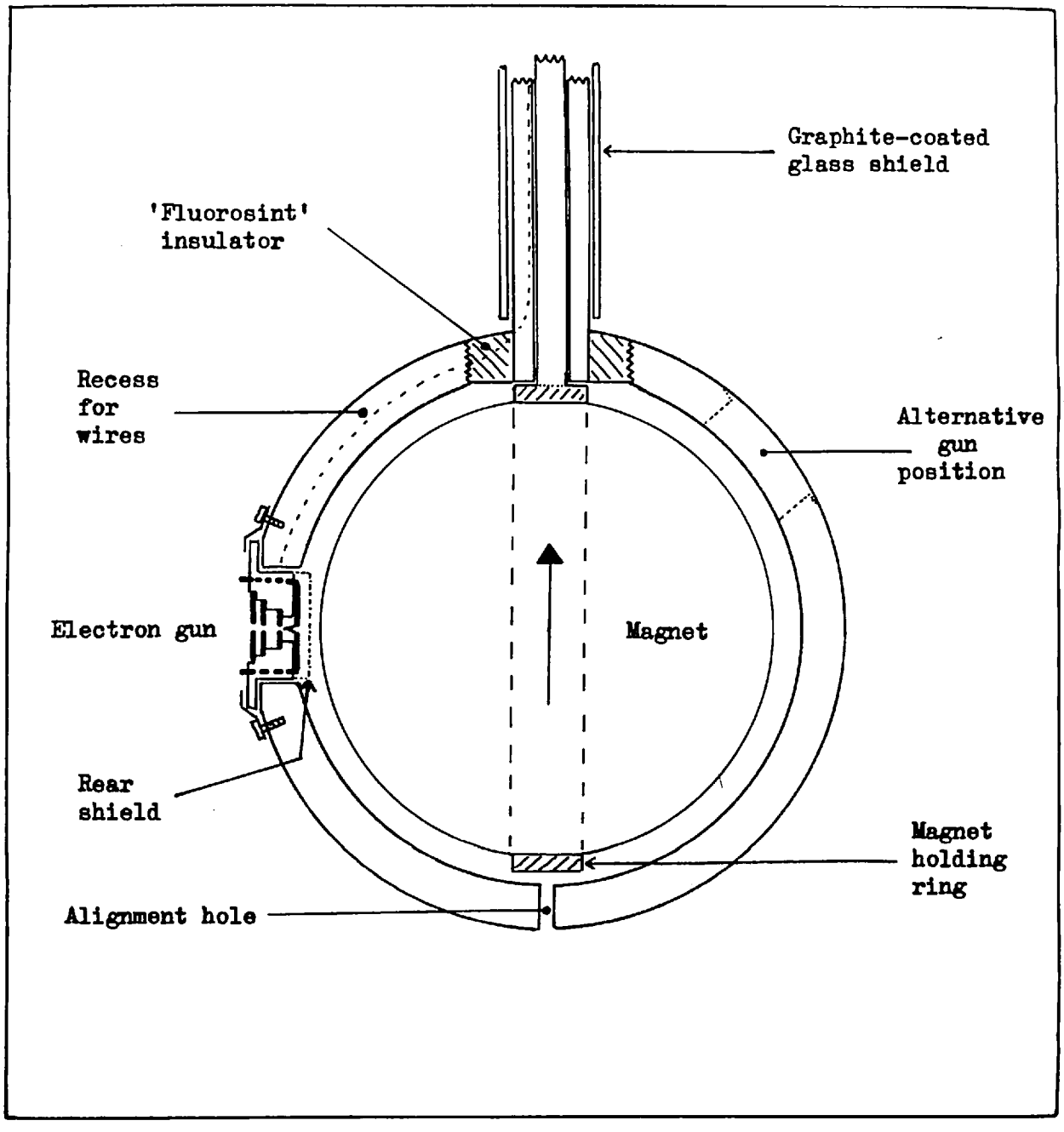

Figure 4.3 Cross-section of the model (actual size).

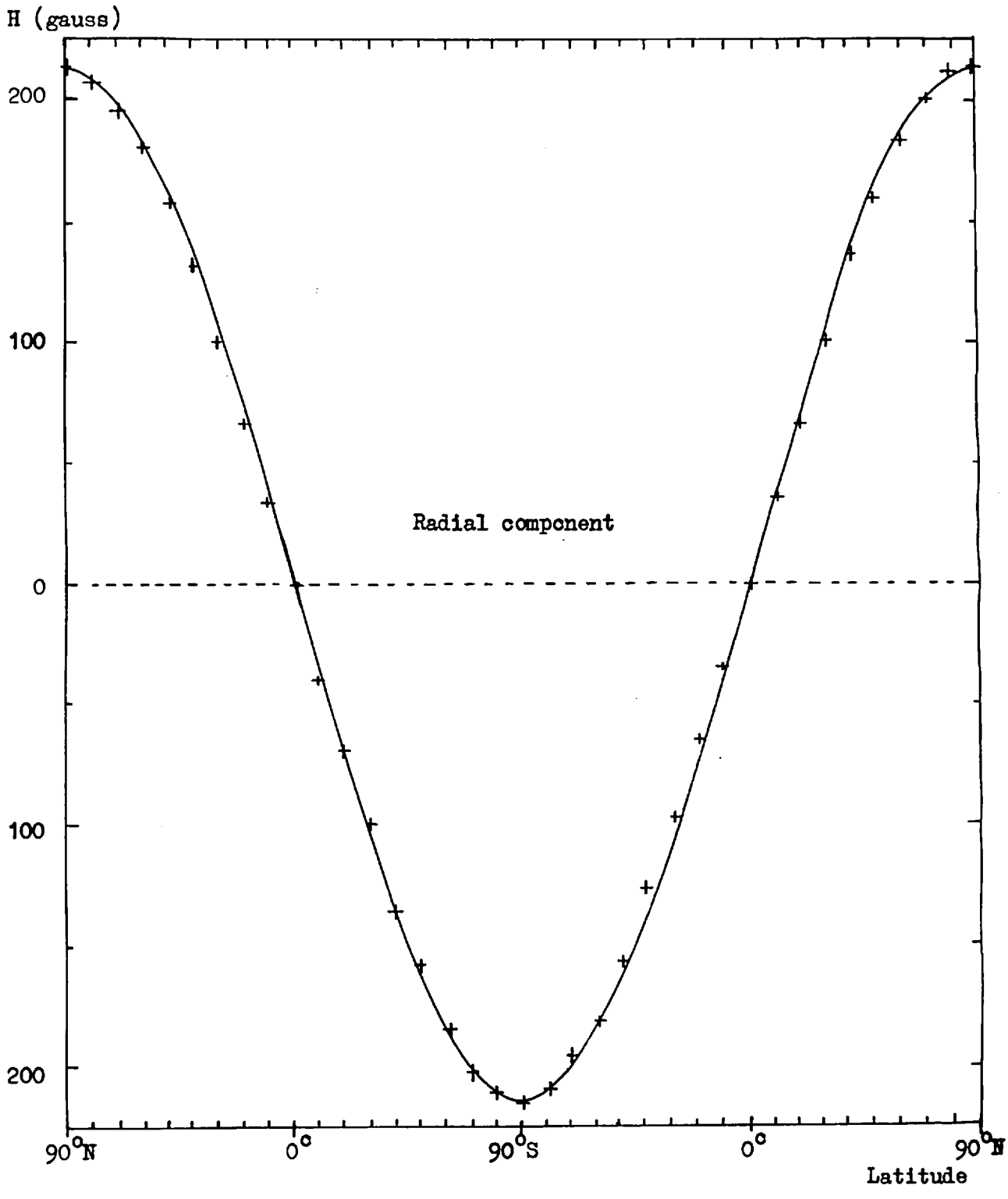

Figure 4.4 A polar great circle survey of the field at the surface of the model produced by the weaker magnet ($M = 10400$ gauss cm^3). The curve is a sine function passing through the experimental zero field points.
(Section 4.3)

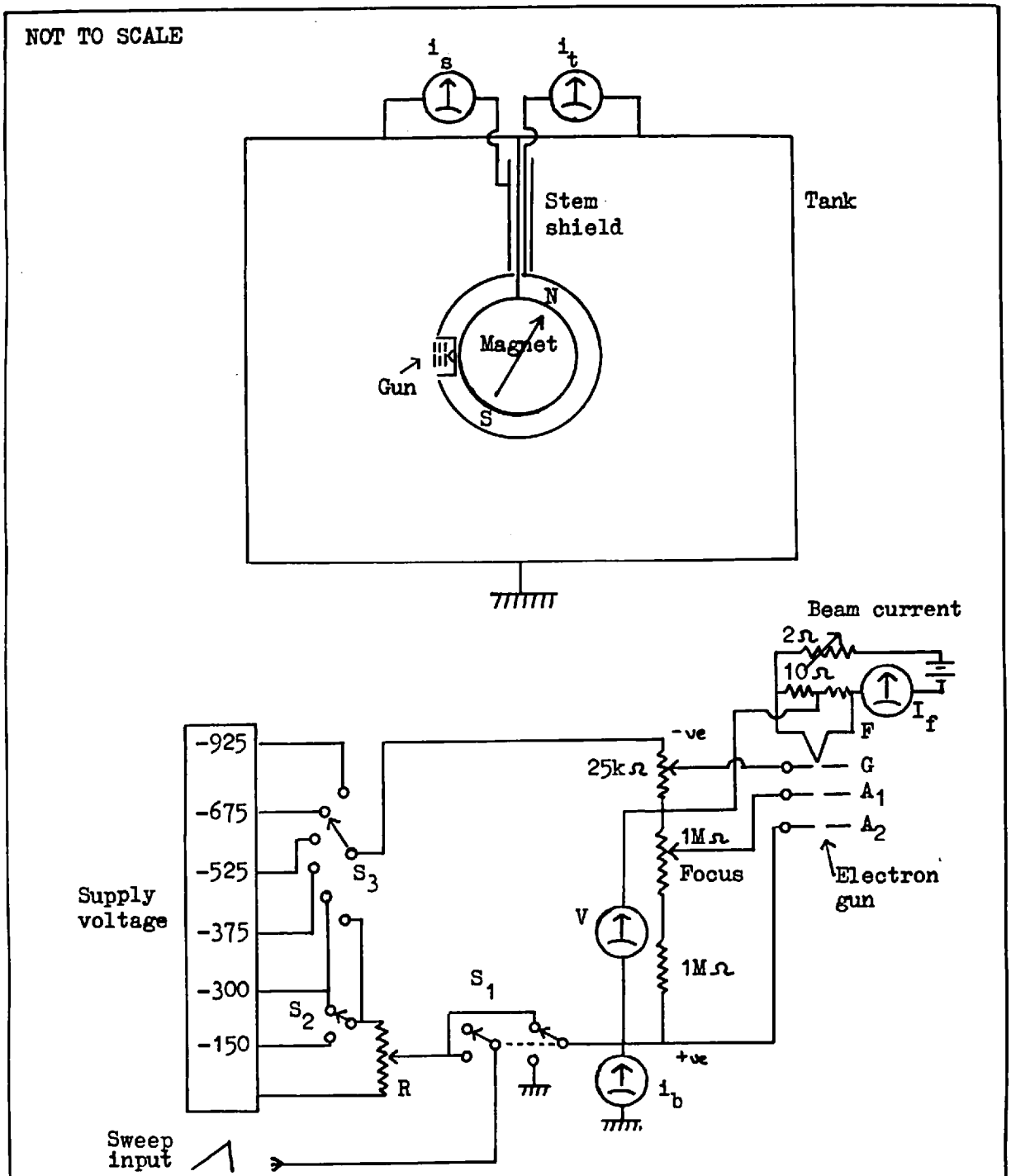

Figure 4.5 Block diagram of electrical connections showing voltage sweep arrangements. Meters indicate monitoring points.

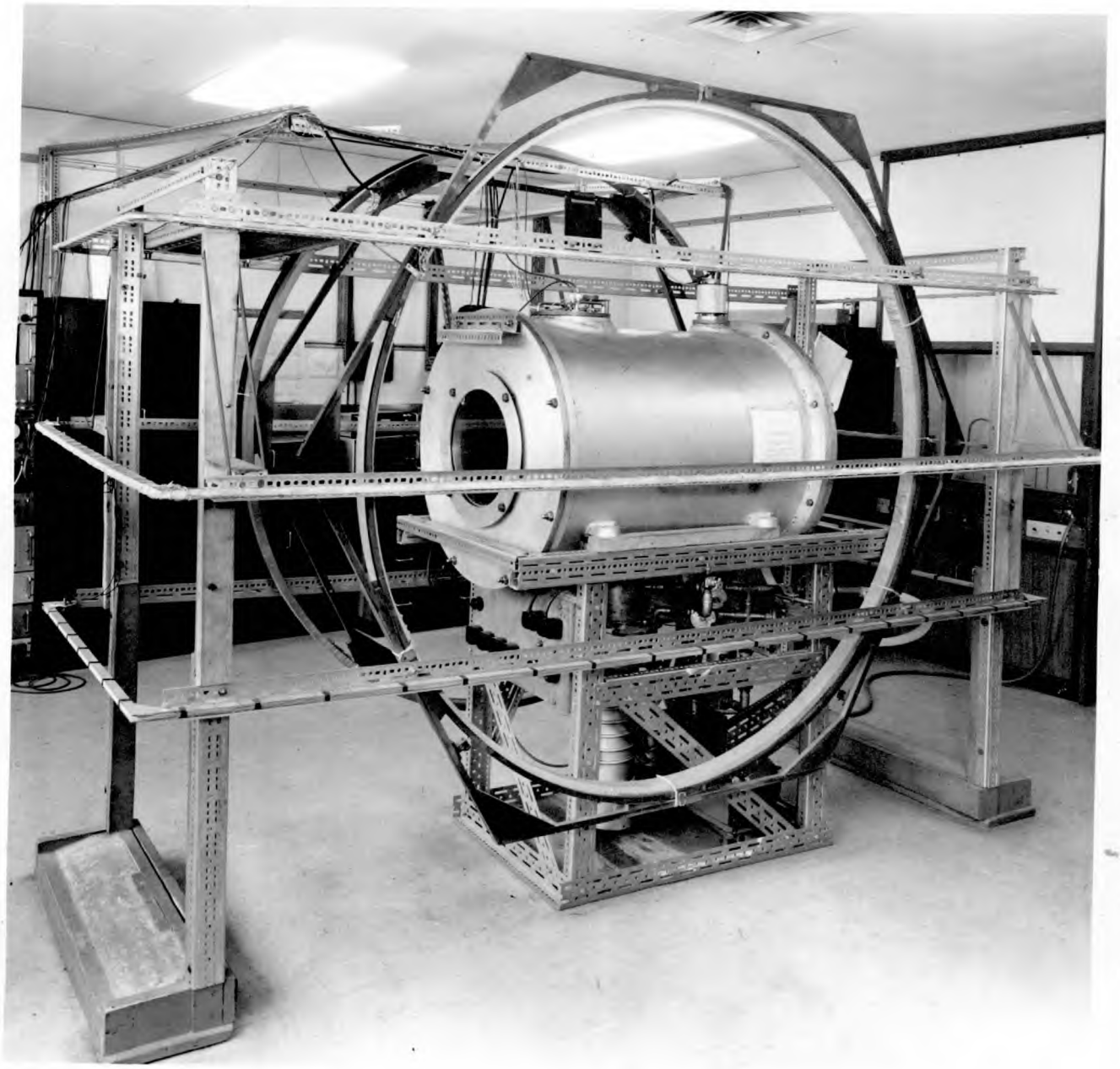

Figure 4.6 General view of the model.

CHAPTER 5

THE EXPERIMENTAL OBSERVATION OF THRESHOLD EFFECTS

5.1 Introduction

In order to interpret the performance of the model in terms of real cosmic ray effects one must determine the characteristics of the detector which the electron gun simulates. We introduce the concept of an 'ideal' cosmic ray telescope as a useful intermediate step in the process of interpretation.

The procedure and errors involved in the experiment are also discussed.

5.2 An analogy between the model threshold curves and cosmic ray effects

Our 'ideal' cosmic ray telescope consists of two thin circular detecting areas which are separated by a given distance along their common axis. Each detector is equally sensitive over its whole area to cosmic ray particles of all energies; however, an artificial lower limit to the rigidity response of the telescope is provided by an electronic discriminator which is sensitive to the rigidity of the particle detected. The telescope is placed at the top of the atmosphere and is aligned so that its axis is radial to the Earth.

Liouville's theorem applied to such a system indicates that, provided all directions of approach within the acceptance cone are accessible to particles at infinity, the counting rate of the telescope will be the same as if it were situated far from the geomagnetic field (Lemaitre and Vallarta 1933, Swann 1933). Thus a plot of the differential counting rate of the 'ideal' telescope as a function of the artificial threshold will be identical to the differential primary spectrum provided that the instrumental threshold

is greater than the geomagnetic threshold everywhere within the telescope acceptance cone.

At the lower values of the instrumental threshold, part of the acceptance cone becomes obscured because some of the trajectories within this cone intersect the Earth or are forbidden by Störmer theory. The curve of differential counting rate as a function of rigidity then departs from the curve which represents the primary differential spectrum by an amount which is proportional to the percentage of the acceptance cone obscured by the geomagnetic effects at the given rigidity. The differential transparency may be defined as being the ratio of the differential counting rate to the extrapolated differential primary spectrum.

Measurements of the performance of the electron gun (section 4.4) showed that the electron beam had approximately circular cross section and uniform current density. Thus the electron gun simulated an 'ideal' cosmic ray telescope of the above type. A curve of differential transparency as a function of rigidity could be obtained directly by plotting the fraction of the beam current which escaped from the field as a function of the simulated rigidity.

5.3 Procedure for the measurement of a given threshold

Before threshold measurements were started, power supplies were allowed to attain thermal equilibrium and the vacuum pressure, degaussing coil currents and gun co-ordinates were checked. Stray magnetic fields were removed by switching off both the ionisation gauge and rotary vacuum pump.

Voltages were applied to the electron gun to produce the required beam divergence and the beam current was monitored for a few minutes. If no change in the value of the beam current could be detected, the accelerating

voltage was slowly increased until the current 'i_t' fell to zero. The automatic display mechanism was adjusted to scan through this value of voltage so that the current 'i_t' varied from $i_t = i_b$ to $i_t = 0$.

Currents were measured in the sequence i_b, i_t, i_b, i_s to obtain a further check on the stability of 'i_b'. Records were rejected if the two curves of 'i_b' as a function of 'V' differed by more than 3% or if 'i_s' was greater than 3% of 'i_b'. The measurement of 'i_b' was repeated with the gun filament supply inoperative to assess the contribution of leakage currents.

The curves were analysed by dividing the voltage scan into 24 equally spaced values and constructing a table of the values of 'i_b', 'i_t', 'i_s' and leakage current 'i_l' for the various voltage values. These voltages were converted to scaled proton rigidities by means of the scaling equation (3.C) and the true beam current 'i'_b' was calculated from the values of 'i_b' and 'i_l'. The quantity $(1 - i_t/i'_b)$ was then plotted as a function of the scaled proton rigidity to obtain the required penumbral differential transparency curve.

5.4 Centring the magnet in the model

This adjustment involves checking that the supporting stem is radial to both the model shell and the magnet and that the magnet is concentric with the shell.

The alignment of the shell relative to the stem was checked by rotating the latter in a lathe and measuring the eccentricity of the shell with a micrometer 'clock' gauge. The small residual eccentricity ($\sim$ 0.1 mm.) which was detected was thought to be negligible since it does not produce a variation in the effective radius of the gun as the shell is rotated and is equivalent to an eccentricity in the geomagnetic field of less than 20 km. Although this small eccentricity might be expected to produce some distortion of the

penumbra, a longitude survey of the penumbral structure revealed no effects which could be attributed to this cause.

The centre of gravity of the magnet was located on the axis of the stem by placing the latter horizontally in two low friction bearings and moving the magnet in the holding ring until the couple exerted by gravity on the stem was zero. The magnetic field of the model was then measured at several positions separated 180° in longitude to check the accuracy of this adjustment. No discrepancies were noticed.

Finally, the magnet was moved along the axis of the stem until it was concentric with the shell. A small hole was drilled in the bottom of the shell to permit a micrometer depth gauge to be used for this purpose. The accuracy of this adjustment could be increased by moving the magnet along the axis of the stem in small increments until the Störmer threshold at magnetically conjugate points occurred at the same value of rigidity.

The final eccentricity of the magnet was estimated to be less than 0.1 mm, the error being in the equatorial plane.

5.5 The alignment of the electron gun

The electron gun must be orientated so that, with the plane of the second anode at a known radius from the centre of the model, the electron beam is directed radially from the model.

The first condition is easily satisfied since the equivalent altitude of the anode plane above the model surface may be determined with a spherometer. Various altitudes may be simulated by altering the thickness of the thin brass shims which are placed under the rim of the gun body.

Since the magnetic deflection of the electron beam within the body of the gun is poorly defined the second condition is difficult to meet. Unless the

electron trajectories within the gun are determined by a theoretical method, this internal deflection is difficult to estimate to better than order of magnitude accuracy (Bland 1962). Therefore the problem was investigated experimentally by comparing the deflections which were produced by the same magnetic field in different guns.

A gun which was twice as long as the 'normal' gun was constructed and observations were made with a fluorescent screen to establish that this gun produced an electron beam which was similar to the beam of the shorter gun. Both guns were placed in turn at the same altitude on the equator of the model and the thresholds which were produced by the two guns were compared. This revealed a difference in threshold which was attributed to the additional deflection in the longer gun.

The Störmer theory of the variation of threshold with zenith angle in the E - W plane was used to deduce the difference in angular deflection in the two guns. The eastward deflection was 5° larger in the longer gun. Since, for small angles, this angular deflection probably is proportional to the length of the gun it has been assumed that the total deflection in the shorter gun is approximately 5°E. Therefore, the shorter gun was tilted 5°W by placing thin brass strips under the rim of the gun body (figure 4.2) and the equatorial threshold was determined at the same altitude as before. This threshold value agreed with the theoretical value which was deduced from the electron voltage, the magnetic dipole moment and the radius of the model to within the possible error of approximately $\pm 4\%$.

Since the threshold at the equator is not a function of the zenith angle in the N - S plane, the alignment of the electron beam in this plane was checked by comparing the penumbral transparency curves at magnetically conjugate points. The measurements of the penumbra at latitude 30° were used

for this purpose because the Störmer threshold may be identified in the differential transparency curves without difficulty at this latitude. This comparison indicated that the error in the zenith alignment in the N - S direction was less than the 2^{o} error which might exist in the geometrical adjustment. Errors in the alignment of the gun in the N - S plane could be separated from the effects which were caused by a displacement of the magnet along the axis of the stem since the latter produces a difference in Störmer threshold at the conjugate points in addition to the penumbral distortion.

5.6 Errors involved in the calibration and data analysis

The errors in the calibration of the model reduce the accuracy with which the absolute values of threshold may be determined. These errors are important only if precision measurements of the penumbra at a given position are required. When threshold perturbations are being studied the calibration errors are negligible compared with the larger random errors which occur in the measurement of the small differences in threshold.

In order of importance the sources of calibration error are :-

1) The determination of the dipole moment M_m.

This involves the measurement of the magnetic field of the model at a known radius on a polar great circle. Errors in the calibration of the magnetometer and in the measurement of the radius produce a possible error in M_m which is of the order $\pm 4\%$. This is the principal source of systematic error in the threshold values. This error could be reduced to approximately $\pm 1\%$ in any future experiment by the use of an absolute field measurement. The electron spin resonance phenomenon in organic free radicals probably could be employed for this purpose (e.g. Codrington, Olds and Torrey 1954).

2) The measurement of the electron accelerating voltage and model radius.

These quantities have possible systematic errors of the order $\pm 2\%$ and

$\pm$ 0.5% respectively. Since $P_e \propto V^{\frac{1}{2}} r_m^2$ these together produce an error of the order $\pm$ 1.5% in P_e.

3) The determination of the mean zenith angle of the electron beam.

The correction discussed in the preceding section produces agreement between the theoretical and experimental thresholds to within the calibration error in the experimental values. If this range of error is expressed in terms of a range of zenith angle in the E - W plane at the equator using Störmer theory, the maximum error in zenith alignment may be estimated as $\pm 4^{\circ}$.

4) The determination of the equivalent superimposed field strengths.

This involves errors of the order $\pm$ 3% in measuring and adjusting the field strengths and $\pm$ 4% in using the dipole moment of the model for scaling purposes. The combined error of $\pm$ 5% is comparable to the uncertainties involved in the graphical analysis.

The random errors which are plotted in figure (6.1) occur during the data analysis in reading co-ordinates from the traces. Although these contribute little uncertainty in the absolute threshold values they become important when small changes in the threshold values are being detected. The latter point is illustrated in figure (7.3) in which it will be noticed that the 1% perturbation produced by a 100 γ field may be determined only to an accuracy of $\pm$ 10%.

Errors in setting the gun co-ordinates due to the reading of scales and torsional effects in the supports are of the order $\pm 0.5^{\circ}$. There is a possible systematic error in the latitude values which is of the same order of magnitude.

CHAPTER 6

THE PENUMBRA

6.1 General

To permit an adequate assessment of the importance of the magnetic deflection of the electron beam within the electron gun it was necessary to use the minimum number of guns in the experiment and to measure the deflection in each gun. Since the magnitude of the internal deflection depends on the degree of focus of the electron beam and on the inclination of the axis of the gun to the zenith direction at the surface of the model, the penumbral investigation was restricted to a study of the differential transparency (section 5.2) 'seen' by a 10°-20° acceptance cone centred at the zenith. A suitable electron beam was obtained by defocussing the tetrode gun or, at the larger latitudes, by using a triode gun (section 4.4).

The penumbra 'seen' from the Earth's surface at latitudes between 0° and 57° has been determined and these observations are compared with measurements of the penumbra 'seen' from an altitude of 1100 km. with a similar acceptance cone. Time limited the latter comparison to latitudes less than 25°.

Although the range of conditions which are represented in these measurements is small the information which has been obtained provides a good independent measure of the latitude and altitude dependence of the penumbra.

6.2 The geometry of the model

The measurements at latitudes less than 40° were performed with the axis of the dipole at an angle of 40° to the supporting stem. This permitted the placing of the gun at any latitude between 40°N and 40°S by the rotation of the shell of the model about the axis of the stem. A larger inclination

could not be employed since this would place the stem within the Störmer inner allowed region (section 4.2). The change of the longitude of the gun during the adjustment of the latitude was unimportant since the magnetic field could be represented to a good approximation by a dipole situated at the centre of the shell (figure 4.4). The relation between the latitude of the gun and the angular rotation of the shell is recorded in Appendix B.

The dipole axis was aligned parallel to the stem for the measurements at latitudes greater than 40°. Latitude adjustments were made by moving the gun to different recesses on the surface of the model. This introduced larger errors in the latitude coordinates but the geometry was more convenient for the application of additional magnetic fields and for the study of longitude dependent effects.

6.3 A summary of the errors involved in the penumbral transparency measurements

1) The absolute values of threshold rigidity.

Errors in the calibration of the model (section 5.6) produce an uncertainty of the order ± 4% in these values. The largest contribution to this uncertainty is the inaccuracy in the measurement of the dipole moment.

2) The mean zenith angle of the electron beam at the gun anode.

Although the geometrical axis of the gun may be aligned to within 0.5° of the zenith the magnetic deflection of the beam within the gun produces a much greater uncertainty in the zenith angle. An approximate correction may be derived by comparing the absolute values of the threshold rigidities produced by two electron guns of differing lengths (section 5.5). The uncertainties in these rigidity values limit the final accuracy of the zenith alignment to $\pm 4^{\circ}$.

At latitudes between 30° and 60° the threshold changes slowly with zenith

angle but rapidly with latitude. The effects of small errors in zenith alignment become less distinguishable from those which are produced by errors in the latitude adjustment of the gun. The absolute value of the threshold at latitude 40° indicates that the maximum Eastward deflection of the electron beam is 10°; however, if the absolute threshold values are normalised to the value 14.9 GV. at the equator the limit is reduced to 5°E.

Even if the electron beam emerges from the gun in a direction parallel to the magnetic field lines the deflection from the zenith at latitude 60° would be less than 20°S. This has been verified by Roberts (1963) who operated the model in an atmosphere of nitrogen at a pressure of 5×10^{-5} mm. Hg. This technique rendered the filamentary beam visible in blue - white light which was emitted from the ionised region along the trajectory. The zenith angle of the beam at the gun anode was approximately 10°S.E. at latitude 55° and viewing conditions were sufficiently good to reveal the spiral motion of the trajectory round the magnetic field lines in the 'horns' of the Störmer inner allowed region.

3) The simulated acceptance cone.

If the shape of the differential transparency curve at the equator (figure 6.1A) is assumed to be caused by the range of threshold which exists within the simulated acceptance oone, a value for the angular width of the latter may be obtained. This assumption is approximately valid only if the electron beam is monoenergetic (section 4.4) and if there is little penumbral structure near the given rigidity. For this reason the check has been applied only at latitudes 0°, 25° and 57°. These latitudes were chosen because large differential transparency changes occur near either the Störmer or the main cone threshold indicating the absence of fine penumbral structure at these

thresholds.

At each latitude, the tangent to the differential transparency curve at the 50% transparency value has been extended to the 0% and 100% values and equation (2.E) has been used to convert the range of rigidity between these intercepts into a range of zenith angle. The cone angle deduced from the range of zenith angle agreed with the expected performance of the electron gun to within 20% in each case.

(It has been assumed that the main cone and Störmer thresholds vary with zenith angle in the E - W plane in a similar way. The curves of Hutner (1939) indicate that this is approximately the case for a small range of angles about the zenith at latitude 20°.)

4) The latitude of the electron gun.

An accurately constructed dipole field was used for the measurements at latitudes less than 40°. The errors in the latitude settings are assumed to be produced only by the geometrical errors in the adjustment mechanism. These are probably less than $\pm 1^{\circ}$ (section 5.6). The distribution of the experimental threshold values (figure 6.3) is in agreement with this suggestion.

A larger magnet was used during the measurements at latitudes greater than 40° to increase the voltage of the electron beam near the threshold. Since this magnet had not been ground to an accurate spherical shape the magnetic field deviated slightly from that of a dipole. This produced a small variation in effective latitude at constant geometric latitude. These effective latitudes could be determined to an accuracy better than $\pm 1^{\circ}$ since the threshold varies rapidly with latitude between latitudes 40° and 60°.

5) The altitude of the electron gun.

The altitude of the electron gun anode above the surface of the model was

determined with a spherometer. The error incurred was ± 10 km. on the geomagnetic scale. No allowance has been made for any penetration of the electric field of the first anode through the aperture of the second anode. This effect might produce an increase of ~ + 1% in the equivalent radius of the model.

6) The magnetic field asymmetry.

The errors in the alignment of the magnet (section 5.4) could produce a variation in effective radius of the order ± 0.2% with longitude. This would produce a longitude variation of threshold at constant latitude of the order ± 0.05 GV. Except at the equator this variation could not be detected in the presence of the errors in the latitude adjustment.

7) Scatter of the electron beam in the residual gas in the tank.

No change in the shape of the differential transparency curves could be detected when the pressure in the vacuum tank was raised by a factor ten above the normal working pressure of 10^{-6} mm. Hg. The mean free path of the electrons is expected to be at least two orders of magnitude greater than the dimensions of the vacuum tank.

6.4 The experimental results

The pairs of differential transparency curves which were obtained at simulated altitudes of 30 km. and 1100 km. between latitudes 0° and 25° are displayed in figure (6.1). The curves which were obtained at the lower altitude between latitudes 30° and 57° appear in figure (6.4).

The arrows 'SC' , 'MC' in the above figures represent the Störmer and main cone thresholds. These are assumed to occur at the rigidity values at which the curves cross the 50% transparency value. An inspection of figure (2.2) indicates that this is a reasonable approximation. Where the differential transparency curve fails to define a Störmer threshold in this

way because the transparency increase is too small (e.g. latitude 19.5°- figure 6.1D) this threshold has been determined by subtracting the Lemaitre - Vallarta penumbral width from the experimental main cone value.

The experimental thresholds have been plotted against latitude in figure (6.3) and curves which represent the theoretical Störmer threshold and the main cone threshold of Lemaitre - Vallarta and Schwartz have been included for comparison. The experimental high altitude thresholds have been scaled in value to allow for the difference in radius.

The distribution of the experimental main cone values in this figure indicates that the percentage width of the penumbra is the same at the two altitudes. This distribution also demonstrates that the variation of the mean zenith angle of the electron beam with latitude was negligible since if this were not the case a systematic displacement of the experimental points relative to the theoretical curve would be noticed.

The Störmer threshold values at latitudes less than 25° are displaced from the theoretical curve. These values were obtained by extrapolating small transparency increases and probably do not represent the Störmer threshold accurately.

The mean transparencies of the curves of figures (6.1) and (6.4) are displayed in figure (6.2). The mean transparency has been defined as 'the area under the differential transparency curve between the Störmer and main cone thresholds expressed as a percentage of the total area between these thresholds'. This mean transparency is equal to the percentage of the primary cosmic ray flux between these two rigidity values which would be recorded at the given latitude by the detector simulated in these measurements.

6.5 A comparison between the present results and the predictions of other workers

Schwartz (1959) has used a digital computer to determine which rigidities are forbidden for the zenith arrival direction at latitudes 30°, 35°, 41°, 45° and 50°. Since these results relate to a single arrival direction which is either allowed or forbidden the penumbral structure may be represented by a series of step function changes in transparency (figures 6.5 and 2.2). To obtain approximate differential transparency curves (section 5.2) for a small angle acceptance cone about the zenith the transparency of these 'Schwartz diagrams' has been averaged over rigidity intervals equal to the range of threshold which occurs in the simulated acceptance cones of figure (6.4). This produces the smooth curves which appear in figure (6.5).

Although the curves of figures (6.4) and (6.5) do not correspond exactly in latitude their similarity in shape and mean transparency is apparent. A closer correspondence in shape could not be expected even if the curves related to the same latitudes since the penumbral structure of the 'Schwartz diagram' is a function of the arrival direction.

The experimental and theoretical mean transparencies should show close correspondence since the mean transparency represents an average property of the penumbra. The experimental values may be compared with the mean transparencies calculated by Schwartz (figure 6.2). The agreement between the two sets of transparency values is excellent at latitudes greater than 40°; however, discrepancies exist at latitudes between 20° and 40°.

The present results confirm Bouckaert's prediction that the penumbral transparency is zero at latitudes less than 20° but indicate that Schwartz is incorrect in assuming that the zero transparency region extends to latitude 25°. Since the penumbra includes a large range of rigidity at latitudes

between 20° and 30° the penumbral corrections of Schwartz differ appreciably from the present predictions in this latitude range (c.f. Bouckaert 1934, Schwartz 1959).

It is unfortunate that the measurements which were made at latitudes 35° and 37.5° were invalidated by recording errors; however, the oscilloscope threshold display demonstrated that the differential transparency curves for these latitudes contain a simple transparency increase near the main cone threshold. This absence of penumbral structure suggests that the mean transparency probably falls to a low value in this latitude region. This behaviour is predicted by Schwartz.

The penumbra at altitudes of approximately 850 km. and 1200 km. has been investigated by Bland (1962). Since the differences between the differential transparency curves at the two altitudes were small it has been assumed that Bland's measurements may be compared with the present measurements at 1100 km. altitude. The general agreement between the two results is evident on inspection of figure (6.2). In addition, the shapes of the curves of figure (6.2) agree with those of Bland.

Figure (6.2) indicates that, compared with the penumbra 'seen' from the Earth's surface, the zero transparency region of the penumbra at 1100 km. altitude is confined to a smaller range of latitude about the equator and the transparency at the higher altitude is generally larger. The present work thus supports Bland's conclusion that the difference between his transparency values and those of Schwartz is caused by the variation of the penumbral structure with altitude.

6.6 The evaluation of 'effective threshold rigidities'

The mean penumbral transparencies of Schwartz have been used by Quenby

and Wenk to evaluate threshold rigidities over a wide range of latitude and longitude (section 2.4). At latitudes less than 20°, thresholds have been established by using the cosmic ray intensity contours of Katz et. al. (1958) to equate the effective threshold at a given point to the calculated threshold at the equator where the penumbral effect is assumed to be zero. The differences between these effective thresholds and the theoretical Quenby - Webber values are attributed to the penumbral effect and indicate that the penumbral transparency is zero for the given acceptance cone at latitudes less than 20°.

The limited range of threshold at the equator prevents the use of the cosmic ray contours to establish thresholds at latitudes greater than 20°. This is unfortunate since, in the latitude range 20° to 40°, the Quenby - Webber calculations have least accuracy and the penumbral effects are large. In view of the differences in this latitude range between the mean transparency values found in this work and the values of Schwartz used by Quenby and Wenk, new penumbral corrections were derived. These produce a maximum alteration to the Quenby - Wenk values of the order -0.5 GV. at latitude 25°. This difference tends to zero at latitudes 20° and 40°.

Schwartz (1959) has indicated that the effective thresholds are dependent on the primary cosmic ray rigidity spectrum when penumbral effects are present. The largest variation of effective threshold would be expected at latitudes where the penumbral rigidity width is large and the differential transparency near the Störmer threshold is much larger than the value near the main cone threshold (e.g. latitude 25° - figure 6.1G). Effective thresholds have been evaluated at latitude 25° for primary differential spectra of the form $dI/dR = R^{-a}$ with 'a' = 0, 2 and 6. Threshold values of 10.9, 10.75 and 10.4

GV. respectively were obtained. (The definition of effective threshold and the method of calculation are stated in Appendix C).

This calculation indicates that during large solar flare events in which the spectrum exponent 'a' may approach the value 6 at 10 GV. (e.g. Webber 1962) the effective threshold at latitudes near 25° may change by ~ -3% due to the spectrum change alone. This change is of the same order as that produced by a 150 γ uniform magnetic field parallel to the dipole axis (figure 2.3). It may be necessary to consider this effect in the analysis of the threshold perturbations which occur during geomagnetic disturbances.

The effective thresholds for 'a' = 0 may be obtained simply by subtracting the penumbral rigidity width multiplied by the mean fractional transparency from the main cone threshold. Since the undisturbed primary cosmic ray rigidity spectrum is characterised by a value of 'a' less than 3 the above calculation indicates that the error introduced by the use of the correction for 'a' = 0 is negligible.

The new corrections for 'a' = 0 at the Earth's surface are presented in figure (6.6). The Schwartz penumbral width and the penumbral corrections which were used by Quenby and Wenk also are indicated.

The penumbral corrections for the 1100 km. altitude have been derived from the high altitude mean transparencies (figure 6.7). These corrections must be added to the Störmer thresholds of Quenby - Wenk for this altitude to obtain the effective threshold rigidities. In this calculation the Schwartz penumbral widths have been scaled to allow for the radius change (section 6.4).

6.7 Atmospheric effects

No attempt was made to simulate an 'atmosphere' in the present experiment.

The observations which were made at a simulated altitude of 30 km. are assumed to represent the conditions at the surface of the Earth. This seems reasonable since ~99% of the atmospheric mass is contained below the 30 km. altitude surface and a comparison of the 'surface' measurements with those which were made at a simulated altitude of 1100 km. indicates that the structure of the penumbra changes slowly with altitude.

The values of effective threshold for instruments situated on the Earth's surface depend on the atmospheric yield functions. An approximate calculation indicates that the error in the threshold introduced by ignoring the yield function dependence is less than +1% for all detectors with acceptance cones of angle less tha 50°.

6.8 Summary and suggestions for further work

These studies of the penumbra have lead to the following conclusions:-

1) If the penumbra is observed from the Earth's surface with a 10° acceptance cone which is centred at the zenith the mean transparency increases from zero at latitude 20° to ~100% at latitude 60°. This agrees with the values quoted by Schwartz at latitudes less than 20° or more than 40°. The measured transparencies are larger then the Schwartz values af latitudes between 20° and 30°.

2) The mean transparencies at the 1100 km. altitude are larger than the values at the Earth's surface for the same acceptance cone and the region in which the transparency is zero is restricted to a smaller range of latitude about the equator as the latitude of observation is increased. This is in general agreement with the work of Bland.

3) Qualitative observations indicate that the mean transparency is larger for larger acceptance cone angles near latitude 25°. Since the penumbra

extends from approximately the zenith to the West horizon at this latitude this transparency increase occurs when the edge of the acceptance cone penetrates further into the penumbral region.

4) A decrease of the order 3% in effective threshold may occur near latitude 25° during the spectrum changes which accompany very large solar flares. This effect is very small at other latitudes and is probably small at this latitude for instruments which have an acceptance cone of angle larger than 30°.

The present investigation could be extended in the following directions:-

1) A more detailed survey of the penumbra at latitudes between 20° and 40°. (The rapid change of penumbral structure with latitude in this latitude range requires that the errors in determining the latitude and zenith angle of the electron beam be as small as possible.)

2) A latitude survey of the penumbra 'seen' by a wide angle acceptance cone.

3) An extension of the observations of the penumbra at satellite altitudes to a wider range of latitudes, altitudes and acceptance cones.

4) A study of the penumbral distortion produced by large magnetic anomalies both at the anomaly and at the magnetically conjugate point. (An increase in the dimensions of the model would permit the simulation of the geomagnetic field to a good approximation. A model 20 cm. in radius would be optimum for ease of field simulation, low power dissipation and acceptable electron gun performance; however, a model 10 cm. in radius could be used with the present vacuum system to investigate the penumbra at latitudes less than 40°. This would permit the simulation of the larger magnetic anomalies with a coil system similar to that used by Bland.)

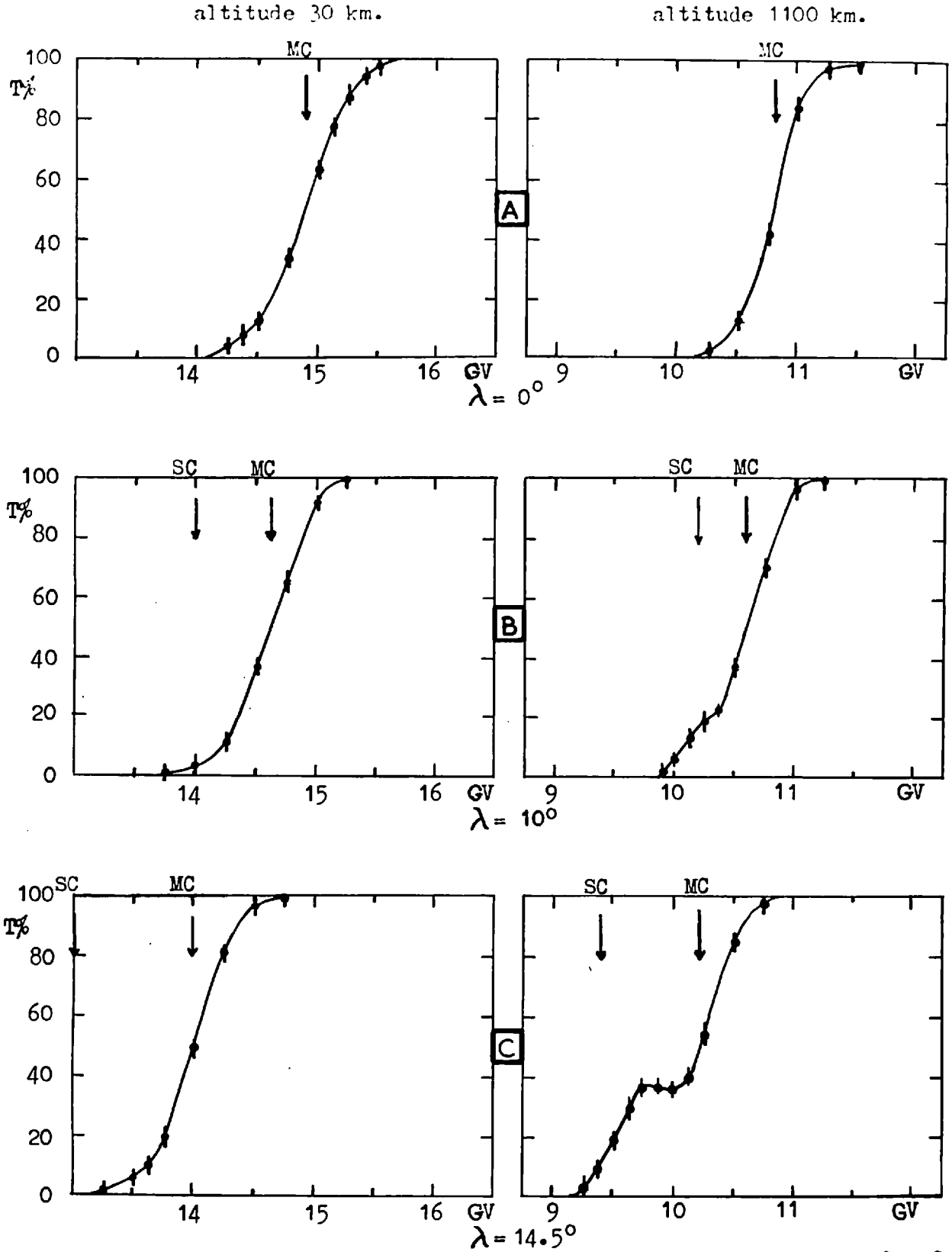

Figure 6.1a Penumbral transparency as a function of rigidity for a 7°–10° acceptance cone centred at the zenith at approximate altitudes of 30 km. and 1100 km. Latitudes 0°, 10°, 14.5°.

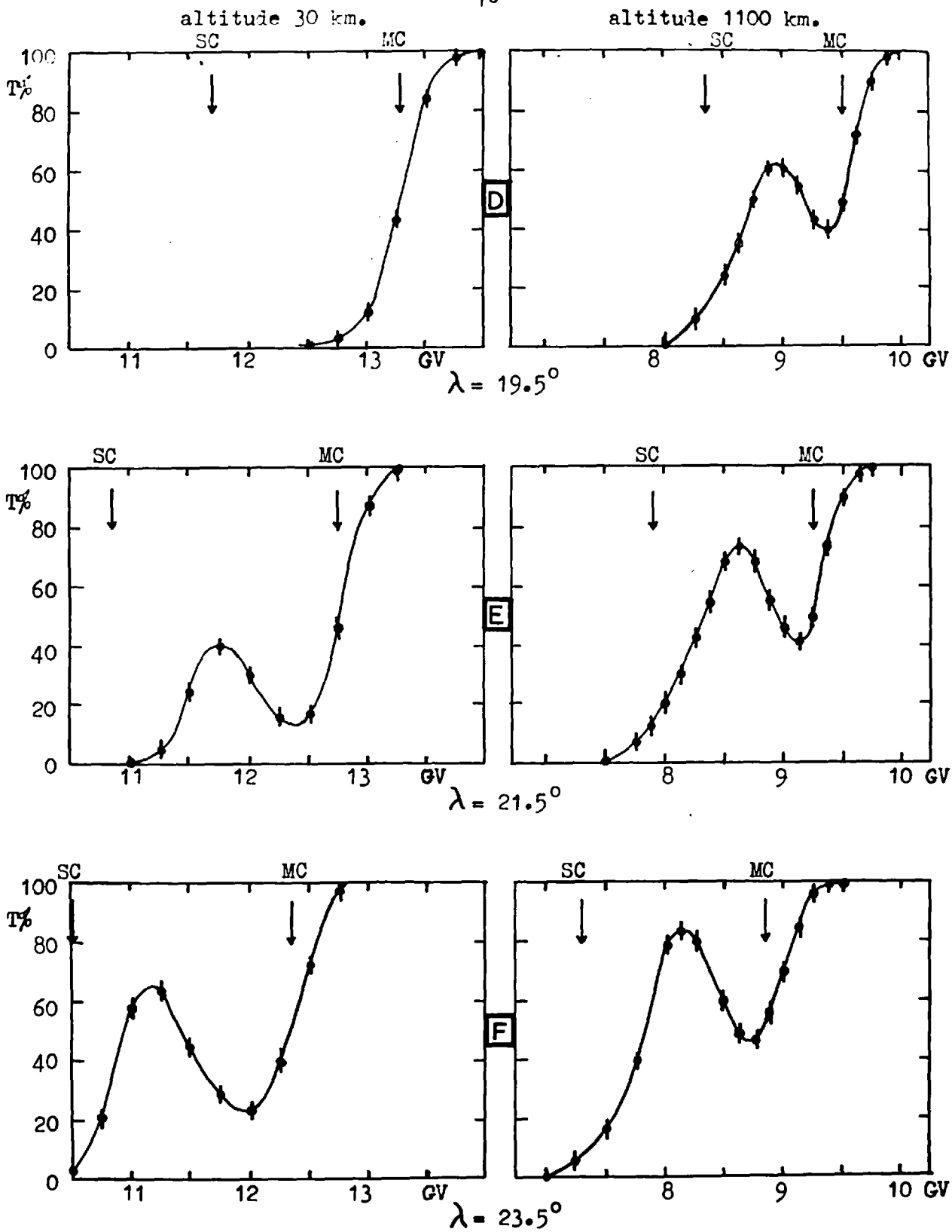

Figure 6.1b Penumbral transparency as a function of rigidity for a 7°-10° acceptance cone centred at the zenith at approximate altitudes of 30 km. and 1100 km. Latitudes 19.5°, 21.5°, 23.5°.

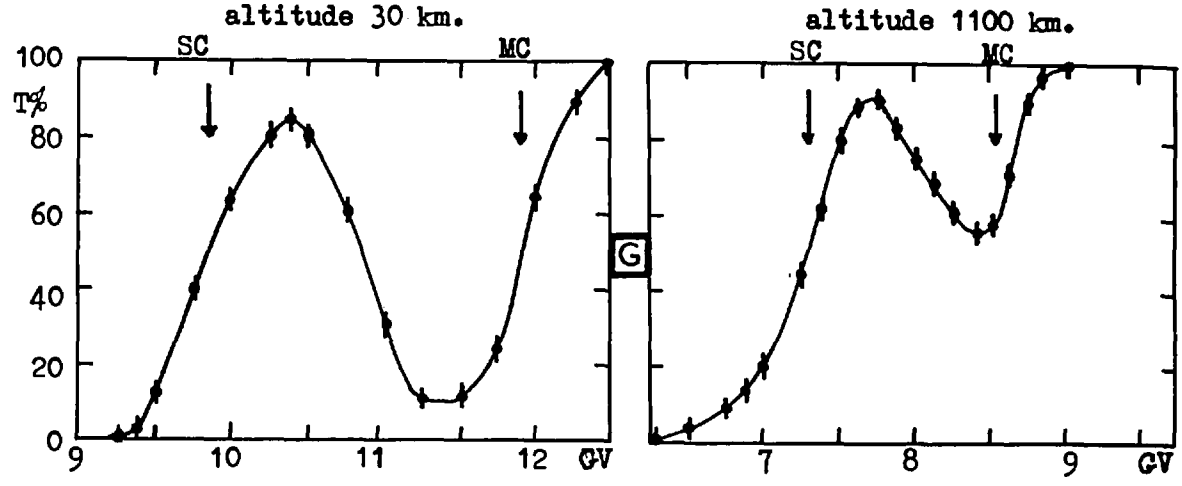

Figure 6.1 Penumbral transparency as a function of rigidity for a 7°- 10° acceptance cone centred at the zenith at approximate altitudes of 30 km. and 1100 km. Latitude 26°.

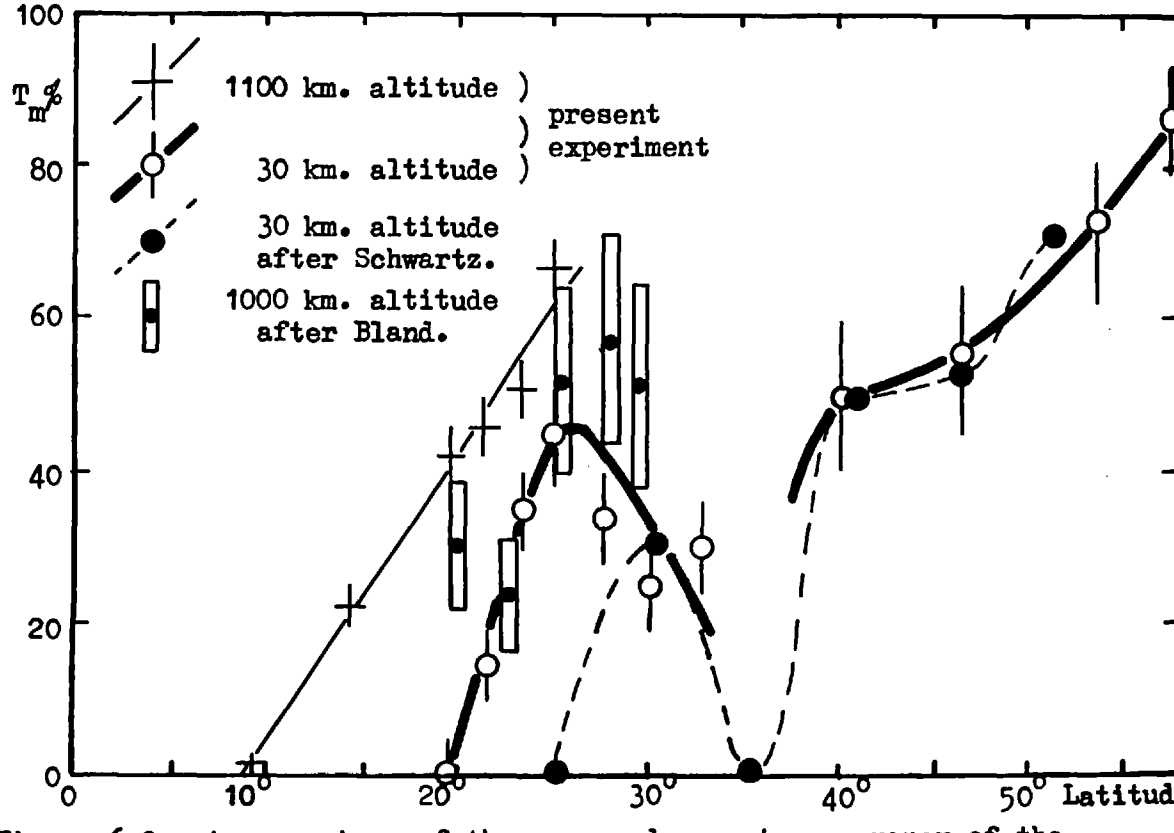

Figure 6.2 A comparison of the measured mean transparency of the penumbra for a 10° acceptance cone centred at the zenith with Bland's results and the theoretical values of Schwartz (section 6.6).

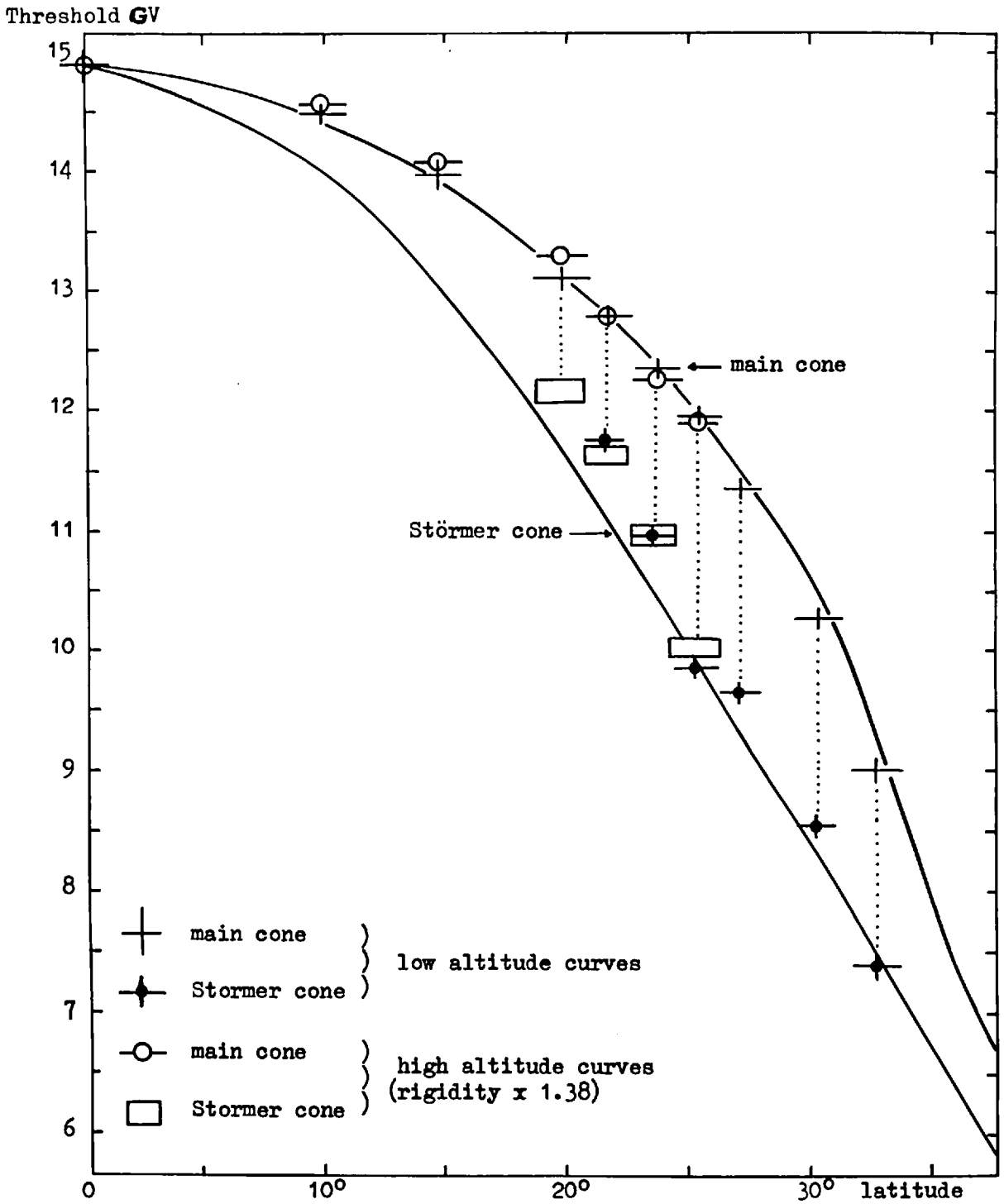

Figure 6.3 A comparison of the experimental Störmer and main cone thresholds with the theoretical curves. The experimental values were obtained from figure 6.1 (section 6.4).

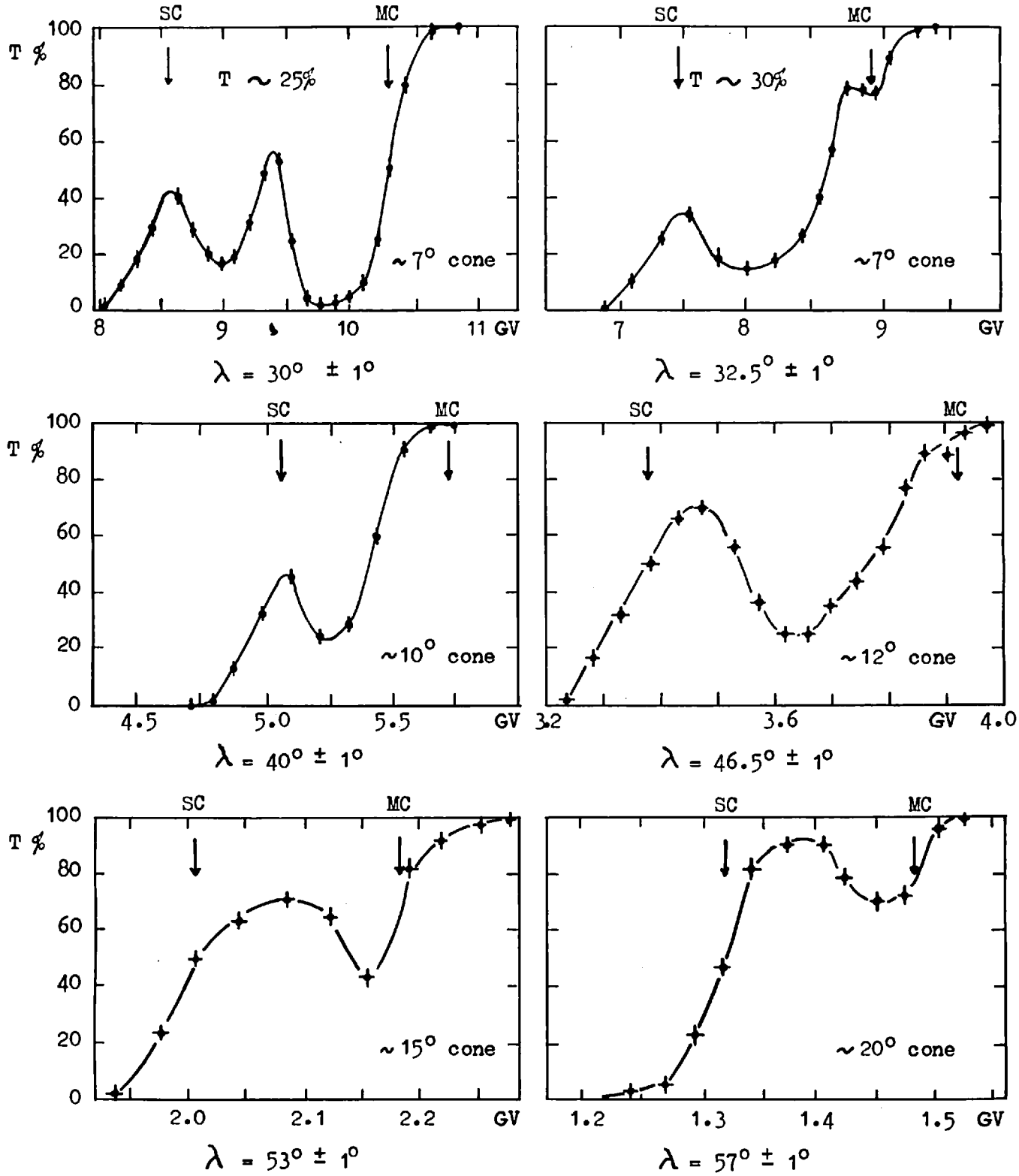

Figure 6.4 Transparency curves for the zenith penumbra at latitudes in the range $30° < \lambda < 57°$.

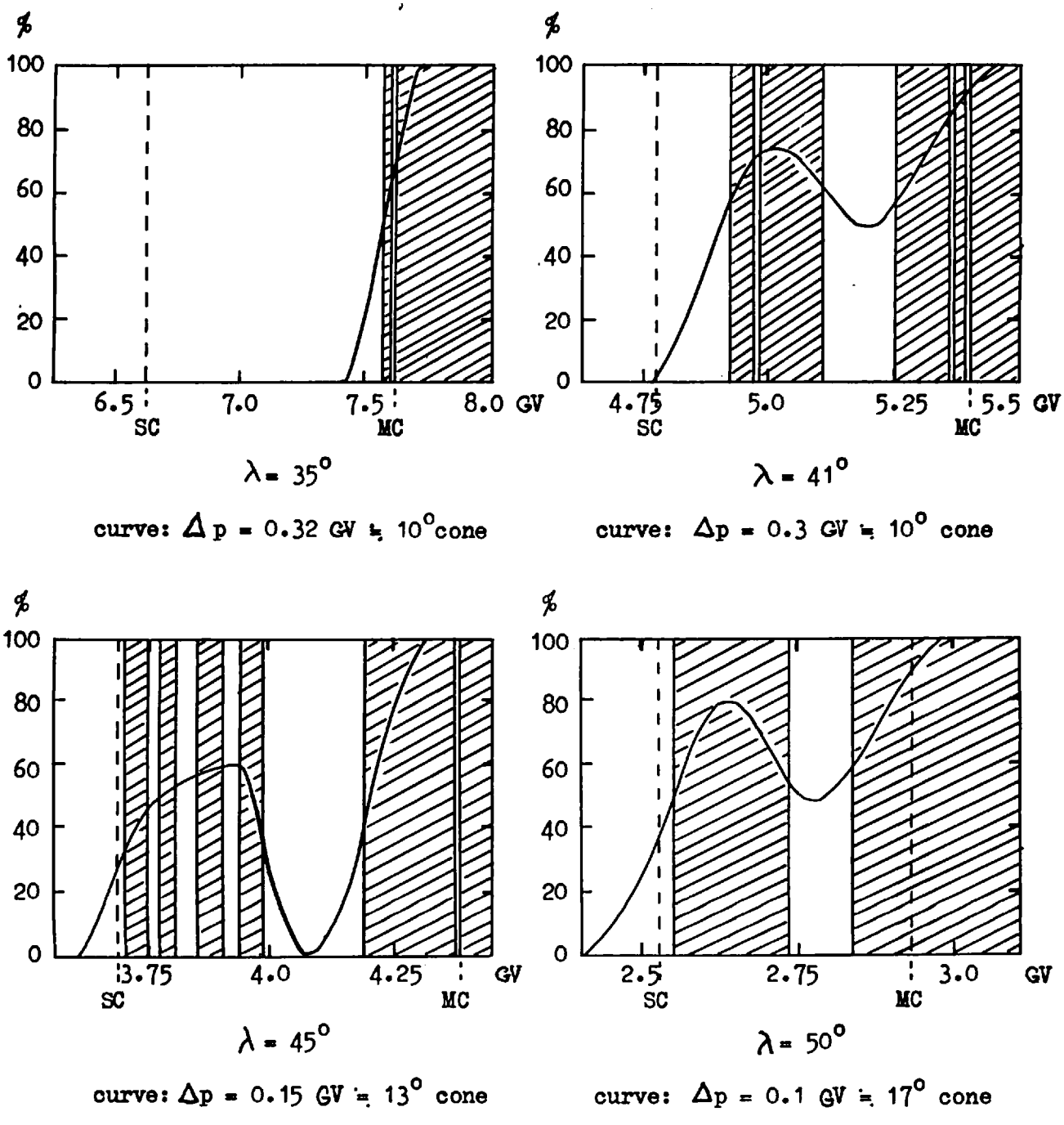

Figure 6.5 Differential transparency as a function of rigidity for line trajectories arriving at the zenith. Curves illustrate the effect of averaging transparencies over given rigidity intervals Δp representing a finite acceptance cone centred at the zenith. (After Schwartz 1958)

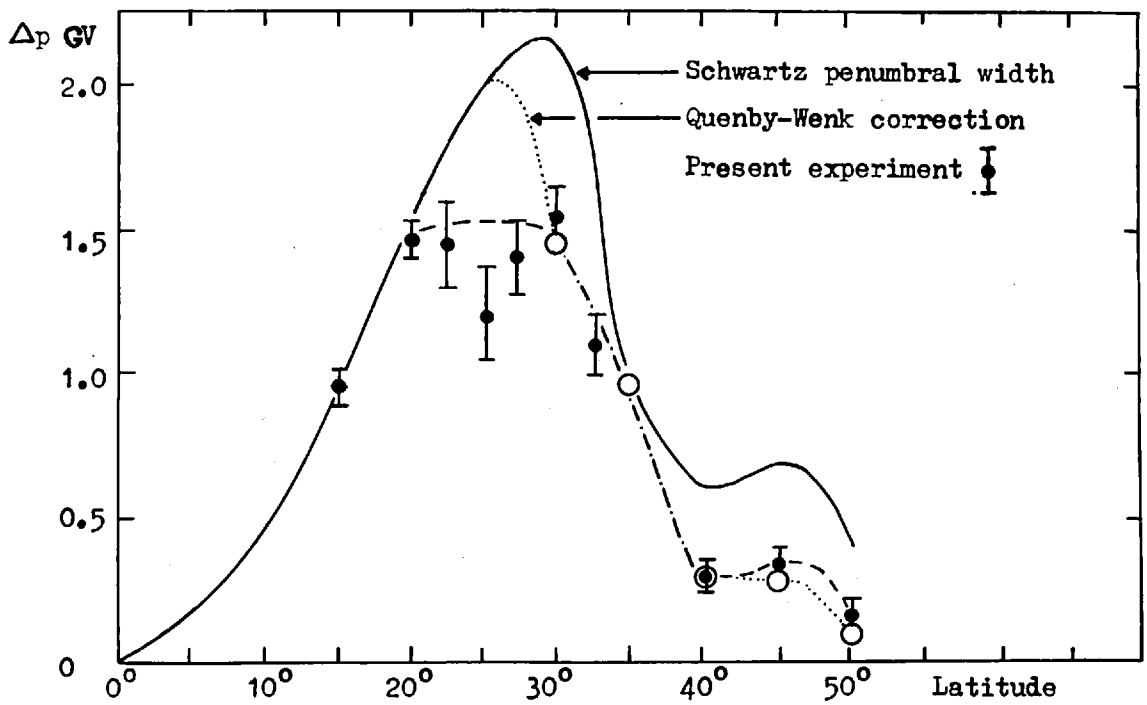

Figure 6.6 A comparison of the penumbral correction obtained in this experiment with the values of Quenby-Wenk and the penumbral width of Schwartz. (section 6.7)

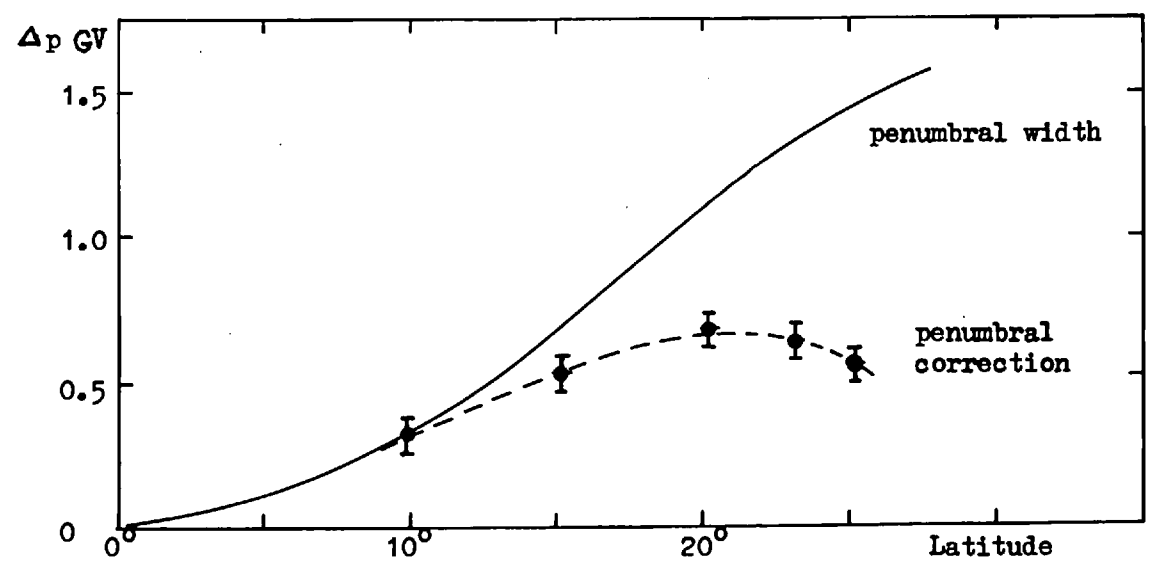

Figure 6.7 The penumbral correction at 1100 km. altitude deduced from the measured transparency and scaled values of the penumbral width of Lemaitre-Vallarta. (section 6.7)

CHAPTER 7

THE THRESHOLD PERTURBATIONS PRODUCED BY SUPERIMPOSING UNIFORM MAGNETIC FIELDS ON A DIPOLE SYSTEM

7.1 General

The first measurements of threshold perturbation demonstrated that the performance of the model agreed with the theoretical predictions (Appendix A) if the superimposed field was parallel to the dipole axis. This result is a useful check on the validity of the method of perturbation measurement since no comparison with theory is possible if the superimposed field is inclined to the dipole axis.

Threshold perturbations were measured for four angles of inclination between the superimposed field and the dipole axis. In each case longitude surveys of the perturbation were performed in the northern and southern hemispheres at latitudes 0°, 25°, 40°, 48° and 53°. This entailed the analysis of more than 500 threshold curves. The study has provided sufficient data to permit the prediction of threshold perturbations to 15% accuracy if a weak uniform magnetic field is superimposed at any angle to the dipole axis.

7.2 The geometry of the model and the generation of the uniform fields

The basic geometry of the model was identical to that used in the penumbral investigation (section 6.2). A similar correction was applied to align the electron beam at the zenith; however, the divergence of the beam was reduced to less than 1° to provide a rapid variation of differential transparency with rigidity near the threshold. This permitted a more accurate measurement of the small perturbations.

The uniform field to be superimposed on the dipole was generated by varying the currents in the degaussing coils. The field was calibrated by the coil and ballistic galvanometer method (section 4.7) and had a uniformity of the order $\pm 2\%$ over the working volume of the tank. The field strength H_M which simulates a given field H_E in the geomagnetic system was calculated from the relation:-

$$\frac{H_M}{H_E} = \frac{\text{(model equatorial field at the radius of the gun anode)}}{\text{(geomagnetic equatorial surface field)}}$$

In the following analysis the longitude at which a given perturbation occurs is specified by an equivalent hour zone. The meridian plane of the model which contains the north pole direction of the superimposed field is defined as the noon meridian. This represents the geometry which exists at the Equinox if a north pole on the Sun produces a field radial to the latter and the angle between the geomagnetic axis and the Earth's rotational axis is ignored.

7.3 The experimental procedure and principal errors

In most cases threshold perturbations could be determined by measuring the voltage displacement of the curves of 'i_t' as a function of 'V' without making corrections for beam current variations. These curves were obtained consecutively for various superimposed field strengths. To establish the stability of the electronic equipment and to ensure an adequate measurement of the position of the unperturbed threshold the first and last curves of the series were obtained in the absence of superimposed field. At each latitude a check was made to ensure that the variation of beam current with voltage and the collection of stray current by the supporting stem were negligible.

It was noticed that changes in the mean transparency of the penumbra

occurred at certain combinations of latitude and superimposed field strength. In each case the magnitude of the transparency change was determined by the construction of the differential transparency curve (section 5.3). These transparency changes are indicated in the discussion of the results (sections 7.4, 7.6).

Two important errors occur in the perturbation measurements. The first is the random error in the measurement of the small displacements of the curves of 'i_t' as a function of 'V'. This is caused mainly by small variations in the gun supply voltages between consecutive voltage scans and by other small electronic instabilities. These effects produce the rigidity errors which are plotted in figure (7.1). The second error occurs in the calibration of the scaled value of the superimposed field strength (section 5.6). This error includes a systematic error of $\pm 5\%$ in the absolute values of superimposed field strength and an additional error of the order $\pm 2\%$ in setting the chosen values of field strength due to current fluctuations in the coil system.

Other errors which include the uncertainties in the absolute values of threshold, in the altitude and latitude of the electron gun and in the mean zenith angle of the electron beam at the surface of the model are negligible compared with the above two errors.

7.4 The threshold perturbations produced by superimposing a uniform magnetic field parallel to the dipole axis

These perturbations were investigated at latitudes 0°, 25°, 40°, 46°, 53° and 57° to check the performance of the model against theoretical prediction. The shape of the differential transparency curve determined whether the perturbation could be measured at the Störmer or main cone positions (figures 6.1, 6.4). Changes in the Störmer threshold could be measured accurately only at latitudes 46°, 53° and 57°.

The measurements at latitude 53° and theoretical predictions of the perturbations produced by superimposed field strengths of 100 γ and 300 γ are presented in figure (7.2). The theoretical values were obtained by the numerical solution of the Störmer equation (Appendix A) and from the curves of Webber (1962). An extrapolation of the line through the experimental points in this figure indicates the field strength which reduces the threshold to zero at this latitude. This field strength is in good agreement with the theoretical values for latitudes 53° and 54° which are indicated in figure (7.2). These two theoretical values were obtained from equation (A.P) (Appendix A).

The perturbations of the main cone threshold at the lower three latitudes are plotted in figure (7.1) together with dash lines which represent the theoretical perturbation of the Störmer threshold (Appendix A equation A.N). Although the difference in the gradients of the theoretical and experimental lines might indicate a small inequality in the magnitude of the perturbations at the Störmer and main cone thresholds, most of this difference could be produced by the calibration error in the superimposed field values.

Increases in differential transparency were observed at latitude 40°. The main increase - from 0% tc ~ 50% for a 100 γ field - occurred near the Störmer threshold. The distortion transformed the differential transparency curve for latitude 40° into a shape which resembled the curve for latitude 30° (figure 6.4). Changes in transparency were absent at the other latitudes for superimposed field strengths less than 500 γ.

7.5 Preliminary experiments with non-axially symmetric field systems

The preliminary measurements of the effects produced by superimposing a uniform magnetic field at various angles to the dipole axis revealed that, to

better than 10% accuracy, the two field components parallel and perpendicular to the dipole axis act independently in producing threshold perturbations. Therefore, the threshold perturbations which would be produced by superimposing a uniform field at any inclination to the dipole axis could be predicted if the perturbations associated with the above two field components were known. Since the perturbations may be predicted satisfactorily if the field component is parallel to the dipole axis (section 7.4) attention was devoted to the measurement of the perturbations produced by superimposing a uniform field perpendicular to the dipole axis.

Observations were made to determine whether the amplitudes of these perturbations are linearly proportional to the strength of the superimposed field. Although the study only included perturbations less than -5% and superimposed field strengths less than 500 γ no deviation from linearity could be detected at any of the latitude positions. The linearity of the relation at latitude 25° is illustrated in figure (7.3).

The change in the sign and amplitude of the threshold perturbation with hour zone and the opposite sign of the perturbation at conjugate points are also illustrated in figure (7.3). A comparable distribution of perturbation was observed at all latitudes except the equator. At the latter position no perturbation could be detected if the superimposed field was accurately perpendicular to the dipole axis - the minimum detectable perturbation was 0.1% for a field strength of 500 γ.

7.6 The threshold perturbations produced by superimposing a 50 γ uniform magnetic field perpendicular to the dipole axis

These perturbations are displayed in figures (7.4) and (7.5). In figure (7.4) the percentage amplitude of the perturbation is plotted as a function of the local hour zone (section 7.2) for latitudes 25°, 40°, 48° and 53°. In

each case a sine curve has been drawn through the experimental points. The amplitude and time of minimum of each curve is tabulated on the right of the figure and the amplitudes are plotted as ● functions of latitude in figure (7.5).

At all latitudes it was noticed that the perturbations had opposite signs at conjugate points. This produces a 12 hr. phase difference between the diurnal threshold perturbation in the northern and southern hemispheres. The curves for the southern hemisphere which correspond to those of figure (7.4) may be obtained from this figure by reversing the signs of the perturbations.

At latitude 25° the superimposed field produced a rigidity translation of the differential transparency curve without changing its shape. Small changes in the shapes of the differential transparency curves at other latitudes complicated the measurement of threshold perturbation by distorting the curves near the Störmer or main cone thresholds. Since the perturbations at these threshold positions rarely differed by more than 10% the general perturbation could be considered, at least to a first approximation, as a simple rigidity translation of the differential transparency curve. This suggests that a cosmic ray detector which has a wide angle acceptance cone would 'see' threshold perturbations which are similar to those of figures (7.4) and (7.5). The sense of the additional changes in threshold produced by these variations in penumbral mean transparency are indicated by the arrows in figure (7.4).

Although the 50 γ field increased the differential transparency by $\sim$ 25% near the Störmer threshold at latitude 40°, this corresponds to an increase of only 5% in mean transparency. A slightly larger increase was noticed at latitude 48°; however, the increase was less than 10% at the position of largest perturbation. These transparency changes are sufficient to distort

the curves of figure (7.4) from the simple sine profile. It was thought more useful to indicate the position and sign of these transparency changes in this figure rather than to correct the curves for this effect since the magnitude of the transparency changes probably is a function of the angle of the acceptance cone of the detector.

7.7 Possible diurnal cosmic ray intensity variations

The diurnal variations of threshold which were described in the preceding section could produce variations in the intensity of the secondary radiation at stations on the Earth's surface. In order to predict the amplitude of these counting rate variations, the change in counting rate produced by a 1% change in threshold must be known as a function of latitude. This has been deduced for sea level nucleon and meson detectors and for mountain altitude nucleon detectors from the tables of Webber and Quenby (1959) (figure 7.7). These results were combined with the values of diurnal threshold change (figure 7.5) to obtain the amplitude of the diurnal counting rate variation which would be produced by a 10 γ uniform field perpendicular to the dipole axis (figure 7.6).

The field geometry represented in figure (7.6) occurs at the Equinox if the 10 γ field is directed radially away from the Sun. The diurnal variations at the Solstice for the same field geometry would be reduced in amplitude by the factor cos 22.5° (~ 0.92). Provided the 10 γ field did not reverse in sense, the phase of the variation at each latitude would be constant in solar time for this radial field model. Alternatively, if the 10 γ field is perpendicular to the ecliptic plane and has constant sense the amplitudes of the diurnal variations would be reduced by the factor cos 67.5° (~ 0.38) but the phase of the variation would be constant in sidereal time.

Although this contribution to the diurnal variation in the cosmic ray intensity is probably small compared with other diurnal effects, the characteristic distribution of phase over the Earth's surface may assist its detection. This aspect of the problem is discussed in chapter 9.

7.8 Summary and suggestions for further work

The application of a uniform magnetic field at various angles to the dipole axis of the model has revealed that the threshold perturbations may be divided into two groups. These contain:-

a) longitude dependent perturbations which are produced by the magnetic field component perpendicular to the dipole axis. A study of the characteristics of this group has permitted the prediction of possible diurnal variations in the intensity of the secondary nucleon and meson components of the cosmic radiation at the Earth's surface.

b) longitude independent perturbations which are produced by the magnetic field component parallel to the dipole axis. The magnitudes of these perturbations agree with the theoretical predictions (Appendix A).

Since the above two field components produce independent perturbations (section 7.5) the present measurements permit the prediction of threshold perturbations for any orientation of the superimposed field relative to the dipole axis.

A future extension of this work could be directed towards discovering the magnitude and phase of the longitude dependent threshold perturbations 'seen' by a large angle acceptance cone. The principal difficulty in this work is likely to be the accurate detection of the small changes in threshold since the differential transparency of the penumbra changes relatively slowly with rigidity for this type of acceptance cone.

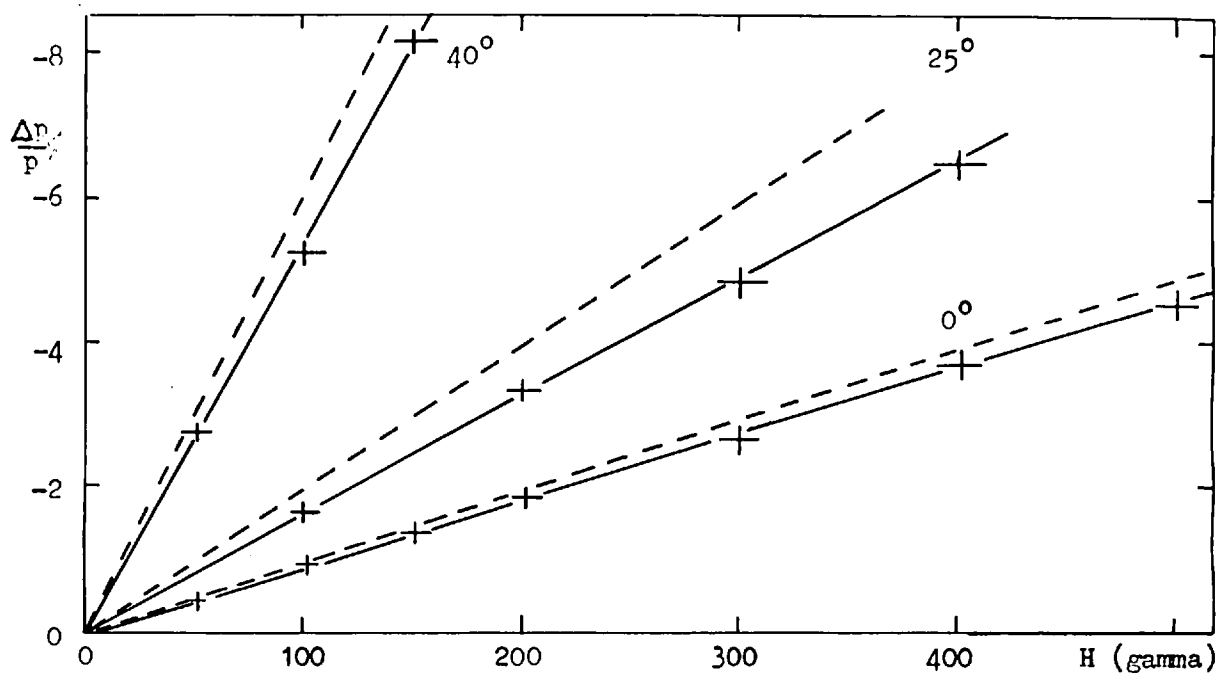

Figure 7.1 Measured percent reduction of threshold at three latitudes as a function of superimposed field strength for a uniform field antiparallel to the dipole equatorial field. The dash lines represent the theory of Appendix'A' (section 7.4)

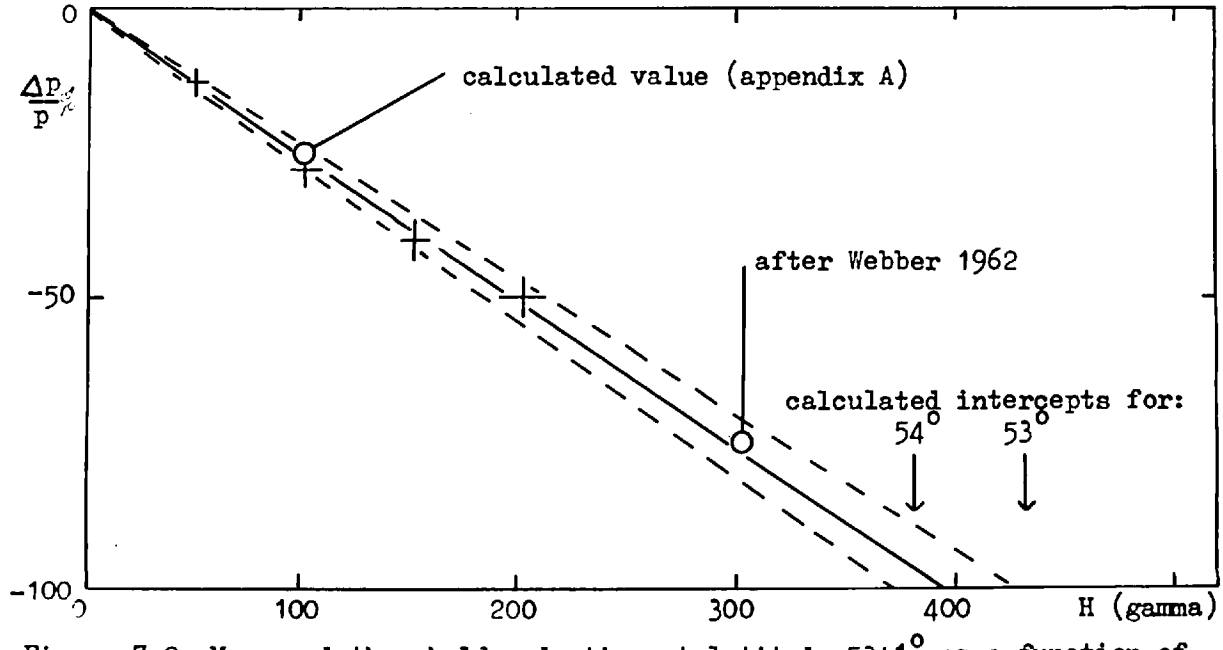

Figure 7.2 Measured threshold reduction at latitude $53\pm1^{\circ}$ as a function of superimposed field strength for a uniform field antiparallel to the dipole equatorial field showing the agreement with the theory of Appendix 'A'. (section 7.4)

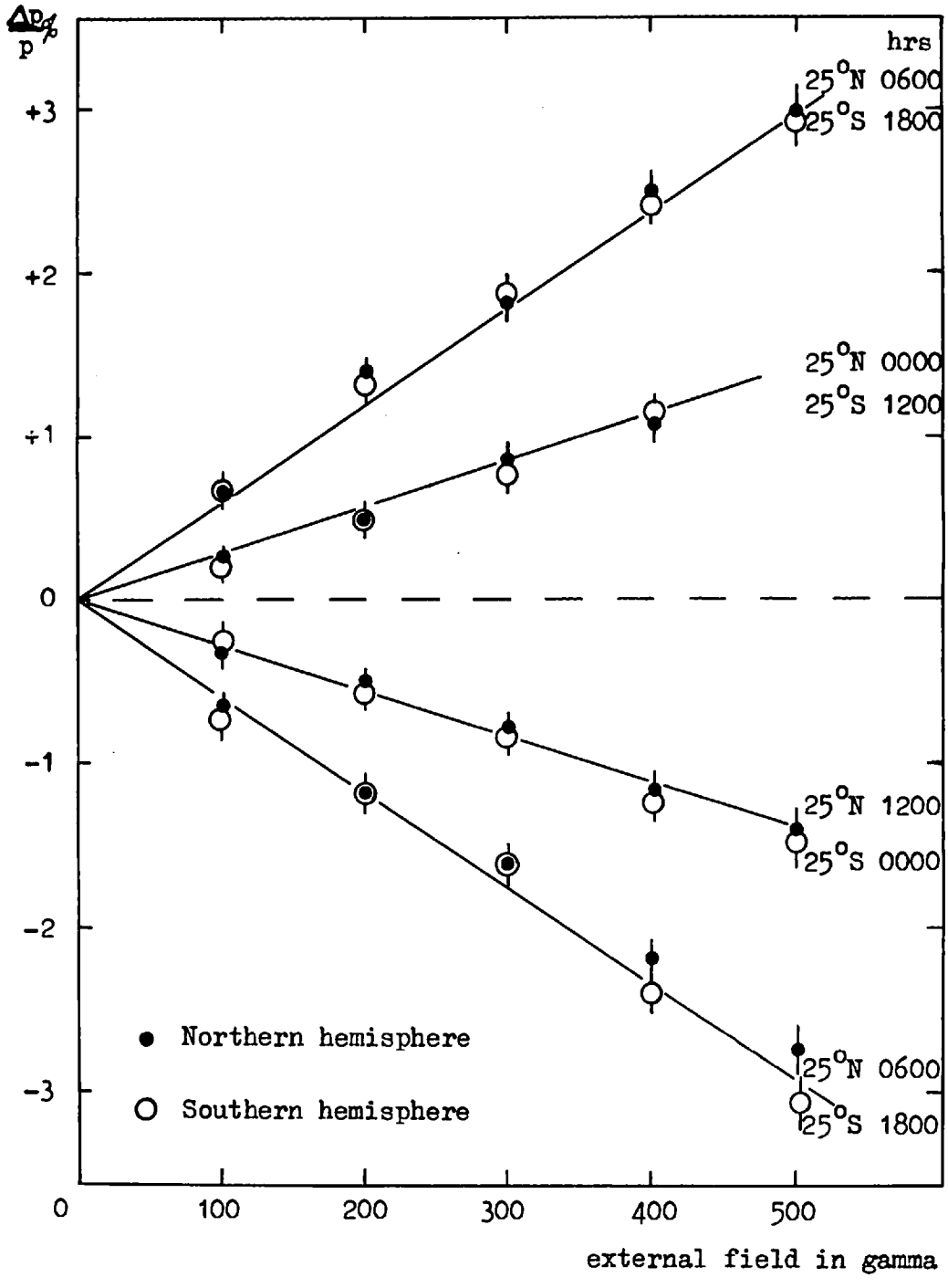

Figure 7.3 Specimen graph obtained at latitude 25° showing percentage change of threshold as a function of field strength for a uniform magnetic field perpendicular to the dipole axis (section 7.5).

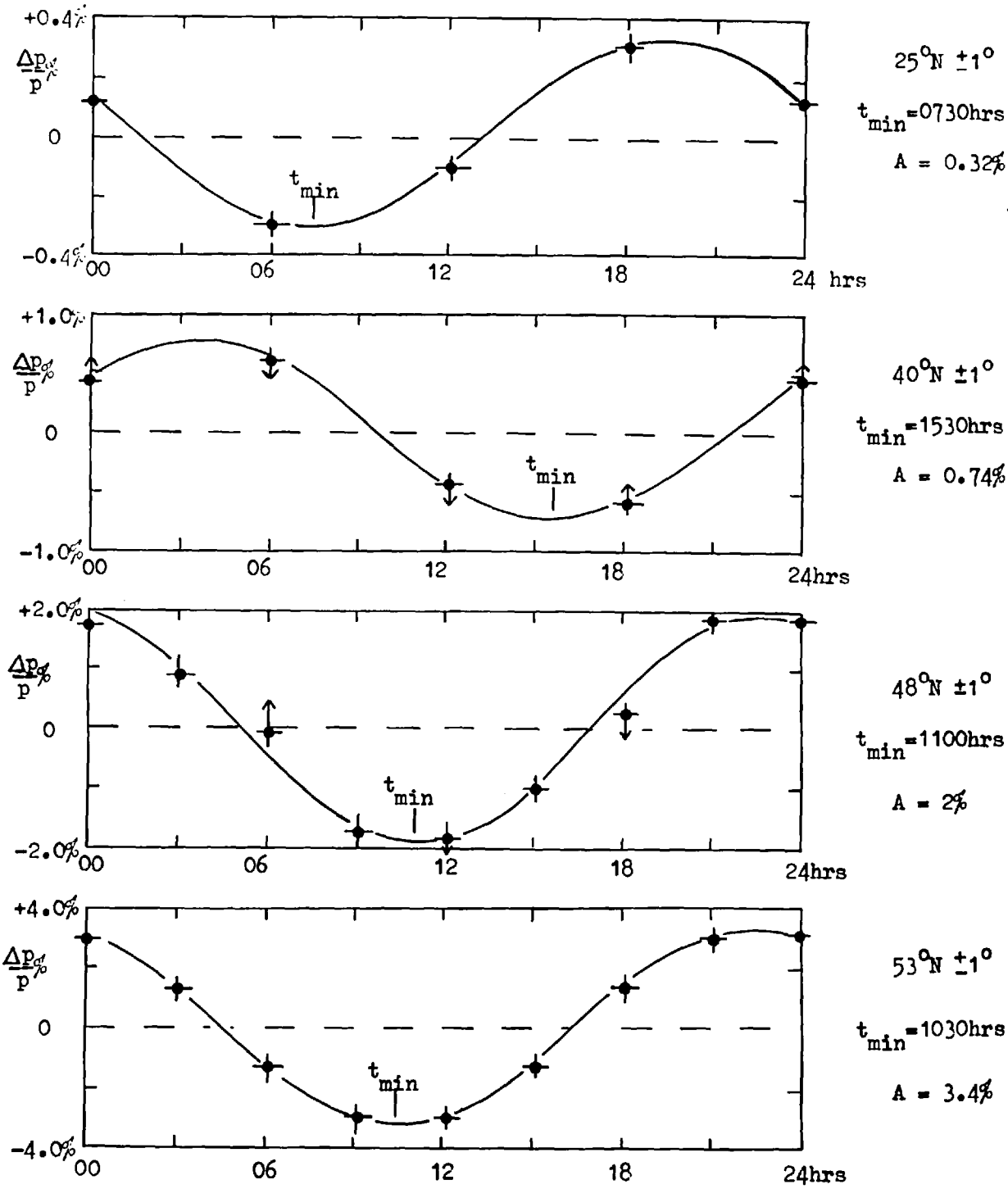

Figure 7.4 Experimental percentage threshold change for a 50γ uniform field perpendicular to the dipole axis. The North pole direction of the superimposed field is at the 12hrs meridian. The threshold change at the equator is less than 0.01%. (section 7.4)

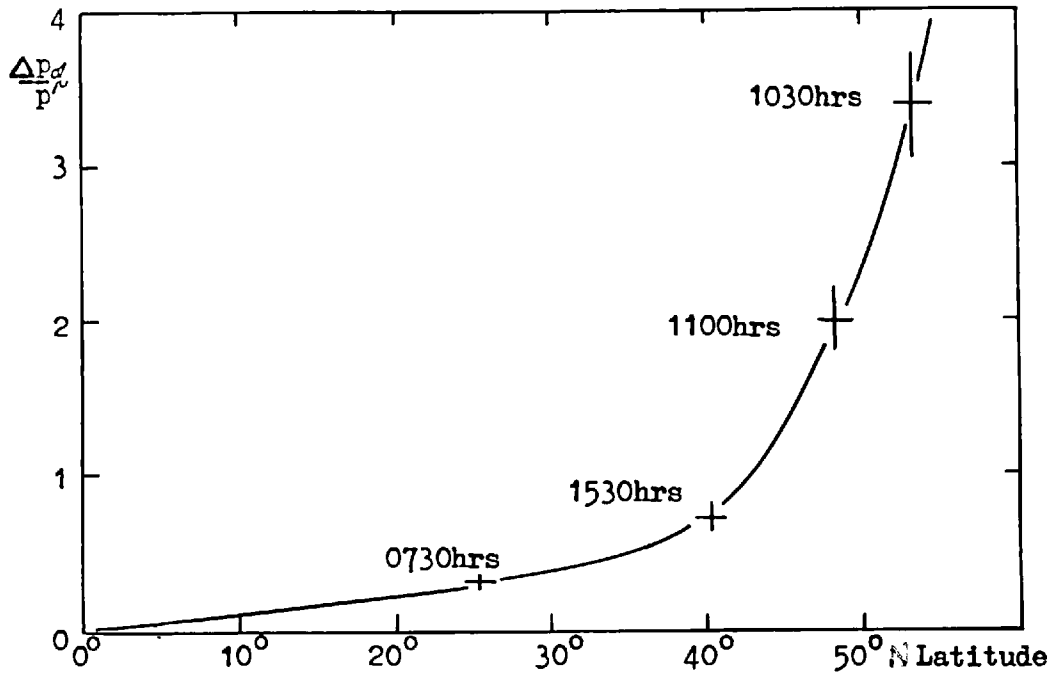

Figure 7.5 The amplitude of the cyclic threshold change shown for a 50 γ field in Figure 7.4 as a function of latitude. The times quoted are the times of minimum threshold at the latitudes corresponding to the experimental points.

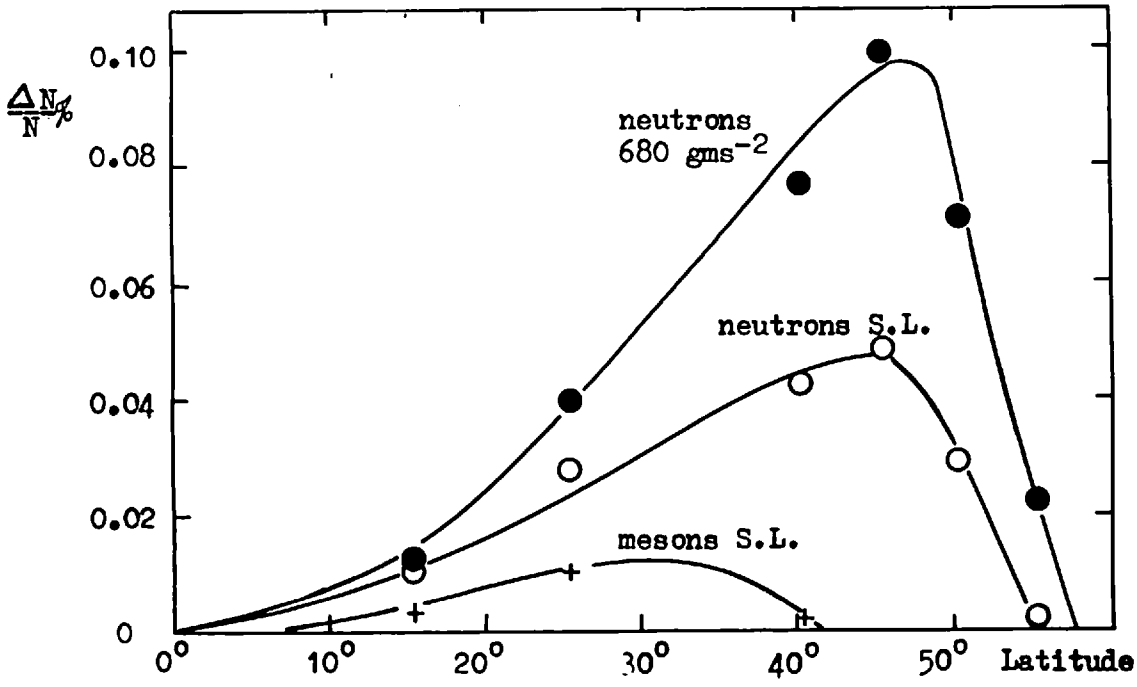

Figure 7.6 Predicted amplitude of the diurnal counting rate variation as a function of latitude for a 10γ uniform field perpendicular to the dipole axis.

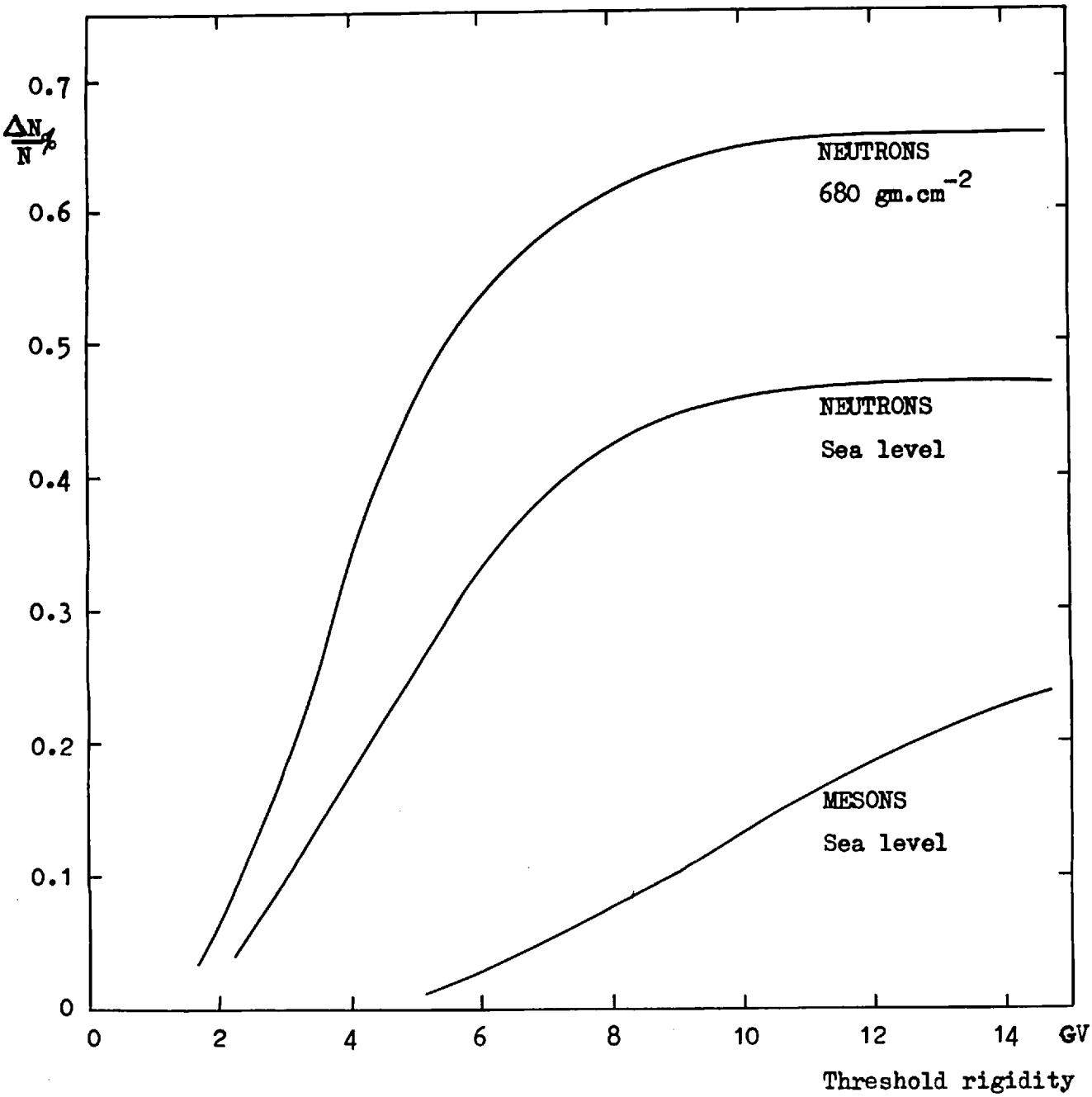

Figure 7.7 Percentage change in counting rate produced by a 1% change in threshold as a function of normal threshold rigidity (section 7.6).

CHAPTER 8

THE THRESHOLD PERTURBATIONS PRODUCED BY MAGNETOSPHERIC 'RING CURRENTS'

8.1 General

The theoretical analyses of Treiman and Ray (section 2.5) predict approximate values for the threshold perturbations which would be produced by a magnetospheric trapped particle system if this system is symmetrically distributed with respect to the geomagnetic axis. Theoretical information on the additional perturbations which might be produced by the asymmetric distortion of this system is not available. The measurements reported in this chapter are the results of a preliminary investigation of this problem.

Since time limited the range of measurements which could be attempted, attention was focussed on the interesting conditions which occur when the control of access of cosmic ray particles to the Earth is transferred from one of the passes between the Störmer forbidden regions to the other (section 2.5). These conditions are interesting for two reasons. The first is that this transfer of control occurs when the 'ring current' is situated between the two passes. Therefore these conditions are probably the most sensitive to perturbations which are caused by a longitude variation of the radial coordinate of the 'ring current'. The second reason is that, for the most probable 'ring current' strength and geometry, the transfer of control occurs at a latitude of observation between 50° and 60°. Although figure (7.7) indicates that neutron monitors are relatively insensitive to threshold perturbations at thresholds less than 3 GV, the large amplitudes of the possible perturbations and the good longitude dispersion of the observing

stations at these latitudes are favourable to the detection of longitude dependent perturbations. In addition, the direct measurement of the threshold during geomagnetic disturbances by balloon instrumentation is not too inconvenient in this latitude region.

Except for the introduction of the ring current structure, the geometry of the model was similar to that used for the observation of the penumbra at latitudes larger than 40°. Intersections between the stem and the Störmer inner allowed region were eliminated by mounting the magnetic axis of the model parallel to the stem (section 6.2).

8.2 The preliminary experiments

The magnetic field of the model 'ring current' should represent the field of a real trapped particle system most accurately near the equatorial position of maximum particle density since the field strength of the 'ring current' reaches a value which is comparable with the local strength of the geomagnetic field in this region. This condition is extremely difficult to fulfil because it requires the use of a large number of currents, some of which must be placed in the Störmer inner allowed region. The wires which carry these currents and their supports present a large obstruction to the electron beam of the model.

Experiments were performed to investigate the extent of this obstruction for a single wire loop. Ray's data (1956) were used to select a geometry which would permit threshold measurements at large latitudes where the outer pass controls the particle motion. An equatorial ring of radius equal to five times the model radius was chosen and the current in the ring was adjusted to simulate a 100 γ reduction in the Earth's equatorial surface field. This 'ring current' would produce a rapid change of slope in the 'ring current' curve of figure (2.4) near latitude 49° and threshold observations should be possible

with the model at latitudes less than 56°.

The threshold perturbations which were produced by this ring current at latitudes less than 45° were in excellent agreement with Ray's predictions. Near latitude 49°, however, the differential transparency curve became badly distorted and a large stray current was collected by the ring structure. This distortion was sufficient to make the determination of the threshold impossible.

It was noticed that, at latitudes less than 49°, the ring structure collected stray current only when the rigidity of the electron beam was larger than the local threshold but that this was not the case at latitudes larger than 49°. This was interpreted as indicating that the inner pass was located within the ring structure and that this pass controlled the electron motion at latitudes less than 49°.

It might be possible to simulate the magnetic field of a trapped particle system without obstructing the electron beam by placing the currents in the Störmer forbidden regions. Time prevented an analysis of this possibility.

8.3 Technical problems

Since it was inconvenient to provide large currents it was necessary to use approximately 30 turns of wire in the ring current structure. The difficulty of supporting these in the vacuum tank with the minimum obstruction of the electron beam was overcome by threading insulated wire inside a glass tube which was bent to the shape required. This tube was suspended by thin wires from ceramic insulators in the top of the vacuum tank. To prevent excessive outgassing P.T.F.E. coated wire was inserted in the tube and the aperture in the tube was sealed with Picein wax.

A coating of colloidal graphite (Aquadag) on the outside of the glass

tube made electrical contact with the wire suspension. This permitted the measurement of the stray current which was collected by the structure. This arrangement was particularly convenient because the power supply for the 'ring current' could be connected to the vacuum tank to avoid the introduction of stray voltages.

A typical ring structure of this type is shown in figure (8.1).

8.4 The experimental results

In view of the difficulties discussed in section (8.2) the investigation was restricted to a determination of the longitude variation of the perturbations which were produced by an asymmetric 'ring current' when the inner pass limited the electron motion. Under these conditions the obstruction of the electron beam was eliminated except at rigidities greater than the threshold and the performance of the model was adequate to permit reliable measurements of the threshold perturbations.

A plan view of the geometry of the asymmetric 'ring current' is shown in figure (8.2). The dimensions of the current loop were chosen to represent approximately the equatorial section of the theoretical magnetosphere of Beard and Jenkins (chapter 9); however, the radial extent of this loop was limited by the dimensions of the vacuum tank. Figure (8.1) illustrates the appearance of the complete model.

This loop should produce the largest longitude variation of threshold perturbation at a latitude of observation which places the Störmer pass near the radial position of the 'ring current'. Therefore, the electron gun was placed at latitude 48° since this locates the inner pass on a circle which is 2 cm. smaller in radius than the minimum radius of the loop. The fact that no stray current was collected by the ring structure at rigidities less than

the threshold verified that the loop did not enter the inner allowed region.

Figure (8.3) shows the longitude dependence of the threshold perturbation at latitude 48°. The longitude coordinates are expressed in terms of hour zones and the noon position occurs at the minimum radius of the loop. At each hour zone the perturbation has been calculated by taking the mean of the two perturbations which were measured at the Störmer and main cone threshold positions. The indicated errors of $\pm 10\%$ are based on an estimate of the uncertainties which were produced by variations in penumbral transparency and by small differences between the perturbation amplitudes at these two threshold positions. The perturbations have the same phase in both hemispheres.

In obtaining data for figure (8.3) the current in the loop was adjusted to produce a threshold perturbation at the 12 hr. position which equalled the amplitude of the perturbation which would be produced at this latitude by superimposing a 25γ uniform field parallel to the geomagnetic dipole axis. The ratio between the percentage perturbations at the 12 hr, and 00 hr. positions was determined for loop currents which corresponded to uniform field strengths of 25γ, 50γ and 100γ. This ratio was found to be 1.5 ± 0.1 to 1 for the three values of current.

The distribution of the experimental points in figure (8.3) suggests that the maximum reduction of threshold occurs approximately two hours earlier than the noon position at this latitude. Since the trajectories which arrive at a latitude of the order 50° cross the pass at a longitude to the east of the arrival point, this behaviour might be expected if it is assumed that the largest perturbation of the trajectories occurs near the pass.

8.5 Conclusions

These measurements have demonstrated that an asymmetric distortion of the

'ring current' may produce threshold perturbations which vary appreciably with longitude. This variation is probably a maximum at the latitudes which correspond to a position of the pass close to the equatorial position of maximum 'ring current' particle density. Since the radial distance of the pass varies rapidly with the latitude of observation, 'ring currents' which are located between 4 and 12 Earth radii from the geomagnetic axis would produce a maximum longitude variation of threshold at a latitude between 45° and 65°. This variation should be small near either the equator or the pole.

The amplitude of the diurnal threshold variation is proportional to the magnetic field strength of the 'ring current'; however, the ratio of the maximum to the minimum percentage reduction of threshold is independent of this field strength. The diurnal threshold variation is presumably a function of the geometry of the 'ring current'. No information on this subject was obtained.

Although this investigation has been very brief, it is thought that these observations indicate some of the characteristics which may be used to recognise the existence of an asymmetric geomagnetic 'ring current'. In future experiments the possibility of placing the 'ring current' wires in the Störmer forbidden regions should be studied. By avoiding the obstruction of the electron beam, this would permit a better measurement of the perturbations which are produced by asymmetric current distributions especially when the outer pass controls the electron motion.

Figure 8.1 The 'ring current' of Figure 8.2 mounted in the vacuum tank.

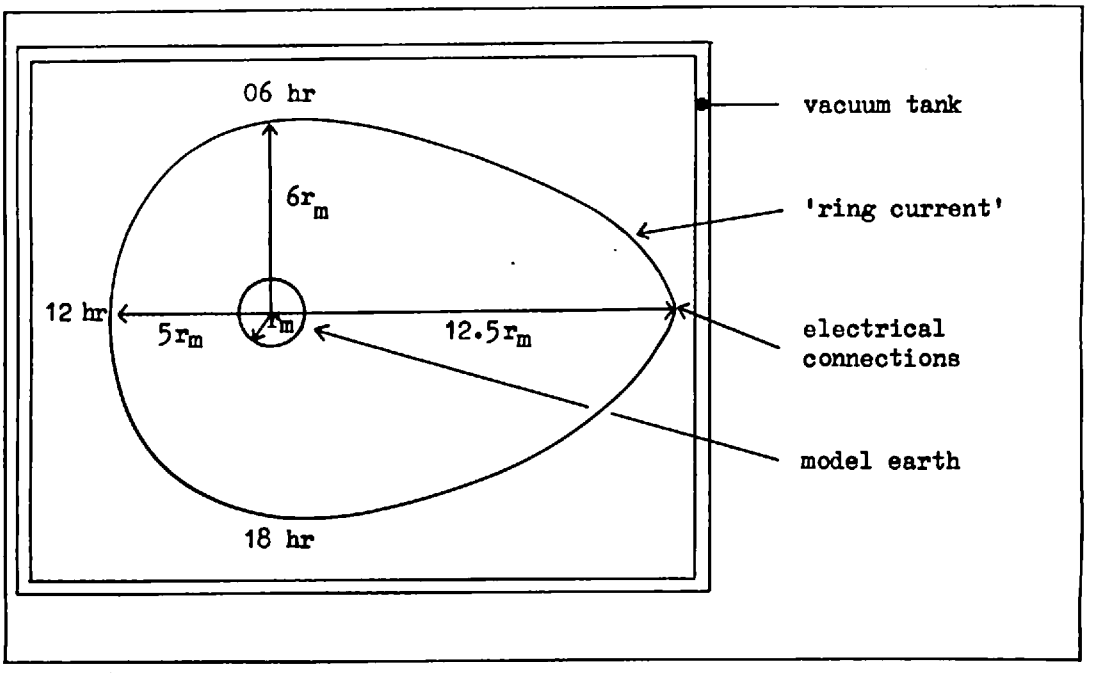

Figure 8.2 Plan of the equatorial section of the tank and model showing the geometry of the asymmetric current.

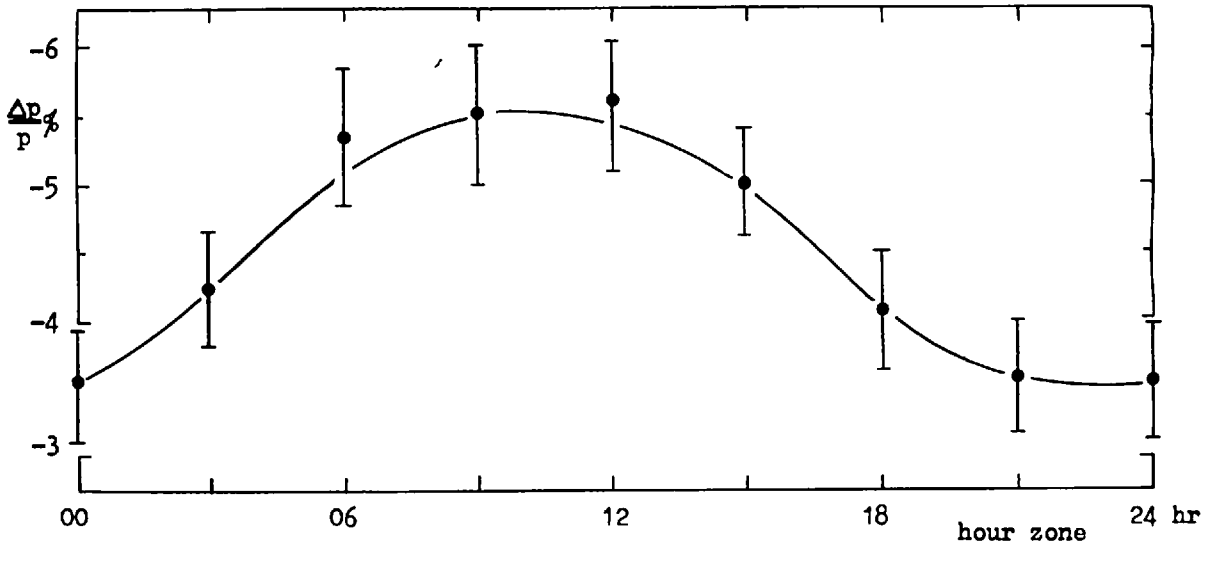

Figure 8.3 The threshold perturbation as a function of longitude for the asymmetric ring current above.

CHAPTER 9

COMMENTS ON THE APPLICATION OF THE PERTURBATION MEASUREMENTS TO THE COSMIC RAY PROBLEM

9.1 Introduction

The measurements which were reported in the preceding two chapters have demonstrated that important longitude variations of threshold may occur if the magnetospheric field possesses longitude asymmetry. In addition, since the magnetic fields which were superimposed on the model were approximately three orders of magnitude smaller than the magnetic field at the surface of the model these measurements also reveal the sensitivity of the thresholds to the distortion of the magnetic field near the Störmer pass. Since only simple field geometries have been simulated in this experiment it is appropriate to consider how the magnetospheric field differs from the model field.

9.2 Magnetospheric distortion and the threshold rigidities

Theory (e.g. Beard 1960, 1962, Spreiter and Briggs 1962, Beard and Jenkins 1962, Midgley and Davis 1962, 1963, Spreiter and Hyett 1963, Spreiter and Jones 1963) and practical observation (e.g. Cahill and Amazeen 1963, Smith, Sonett and Dungey 1963, Heppner et. al. 1963) indicate that the geomagnetic field is confined within an approximately egg shaped cavity by the pressure of the solar plasma stream (c.f. Bierman 1957, Parker 1961, Blackwell and Ingham 1961, Bridge et. al. 1962, Neugebauer and Snyder 1962). In addition a region of turbulent magnetic field and plasma which has a radial thickness of several Earth radii exists outside the magnetospheric boundary (Cahill and Amazeen 1963).

The existence of this magnetospheric boundary must produce serious

perturbations of the geomagnetic threshold rigidities when the Störmer pass is located near the boundary. This is confirmed by the work of Obayashi (1961) who has shown that the threshold rigidity is increased by an order of magnitude at latitude 80° and by a factor of two at latitude 65° if the geomagnetic field is terminated at a geocentric distance of ten Earth radii. Unfortunately the real geomagnetic field differs considerably from the axially symmetric field of Obayashi and some geomagnetic flux might 'leak' through the magnetospheric boundary, especially in the night hemisphere. This could reduce the thresholds to zero at some longitudes in the polar regions.

It is probable that the existence outside the magnetospheric boundary of a region of turbulent magnetic field and plasma prevents the access of any large scale regular interplanetary field to the inner maghetosphere. Therefore the present measurements and the theoretical predictions of figure (2.5) cannot be used directly to interpret experimentally observed threshold perturbations in terms of the strength of a regular interplanetary field. However, the current which may flow on the surface of the magnetospheric boundary might produce a magnetic field within the cavity which has a large scale uniformity and consequently would produce regular threshold perturbations. The present results provide a useful guide to the way in which the latter threshold perturbations are distributed on the Earth's surface.

The observation by Davis and Williamson (1962) (c.f. Akasofu and Cain 1962, Akasofu 1963) of a large flux of protons at an equatorial geocentric distance of approximately three Earth radii suggests that the 'ring current' may be situated at a smaller geocentric distance than was estimated earlier (c.f. Akasofu, Cain and Chapman 1961, Apel, Singer and Wentworth 1962). This is in agreement with the work of Akasofu and Lin(1963) also Akasofu, Chapman and Venkatesan(1963).

If in fact the 'ring current' is located at a geocentric distance between two and three Earth radii the discontinuity of the ring current curve of figure (2.4) would occur at a latitude of approximately 40°. Thus, since the threshold perturbations which are produced by the presence of the magnetospheric boundary or by weak superimposed uniform magnetic fields are small at this latitude, a knowledge of the latitude dependence of the experimentally observed perturbations might permit the identification of the ring current effects.

9.3 Concluding remarks

The perturbation measurements which were reported in chapters 7 and 8 have revealed the complexity of the threshold perturbations which accompany the asymmetric distortion of the magnetosphere. In particular the longitude dependent perturbations are interesting because, in the absence of an enhanced flux of relatively low energy solar flare particles, threshold perturbations which have a diurnal variation are more easily detected than perturbations which are longitude independent. In addition, the characteristic opposite phase of the perturbations at magnetically conjugate points which is produced by the asymmetric uniform fields enables this type of longitude dependent perturbation to be distinguished from the longitude dependent perturbations which accompany an asymmetric 'ring current'. Therefore these results demonstrate the need for correlation between threshold perturbations which are observed at many different longitudes and latitudes in the analysis of geomagnetic storm phenomena. Ideally, threshold perturbations should be measured at a minimum of two pairs of conjugate points which are separated in longitude by approximately 180°.

The possibility of simulating the asymmetric magnetosphere in the model

is worth further study. An attractive method would be to place a second dipole outside the vacuum tank on the 'sunward' side of the model to compress the model field in this direction. The moment of this dipole must have the same sign as the moment of the model. The 'night side' of the model field could be extended by placing a third dipole of opposite sense on this side of the model at a suitable distance. Additional weaker dipoles could be used to adjust the compression of the model field in the morning and evening sectors. This method has the advantages that the field at a given point may be calculated relatively easily and that the electron beam within the vacuum tank is unobstructed.

It will be interesting to see if the large diurnal threshold variations at latitudes of the order 50° which are predicted by the present experiment are found in this more accurate simulation of the real magnetosphere.

CHAPTER 10

A MODEL TRAPPED PARTICLE SYSTEM ?

10.1 Introduction

When the penumbra was observed at latitudes larger than 50° an unexpected instability appeared on the differential transparency curve at rigidities just less than the Störmer threshold. This may be seen in the photograph of the oscilloscope threshold display (figure 10.1). No similar phenomenon occurred at latitudes less than approximately 50°.

An analysis of the electronic circuitry demonstrated that this instability could not be attributed to the presence of faulty electrical connections, oscillation in the display device or oscillations in the model system which might be produced by electron transit time effects. Therefore the possibility that the instability was produced by the trapping of secondary electrons or ions in the model field was investigated.

10.2 The experimental observations

The electron current which was returned to the surface of the model (i_t in figure 4.5) was observed with an oscilloscpoe as the electron accelerating voltage 'V' was increased slowly by hand from a value considerably less than the Störmer threshold value. When the value of 'V' approached the Störmer threshold it was noticed that 'i_t' contained an a.c. component which looked similar to electronic 'noise' and had an amplitude which was equal to a few percent of the d.c. component.

At a few values of 'V' near the Störmer threshold one frequency component became predominant. This is illustrated in figure (10.2). The frequency of this a.c. component is approximately 8 kc/s; however, by slightly varying the

voltage 'V' several discrete frequencies in the range 8 - 10 kc/s could be excited. No a.c. component could be detected when the value of 'V' was larger than the main cone threshold value.

When these discrete frequencies were excited an a.c. voltage was induced on a metal foil which was attached to the glass window of the vacuum tank (figure 4.6) and on a thin wire which projected into the vacuum tank in the equatorial plane of the model. A large voltage was induced on the wire only if the latter entered the working volume of the tank. This voltage was a maximum if the wire reached to within three model radii from the surface of the model. These voltages were applied to a radio receiver and via an amplifier to a loudspeaker.

It was noticed that, when the frequencies of approximately 10 kc/s were excited, the radio receiver detected a large increase in 'noise' at frequencies between 800 and 900 kc/s. There was a smaller increase in noise at harmonically related frequencies between 1.5 and 10 mc/s. No noise could be detected at approximately 450 kc/s. Some unstable tones at frequencies between 1 and 2 kc/s were detected. These were relatively small in amplitude and, using the oscilloscope display as a guide, were attributed to beats between the larger frequency components.

Changes in the frequency of the 8 - 10 kc/s component could be produced by varying the accelerating voltage 'V', the electron beam current, the current in the degaussing coils, the strength of electric fields in the vacuum tank and the gas pressure in the tank. In most cases the relation between the frequency and a given variable could be determined only qualitatively because the other variables could not be stabilised with sufficient accuracy. However, it was apparent that the discrete frequencies were most sensitive to small changes in

the degaussing coil current and in the voltage 'V'.

The r.f. 'noise' which was detected by the radio receiver was insensitive to changes in any of the variables provided that the frequency of approximately 10 kc/s was present. Small changes in the frequency of this r.f. component could not be detected because of the large band-width of the noise spectrum (approximately 100 kc/s).

The experimental observations may be listed:-

1) The principal frequencies of oscillation were in the ranges 8 - 10 kc/s and 800 - 900 kc/s. Several discrete frequencies in the l.f. range could be excited by adjusting the accelerating voltage 'V'.

2) The application of a potential of +10 volts to the surface of the model produced a 10 - 20% decrease in the frequencies of the discrete l.f. components.

3) Although the discrete frequencies could be excited only by selecting suitable values of the accelerating voltage 'V', the exact relation between these frequencies and this voltage could not be determined because changes in the latter varied the frequency in an irregular series of steps. Small irregular changes in frequency also were produced by large changes in the electron beam current.

4) The presence of magnetic field strengths of the order 10^{-2} gauss in the vacuum tank produced changes of approximately 10% in the frequencies of the l.f. components. The variation of frequency was irregular.

5) An increase in the gas pressure in the tank increased the frequency of l.f. oscillation by a few percent but oscillation was prevented if the gas pressure was larger than 5×10^{-6} mm. Hg. - five times the normal working pressure.

6) Oscillation could be prevented by placing a metal baffle in the equatorial plane of the model at a distance of four model radii from the model. The baffle was approximately three model radii square and was connected electrically to the tank. Oscillation also was prevented if the baffle was placed symmetrically about the equator in a meridian plane of the model. The prevention of oscillation was independent of the longitude of the baffle relative to the electron gun and both l.f. and r.f. components were removed.

7) The amplitude of the a.c. voltage which was induced on a wire which projected into the model field was largest when the wire projected equatorially into the field to an 'L' value of between three and five.

It will be noticed that observations 4) and 6) indicate that the oscillatory effects did not occur in the electron gun since if this were the case the presence of the baffle or the relatively weak magnetic fields would not affect the oscillation.

10.3 A possible explanation

The rigidities of particles which may be trapped in orbits of the Van Allen type were distinguished from the larger rigidities which correspond to periodic Störmer orbits by projecting one cycle of the particle orbit into the equatorial plane of the model. It was thought that particles which had a 'projected gyroradius' which was larger than the radius of the model would be unlikely to provide a trapped particle system which could produce the observed oscillations.

Singly charged ions with atomic weight larger than 10 must possess energies less than 0.1 eV to fulfil the above trapping condition. Since ions with these energies have characteristic oscillation frequencies in the model

which are less than 1 kc/s, trapped ions may be eliminated as a possible source of the observed oscillation. Similarly the oscillation is not related to the cyclotron frequencies of ions or electrons in the model field since these frequencies are less than 1kc/s or larger than 3 mc/s respectively. There is a possible exception in that ions which describe the circular equatorial Störmer orbit may produce a frequency of approximately 10 kc/s. Since this orbit is unstable and lies entirely within the inner Störmer forbidden region where the electron beam cannot produce ionisation this orbit is an unlikely source of the observed phenomenon.

The consideration of the size of the gyroradius indicates that electrons with energies less than 5 eV may be trapped in Van Allen type orbits. The most important source of low energy electrons in the model is the secondary emission which occurs where the primary electron beam returns to the surface of the model. These electrons have a relatively small mean free path and probably lose energy rapidly by collisions with gas molecules until their energies fall below the minimum excitation potential of the gas molecules. Since there is a large partial pressure of oil vapour in the vacuum system the oil molecules, which have a small minimum excitation potential and large collision cross-section, dominate in collision effects. Thus an abundance of electrons with energies less than 1 eV might be expected.

The large flux of electrons which struck the model in the 'horns' of the inner Störmer allowed region produced dark lines on the graphite surface (figure 10.3). One of these lines passes through the position of the electron gun anode and both have widths of approximately 1 mm. which is considerably less than any of the ion gyroradii. The two local patches of more intense darkening are probably impact points of the primary electron beam.

A comparison with the threshold measurements indicates that these dark lines follow the contours of constant effective threshold.

The existence of these lines is thought to indicate that appreciable secondary emission probably occurs at the surface of the model and that this secondary emission is uniformly distributed in longitude.

Assuming that the low energy secondary electrons which are produced near the model are trapped on the magnetic field line shell which passes through these dark lines ($L \fallingdotseq 3.7$) the drift and mirror periods of these particles may be associated with the observed frequencies. Elliot's equations (Elliot 1963) indicate that an electron of energy E eV in the model possesses mirror and drift frequencies f_m and f_d which are related to the L value of the magnetic shell on which they are trapped by the equations:-

$$\left.\begin{aligned} f_m &\fallingdotseq 3.26 \times 10^6 \frac{E^{\frac{1}{2}}}{L} \quad / \text{sec} \\ f_d &\fallingdotseq 10^4 \, L \, E \quad / \text{sec} \end{aligned}\right\} \text{ for small E}$$

If 'L' and 'E' are eliminated alternately from these equations:-

$$E^{3/2} \fallingdotseq \frac{f_d \, f_m}{3.26 \times 10^{10}}$$

$$L^{3/2} \fallingdotseq 3.26 \times 10^4 \frac{f_d^{\frac{1}{2}}}{f_m}$$

If the observed frequencies of 850 kc/s and 9 kc/s are identified with $2f_m$ and f_d respectively, the values $L = 3.76$, $E = 0.24$ eV are obtained. This is in good agreement with the postulate that the magnetic field shell $L \fallingdotseq 3.7$ is the most probable position of the trapped particle system. Alternatively, if the 850 kc/s frequency is equated to f_m rather than to $2f_m$ the values $L \fallingdotseq 2.4$, $E \fallingdotseq 0.38$ eV are obtained. A large density of trapped electrons is unlikely to occur on this shell, however, since it is entirely within the

inner Störmer forbidden region.

In order to couple energy into an external system some degree of bunching or asymmetry must occur in this trapped electron system. The mechanism which is responsible for this bunching is obscure. The preferential detection of the second harmonic of the mirror frequency is consistent with the approach of any bunch or asymmetry in the electron system to the sensing electrode twice per mirror period.

Of the observations which are listed in the preceding section, 2, 4, 6 and 7 are consistent with the characteristics of a trapped electron system of this type. The dependence of the oscillation frequency on the primary electron accelerating voltage (observation 3) is probably caused by small variations in the mean energy or density of the trapped electrons which are produced by changes in the primary electron trajectory. The dependence of the oscillation frequency on the gas pressure is difficult to reconcile with the properties of a trapped particle system.

10.4 Summary

It has been shown that oscillatory phenomena in the model may be produced by the trapping of low energy electrons on the magnetic field shell which passes through the position of the electron gun. An adequate method for bunching the trapped electrons has not been found.

Other experiments which appear to be possible are:-

1) The use of the dark line phenomenon (figure 10.3) to map contours of constant effective threshold at large latitudes. This would require the use of a large model to permit a good simulation of the geomagnetic field. A coating of fluorescent material would permit a rapid visual inspection.

2) A study of the dynamics of trapped particle systems.

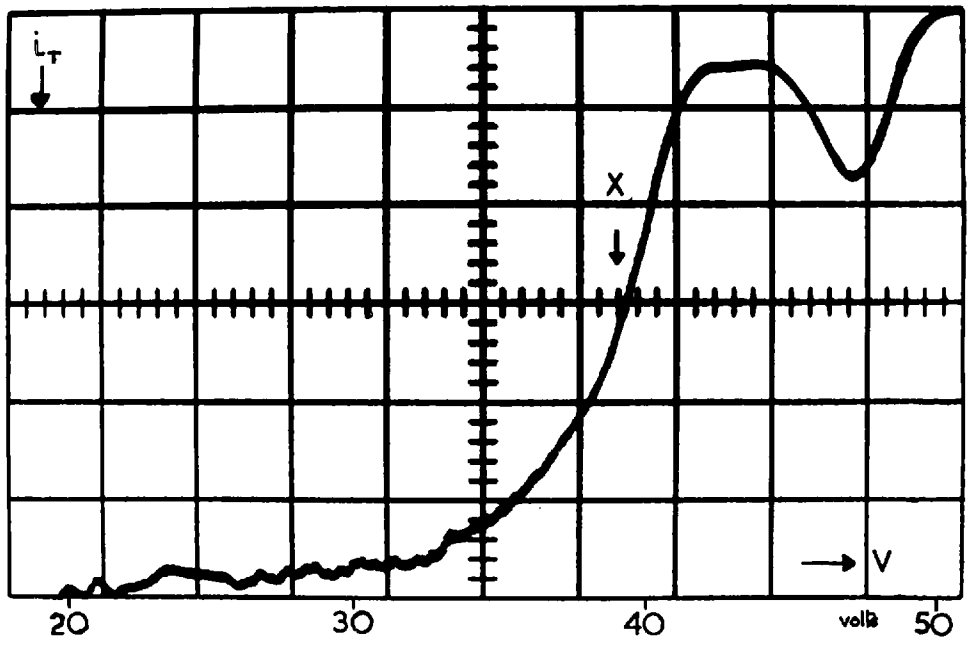

Figure 10.1 The threshold at latitude 57° illustrating the instability at rigidities below the Störmer threshold (section 10.2)

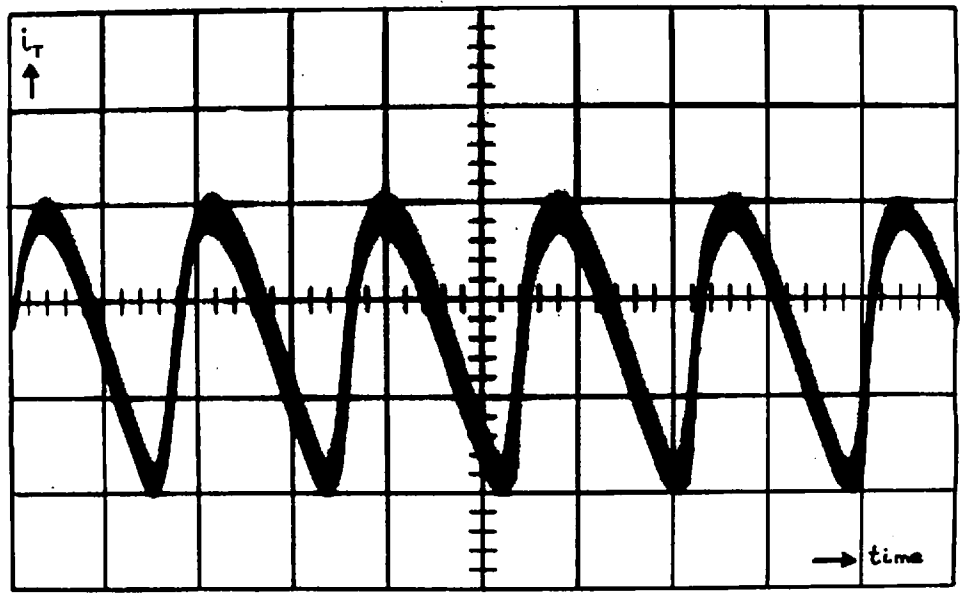

Figure 10.2 Oscillatory waveform observed with an accelerating voltage of ~38 volts, represented by 'X' in the upper curve (section 10.2).

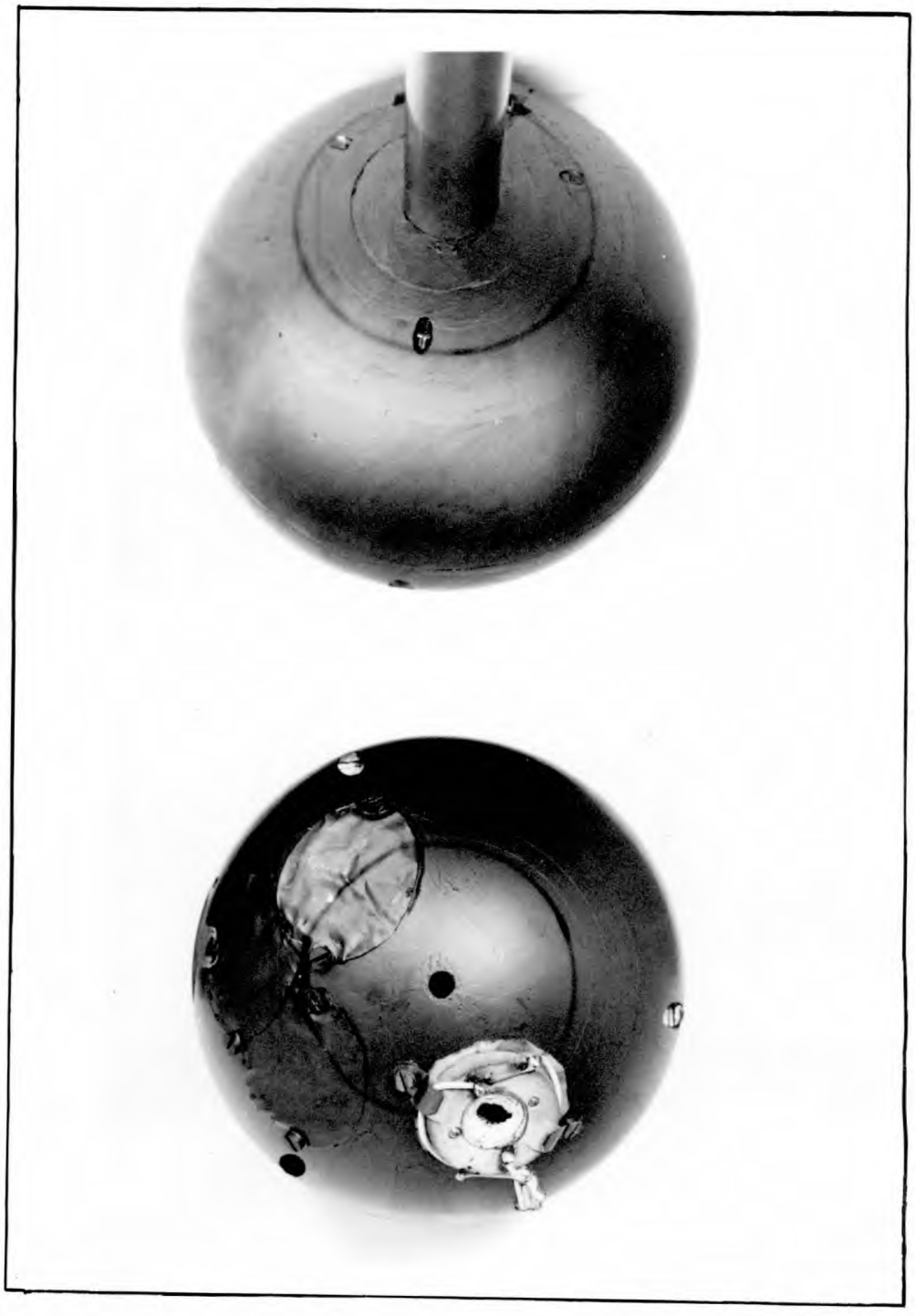

Figure 10.3 Photographs of the polar regions of the model showing the dark lines following contours of constant L value. The axis of the magnet is parallel to the stem (upper photograph).

ACKNOWLEDGEMENTS

I would like to thank Professor P.M.S. Blackett for providing me with the opportunity of working in his laboratories.

I would also like to thank my supervisor, Professor H. Elliot for suggesting this work, for continued encouragement and for ensuring that the work maintained close ties with the field of cosmic ray physics.

My early work was performed in conjunction with Dr. C.J. Bland to whom I am indebted for a particularly pleasant and profitable partnership.

I am indebted also to Mr. A. Bewick for considerable instruction in the art of designing transistor circuits and for preventing the larger electronic catastrophies, and to Dr. J.J. Quenby for allowing me to use his unpublished calculations of threshold perturbation.

I would like to thank the Misses A. Benton and C. Fogg for performing several calculations and for helpful suggestions in the preparation of this thesis, Mr E. Sparkes for practical assistance and advice in the preparation of the diagrams and photographs, and Mr. F. Martin for correcting my metalwork techniques.

Finally, I wish to thank the Department of Scientific and Industrial Research for grants which have permitted the execution of this work.

REFERENCES

Akasofu S-I, 1963, Space Sci. Reviews 2, 91.

Akasofu S-I. and Cain J.C.,1962, J. Geophys. Res. 67, 3537.

Akasofu S-I., Cain J.C. and Chapman S., 1961, J. Geophys. Res. 67, 2645.

Akasofu S-I., Chapman S. and Venkatesan D., 1963, J. Geophys. Res. 68, 3345.

Akasofu S-I. and Lin W.C., 1963, J. Geophys. Res. 68, 973.

Alfvén H., 1950, Cosmical Electrodynamics, Oxford University Press, 1950.

Apel J.R., Singer S.F. and Wentworth R.C., 1962, Advances in Geophysics G,131. Academic Press, New York, 1962.

Bailey D.K., 1962, Proc. Intl. Conf. on Cosmic Rays and the Earth Storm, Kyoto, Japan, 1961, 1, 106.

Beard D.B., 1960, J. Geophys. Res. 65, 3550.

Beard D.B., 1962, J. Geophys. Res. 67, 477.

Beard D.B. and Jenkins E.B., 1962, J. Geophys. Res. 67, 4895.

Bennett W.H.,195 , Rev. Sci. Inst. 30, 2.

Bierman L., 1957, Observatory 77, 109.

Birkeland K., 1901, Vid. Selsk. Skr. Math. Nat. Kl. 1 (in Norwegian) (some translation in Störmer's Polar Aurora O.U.P.)

Blackwell D.E. and Ingham M.F., 1961, Mon. Not. Roy. Astronomical Soc.,122,113.

Bland C.J., 1962, Phil. Mag. 7, 1487., also Ph.D. thesis, London University 1961.

Block L.,1955, Tellus 7, 65.

Block L.,1956, Tellus 8, 234.

Block L.,1958, Proc. I.A.U. Symposium No. 6, 312.

Bouckaert L., 1934, Ann. Soc. Sci. Bruxelles, 54, 174.

Bowen I.S., Millikan R.A. and Neher H.V., 1938, Phys. Rev. 53, 855.

Bridge H.S., Dilworth C., Lazarus A.J., Lyon E.F., Rossi B., Scherb F., 1962, J. Phys. Soc. Japan, 17, Suppl. A-2 553.

Brown W.E. and Sweer J.H., 1945, Rev. Sci. Inst., 16, 10, 276.

Bruche E., 1931, Terr. Mag. 36, 41.

Brunberg E-Å. and Dattner A., 1953, Tellus 5, 135.

Cahill L.J. Jr. and Amazeen P.G., 1963, J. Geophys. Res. 68, 2121.

Clay J., 1927, Proc. Roy. Acad. Amsterdam 30, 1115

Codrington R.S., Olds J.D. and Torrey H.C., 1954, Phys. Rev. 95, 607.

Coleman P.J. Jr., Sonett C.P. and Davis L., 1960, Phys. Rev. Letters 5, 43.

Compton A.H., 1933, Phys. Rev. 43, 387.

Compton A.H. and Turner R.N., 1937, Phys. Rev. 52, 799.

Craig H., 1947, Proc. Phys. Soc. 59, 804.

Davis L.R. and Williamson J.M., 1962, I.G.Y. Bulletin 58, 223.

Elliot H., 1963, Reports on Progress in Physics 26, 145.

Finch H.P. and Leaton B.R., 1957, Mon. Not. Roy. Astronomical Soc. Geophys. Suppl. 1, 1, 314.

Firor J., 1954, Phys. Rev. 94, 1017.

Fermi E., 1949, Nuclear Physics, Chicago University Press, 224.

Gregg J., 1947, Rev. Sci. Inst. 18, 2, 77.

Hatton C.J. and Marsden P.L., 1962, Phil. Mag. 7, 1145.

Haynes S.K. and Wedding J.W., 1951, Rew. Sci. Inst. 22, 97.

Heppner J.P., Ness N.F., Scearce C.S. and Skillman T.L., 1963, J. Geophys. Res. 68, 1.

Hultqvist B., 1958, Arkiv for Geofysik 3, 4, 63.

Hultqvist B., 1962, 'Studies of ionospheric absorption of radio waves by the cosmic noise method' Report of the Kiruna Geophysical Observatory.

Hutner R.A., 1939, Phys. Rev. 55 15, 614.

Johnson T.M. and Street J.C., 1933, Phys. Rev. 43, 381.

Jory F.S., 1956, Phys. Rev. 102, 4, 1167.

Katz L., Meyer P. and Simpson J.A. Il Nuovo Cimento 8, Suppl. 2, 277.

Kasper J.E., 1959, Il Nuovo Cimento 11 Suppl. 1, 1.

Kellogg P.J., 1960, J. Geophys. Res. 65, 9, 2701.

Kellogg P.J. and Winckler J.R., 1961, J. Geophys. Res. 66, 3991

Klemperer O., 1953, 'Electron Optics' Cambridge University Press, 264 et. seq.

Kodama M., 1959, J. Geomag. and Geoelec. 10, 37.

Kodama M., Kondo I. and Wada M., 1957, J. Sci. Res. Inst., Japan, 51, 138.

Kodama M. and Miyazaki Y., 1957, Rep. of Ion. Res. in Japan 11,99.

Lemaitre G., 1935, Ann. Soc. Sci. Bruxelles 54, 162.

Lemaitre G. and Vallarta M.S., 1933, Phys. Rev. 43, 87.

Lemaitre G. and Vallarta M.S., 1936 a, Phys. Rev. 49, 719.
b, Phys. Rev. 50, 493.

Little C.G. and Leinbach H., 1959, Proc. I.R.E. 47, 315.

Lust R., 1957, Phys. Rev. 105, 1827.

MacDonald F.B., 1956, Phys. Rev. 104, 1723.

Malmfors K.G., 1945, Arkiv fur Math. o.Fysik 32A, 8.

Marsden P.L. and Wilson J.G., 1958, Il Nuovo Cimento 8, Suppl. 2, 228.

Mathews T., Thambyahpillai T. and Webber W.R., 1961, Mon. Not. Roy. Astro. Soc. 123, 2, 97.

McCracken K.G., 1962, J. Geophys. Res. 67, 423.

McCracken K.G., Rao U.R. and Shea M.A., 1962, Mass. Inst. Tech., Report 77.

McIlwain C.E., 1961, J. Geophys. Res. 66, 3681.

Midgley J.E. and Davis L. Jr., 1962, J. Geophys. Res. 67, 499.

Midgley J.E. and Davis L. Jr., 1963, J. Geophys. Res. 68, 5111.

Neher H.V. and Peterson V.Z. and Stern E.A., 1953, Phys. Rev. 90, 655.

Neugebauer M. and Snyder C.W., 1962, Science 138, 1095.

Obayashi T., 1961, Arkiv fur Geofysik 3, 507. also J. Geomag. and Geoelec. 13, 26.

Obayashi T. and Hakura Y., 1960, J. of Radio Res. Lab. of Japan 7, 27.

Parker E.N., 1961, Astrophysical Journal 133, 1014.

Pfotzer G., 1958, Il Nuovo Cimento 8, Suppl. 2, 220.

du Plooy N.F., Kühn G.J., Maree J.P., Stoker P.H. and Van der Walt A.J., 1963, J. Geophys. Res. 68, 3123.

Pomerantz M.A. and Agarwal S.P., 1962, Phil. Mag. 7, 1503.

Quenby J.J., 1960, Private Communication.

Quenby J.J. and Webber W.R., 1959, Phil. Mag. 4, 90.

Quenby J.J. and Wenk G.J., 1962, Phil. Mag. 7, 1457.

Ray E.C., 1956, Phys. Rev. 101, 1142.

Ray E.C., 1963, N.A.S.A., G.S.F.C. Rept. X-611-63-43.

Roberts A.M., 1963, Private Communication.

Rothwell P., 1958, Phil. Mag. 3, 961.

Rothwell P. and Quenby J.J., 1958, Il Nuovo Cimento 8, Suppl. 2, 249.

Sandström A.E., 1958, Il Nuovo Cimento 8, Suppl. 2, 263.

Sauer H.H., 1963, J. Geophys. Res. 68, 957.

Sauer H.H. and Ray E.C., 1963, State Univ. Iowa Res. Rept. 63-8, 19, March 1963.

Schluter A., 1958, Il Nuovo Cimento 8, Suppl. 2, 263.

Schremp E.J., 1938, Phys. Rev. 54, 158.

Schwartz M., 1959, Il Nuovo Cimento 11, Suppl. 1, 27.

Simpson J.A., Fenton K.B., Katzman J. and Rose D.C., 1956, Phys. Rev. 102, 1648.

Spreiter J.R. and Briggs B.R., 1962, J. Geophys. Res. 67, 37.

Spreiter J.R. and Hyett B.J., 1963, J. Geophys. Res. 68, 1631.

Spreiter J.R. and Jones W.P., 1963, J. Geophys. Res. 68, 3555.

Storey J.R., 1959, Phys. Rev. 113, 297, 302.

Störmer C., 1907, Arch. Sci. phys. nat. Geneve. Oct. 1907, 347.

Swann W.F.G., 1933, Phys. Rev. 44, 224.

Treiman S.B. 1953, Phys. Rev. 89, 130.

Vallarta M.S., 1935, Phys. Rev. 47, 647.

Vallarta M.S., 1938, An Outline of the Theory of the Allowed Cone of Cosmic Radiation (Toronto, 1938).

Vallarta M.S., 1961, Handbuch der Physik 46, 1. (Springer - Verlag)

Villard M.P., 1906, Ann. de Chimie et de Physique 8^{me} series, 9.

Webber W.R., 1962, Prog. in Cosmic Ray Physics, North Holland Publishing Co.

Webber W.R., 1963, J. Geophys. Res. 68, 3065.

Webber W.R. and Quenby J.J., 1959, Phil. Mag. 4, 654.

APPENDIX A

A THEORETICAL ANALYSIS OF THE THRESHOLD PERTURBATIONS WHICH ARE PRODUCED BY SUPERIMPOSING A UNIFORM MAGNETIC FIELD PARALLEL TO THE AXIS OF A MAGNETIC DIPOLE

A.1 General

Quenby (1960) has obtained a numerical solution of the Störmer equation which represents the motion of a charged particle in an axially symmetric combination of uniform and dipole magnetic fields. This review of the method illustrates how the threshold perturbations may be determined either from an approximate equation which is valid at equatorial latitudes or by using a simple procedure to obtain a numerical solution which is valid at all latitudes.

The notation and unit system of section (2.2) have been used and for ease of comparison the equations which are derived in this section bear the same index letters as the corresponding equations in section (2.2).

A.2 The basic equation

The vector potential which represents the combination of the uniform and dipole magnetic fields is:-

$$\underline{A} = \frac{M_e \cos\lambda}{r^2}\,\underline{i}_\phi - \frac{r}{2} H_z \cos\lambda\,\underline{i}_\phi \qquad \ldots\ldots (A.A)$$

where H_z is the uniform field strength. H_z is positive if H_z and the dipole equatorial field have the same sense. The use of this vector potential changes equation (2.D) to:-

$$r\cos\lambda\cos\psi + \left(\frac{M_e}{r^2} - \frac{rH_z}{2}\right)\frac{r\cos^2\lambda}{R_e} = \text{constant} \qquad (A.D)$$

Therefore equation (2.E) becomes:-

$$R\cos\lambda\cos\psi + \frac{\cos^2\lambda}{R}\left(1 - \frac{M_e^{\frac{1}{2}} H_z R^3}{2P_e^{\frac{3}{2}}}\right) = 2\gamma \qquad \ldots\ldots (A.E)$$

This is the basic 'Störmer' equation of Quenby's method: however, since this equation contains the term P_e the method which was used to solve equation (2.E) cannot be used in this case.

It can be shown that the Störmer allowed region which is obtained from equation (A.E) may be divided into two parts by a suitable choice of the constant γ as in the case of a simple dipole field. The minimum value of γ which produces this division is a function of both P_e and H_z.

Since $\cos\lambda = 1$ at the equatorial pass between the inner and outer allowed regions and $\cos\psi = 0$ for an orbit at grazing incidence at the pass these values are used in equation (A.E) to yield:-

$$R_j + \frac{1}{R_j} - \delta R_j^2 = 2\gamma \qquad \ldots\ldots \text{(A.K)}$$

where $\delta = \dfrac{M_e^{\frac{1}{2}} H_z}{2 P_e^{3/2}}$ and R_j is the radial co-ordinate of the pass in Störmer units.

An inspection of the graph of 2γ as a function of R for various values of δ indicates that the correct minimum value of γ is obtained by putting $\dfrac{\partial\gamma}{\partial R} = 0$. Whence:-

$$1 - R_j^2 + 2\delta R_j^3 = 0 \qquad \ldots\ldots \text{(A.L)}$$

This equation must be solved for R_j either numerically or by an approximate method.

A.3 <u>An approximate solution of equation (A.E) which is valid for small values of δ.</u>

Since in equation (A.L) $R_j \to 1$ if $\delta \to 0$ the substitution $R_j = 1 + \alpha$ is valid for small δ. If this substitution is made and equation (A.L) is solved for α :-

$$\alpha \sim \frac{\delta}{1 - 3\delta} \sim \delta \quad \text{to first order.}$$

Whence putting $R_j = 1 + \delta$ in equation (A.K), $2\gamma = 2 - \delta$ to first order.

If this value of 2γ is used in equation (A.E) and the zenith arrival direction at the Earth's surface is selected by putting $\cos\psi = 0$:-

$$\frac{\cos^2\lambda}{R_e}\left(1 - \delta R_e^3\right) = 2 - \delta$$

Now $R_e \to \frac{1}{2}\cos^2\lambda$ when $\delta \to 0$ (section 2.2). Therefore the substitution $R_e = \frac{1}{2}(1+\rho)\cos^2\lambda$ is made and the above equation is solved for ρ to yield:-

$$R_e = \tfrac{1}{2}\left\{1 + \frac{\delta}{2}\left(1 - \tfrac{1}{4}\cos^6\lambda\right)\right\}\cos^2\lambda$$

Thus:-

$$P_e = \frac{M_e}{r_e^2}R_e^2 = \frac{M_e}{4r_e^2}\left\{1 + \delta\left(1 - \tfrac{1}{4}\cos^6\lambda\right)\right\}\cos^4\lambda$$

—— to first order.

If the constants are evaluated and P_e is expressed in units of 10^9 practical volts this equation becomes:-

$$P_{e(G.V.)} = 14.9\left\{1 + 7.4 \times 10^{-3}\Delta H\, P_e^{-\frac{3}{2}}\left(1-\tfrac{1}{4}\cos^6\lambda\right)\right\}\cos^4\lambda \quad \ldots(A.M)$$

where ΔH is the superimposed field strength in units of 10^{-5} gauss.

Since three approximations to first order have been made in this derivation, a comparison was made between the values of threshold which were obtained from this equation and the values which were obtained by numerical solution. It was found that the error in the percentage perturbation increases with ΔH and with λ; however, this error is less than approximately -10% of the perturbation for $\Delta H \leq 100$ gammas and $\lambda \leq 30^\circ$. (1 gamma = 10^{-5} gauss). Thus within this range of application equation (A.M) may be simplified without involving serious error by replacing P_e in the bracket by the unperturbed Störmer value. This gives:-

$$P_{e(G.V.)} = 14.9\left\{1 + 1.29 \times 10^{-4}\Delta H\,\frac{\left(1-\tfrac{1}{4}\cos^6\lambda\right)}{\cos^6\lambda}\right\}\cos^4\lambda \quad \ldots(A.N)$$

This equation has been used to obtain the data for figure (2.3).

A.4 The procedure for obtaining the numerical solution which is valid at all latitudes

The steps are:-

1) Equation (A.L) is solved graphically for R_j. It is noticed that if H_z is negative, δ is negative and R_j is in the range $0 \leq R_j \leq 1$. Therefore is plotted as a function of R_j for values of R_j between 0 and 1.

2) Graphs of δ as a function of P_e are constructed for a selection of values of H_z in the range of interest. The range of P_e should represent the range of values of the geomagnetic thresholds.

3) The above two steps provide R_j as a function of δ, δ as a function of P_e and hence also R_j as a function of P_e. These values of R_j and δ are inserted in equation (A.K) to provide 2γ as a function of P_e. A family of curves with H_z as parameter may be constructed.

4) The conditions for zenith incidence at the Earth's surface ($\cos\psi = 0$, $R = R_e$) are inserted in equation (A.E) to give:-

$$2\gamma = (1 - \delta R_e^3) \frac{\cos^2\lambda}{R_e}$$

If δ is obtained from 2) above and R_e is obtained from the expression for the Störmer unit this equation permits the construction of a family of graphs of 2γ as a function of P_e with the latitude λ as a parameter.

5) The families of curves of 2γ as a function of P_e which were obtained in steps 3) and 4) above are plotted on a common abscissa. The points where the H_z parameter curves cross the λ parameter curves are the threshold values at the various combinations of latitude and field strength.

This procedure has been used to obtain the data for figure (2.4).

A.5 An expression for the minimum latitude at which negative values of H_z reduce the zenith thresholds to zero

Since $\delta \to -\infty$ as $P_e \to 0$ equation (A.L) indicates that $R_j \to (2\delta)^{-1/3}$ at

this limit. The use of this value of R_j in equation (A.K) reveals that the corresponding limiting value of 2γ is $\frac{3}{2}(2\delta)^{\frac{1}{3}}$. If δ and R_e are expressed in terms of H_z, M_e, r_e, P_e, the zenith arrival direction at the Earth's surface is selected by placing $\cos\psi = 0$ and this value of 2γ is used equation (A.E) becomes:-

$$\cos^2\lambda = \frac{\frac{3}{2} M_e^{-\frac{1}{6}} H_z^{-\frac{1}{3}}}{\frac{M_e^{\frac{1}{2}}}{r_e} + \frac{H_z r_e^2}{2M_e^{\frac{1}{2}}}}$$

Since the second term in the denominator is less than 1% of the first term for H_z less than 500 gamma, it may be ignored. The expression then may be simplified by substituting $H_e = M_e / r_e^3$ to give:-

$$\cos^2\lambda = \frac{3}{2}\left(\frac{H_z}{H_e}\right)^{\frac{1}{3}} \qquad \ldots\ldots \text{(A.P)}$$

or - $$\cos^6\lambda = 1.09 \times 10^{-4} \Delta H$$

where ΔH is the strength of the superimposed field in units of 1 gamma. This equation is plotted in figure (2.5). A similar equation has been obtained by Obayashi (1961).

APPENDIX B

THE LATITUDE OF THE GUN AS A FUNCTION OF THE ANGULAR ROTATION Θ OF THE SUPPORTING STEM

The geometry of the model is:-

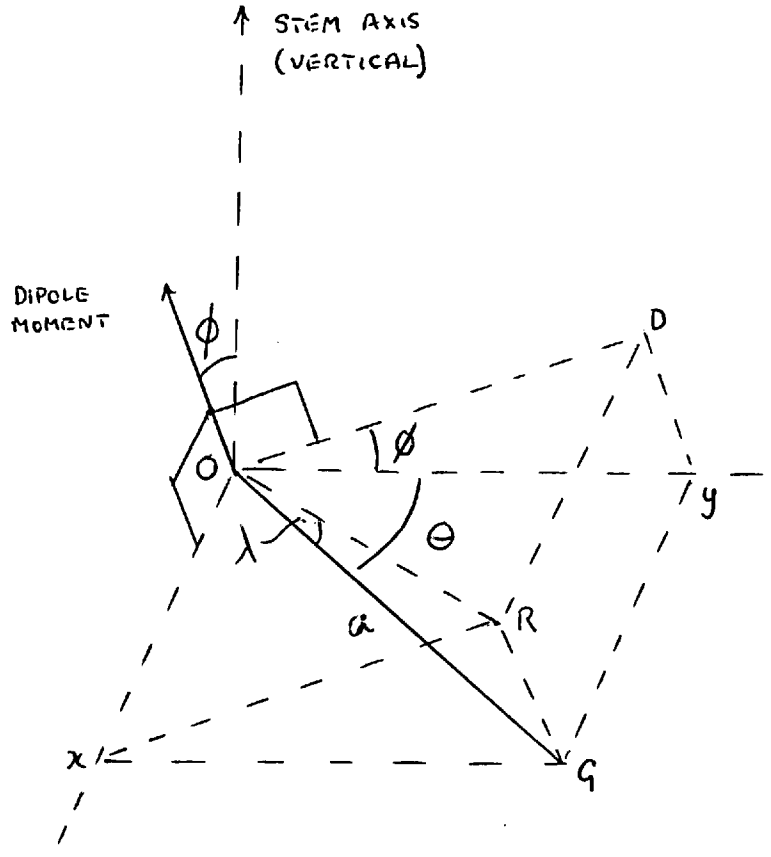

where xOD is the equatorial plane of the dipole and the gun G rotates at a radius 'a' about 'O' in the xOy plane. The gun rotates through an angle 'Θ' about the axis of the stem from the position of maximum latitude at 'y'.

In order to calculate the latitude of the gun in terms of Θ and ϕ, the radius OG = a is resolved into components Ox = a sin Θ and Oy = a cos Θ. Oy is projected on to OD so that OD = a cos Θ cos ϕ. Hence:-

$$(OR)^2 = (Ox)^2 + (OD)^2$$

$$= (a \sin\theta)^2 + (a \cos\theta \cos\phi)^2$$

where ϕ is the angle between planes Oxy and OxD.

Thus:-

$$\cos^2\lambda = \frac{(OR)^2}{a^2} = \sin^2\theta + \cos^2\theta \cos^2\phi$$

$$= 1 - \cos^2\theta \sin^2\phi.$$

APPENDIX C

THE EVALUATION OF EFFECTIVE THRESHOLD RIGIDITIES IN THE PRESENCE OF PENUMBRAL EFFECTS

The differential rigidity spectrum of the primary cosmic radiation may be represented by:-

$$\frac{dI}{dR} = A\,P^{-a}\,dP$$

where 'A' and 'a' are constants. If the rigidity dependence of the penumbral differential transparency at a given latitude is represented by the function 'T' the total primary intensity which is 'seen' by a detector situated at the top of the atmosphere is:-

$$I = \int_0^{\infty} A\;G\;P^{-a}\;T\,dP$$

where the constant 'G' represents the geometrical factor of the detector and 'T' depends on the geometry of the acceptance cone. Thus an effective threshold P_E may be defined by the relation:-

$$\int_{P_E}^{P_x} AGP^{-a}dP = \int_{0}^{P_x} A\,G\,P^{-a}\;T\;dP$$

where the limit of integration P_x may be any rigidity which is larger than the maximum rigidity of the penumbra (i.e. for all $P \geqslant P_x$, $T = 100\%$).

In order to calculate P_E for the curves of figure (6.1) the right-hand integral was replaced by the summation $\sum_{P=0}^{P=P_x} A\,P_i^{-a}\,T_i \Delta P$ in which ΔP is chosen to give ~ 10 values of P_i between the Störmer and main cone thresholds.

Thus if the left-hand side of the above equation is integrated and this summation is used:-

$$\frac{P_E^{1-a} - P_x^{1-a}}{a-1} = \Delta P \sum_{P_i=0}^{P_i=P_x} P_i^{-a}\,T_i$$